# THE ROLE OF THE N-TERMINAL DOMAIN IN THE DYNAMICS OF HSP27 EQUILIBRIUM DISSOCIATION

By

Ezelle Teresa McDonald

Dissertation

Submitted to the Faculty of the

Graduate School of Vanderbilt University

in partial fulfillment of the requirements

for the degree of

DOCTOR OF PHILOSOPHY

in

Molecular Physiology and Biophysics

May, 2012

Nashville, Tennessee

Approved:

Charles E. Cobb, Ph.D.

Albert H. Beth, Ph.D.

Phoebe L. Stewart, Ph.D.

Louis J. De Felice, Ph.D.

I dedicate this dissertation work to my parents, David and Ezell McDonald.

To my brother David and Aunt Mary for all of their love and support

## ACKNOWLEDGEMENTS

This dissertation work would not have been possible without financial support from the National Eye Institute and National Institutes of Health. I would like to express my deepest gratitude to my advisor, Dr. Hassane Mchaourab, for his encouragement, support, and mentorship. He has provided me with extraordinary experiences and opportunities at each stage of my academic development. His wisdom, knowledge, and commitment to the highest standards have both inspired and motivated me.

A special thanks and appreciation go to my dissertation committee members: Dr. Charles E. Cobb, Dr. Albert H. Beth, Dr. Phoebe L. Stewart, and Dr. Louis J. De Felice. I am grateful to my dissertation committee for their encouraging words, thoughtful criticism, and expertise for the betterment of my dissertation work. I would like especially like to thank Angie Pernell and Alyssa Hasty for their support. I offer my deepest regards to members of the Mchaourab lab and the Molecular Physiology and Biophysics Department for supporting me in all aspects of my dissertation project. I would like to thank Dr. Hanane Koteiche for her patience in teaching me molecular biology techniques. I would also like to thank Dr. Richard Stein and Dr. Smriti for all their advice and suggestions. A special thanks goes to Guangyong Yang, Edward Monson, and Sanjay Mishra for all of their help with protein expression, purification, and light scattering experiments. I owe my deepest gratitude to my family for always encouraging me with best wishes, through good times and bad.

## TABLE OF CONTENTS

## LIST OF FIGURES

## LIST OF ABBREVIATIONS

| Abbreviations | Description |
|---|---|
| NiEDDA | nickel (II) ethylenediamine-diacetate |
| T4L | T4 lysozyme |
| EPR | electron paramagnetic resonance |
| HSP | heat shock protein |
| SEC | size-exclusion chromatography |
| ATP | adenosine triphosphate |
| Cryo-EM | cryogenic electron microscopy |
| DTT | dithiotheritol |
| IAP | proxyl iodo acetamide |
| MTSSL | methanethiosulfonate spin label |
| PMSF | phenyl methyl sulfonyl fluoride |
| SDSL | site-directed spin labeling |
| sHsps | small heat shock proteins |
| Hsp16.5 | heat shock protein 16.5 |
| Hsp16.9 | heat shock protein 16.9 |
| Tsp36 | Taenia saginata |
| Hsp20 | heat shock protein 20 |
| Hsp27 | heat shock protein 27 |
| $\alpha$A | alphaA-crystallin |
| $\alpha$B | alphaB-crystallin |

TNF ..... tumor necrosis factor

PDI ..... protein disulfide isomerase

PPI..... peptidyl prolyl cis-trans isomerase

MAPKAP ..... mitogen activated protein kinase activating kinase

Trp ..... tryptophan

Pro ..... proline

Phe ..... phenylalanine

Arg ..... arginine

His ..... histidine

Leu ..... leucine

Ser ..... serine

Ala ..... alanine

Ile..... isoleucine

Glu..... glutamic acid

Tyr ..... tyrosine

Gln..... glutamine

Thr ..... threonine

Val ..... valine

Gly ..... glycine

RT..... room temperature 23$^{o}$C to 25$^{o}$C

FRET ..... fluorescence resonance energy transfer

# CHAPTER I

# INTRODUCTION

## Non-covalent Interactions Contribute to Protein Stability and Structure

Proteins fold into stable conformations where hydrophobic residues are buried on the inside of the protein and polar residues are solvent accessible. Non-covalent interactions significantly contribute to the conformational stability of proteins. These stabilizing interactions include hydrogen bonds, hydrophobic forces, and electrostatic interactions. Stabilizing interactions are disrupted by extremes in temperature or pH and by the addition of alcohols, sodium dodecyl sulfate (SDS), and denaturants such as urea, and guanidium chloride. Therefore under these conditions, the likelihood of protein unfolding (denaturation) is increased. A protein's folded state is maintained through the delicate balance of stabilizing and destabilizing interactions. An example of a destabilizing interaction occurs when a charged group is surrounded by hydrophobic residues on the inside of the protein. This destabilizing effect will promote the unfolding of proteins. For that reason, it becomes abundantly clear the level of intricacy inherent in the protein folding process.

The complex nature of the folding process can be described by the following isothermal Gibbs free energy equation:

$$\triangle G = \triangle H - T\triangle S \qquad (1)$$

where $\triangle G$ is the Gibbs free energy; $\triangle H$ the enthalpy; and $\triangle S$ the entropy.

The Gibbs free energy reflects the difference in contribution from non-covalent interactions (enthalpy) and intrinsic ordering of the system (entropy). To further illustrate the point, the transition from an unstructured conformation to an ordered structure gives rise to unfavorable conformational entropy. As a matter of fact, conformational entropy works against protein folding, favoring unfolded conformations. In order for a protein to fold, it must overcome destabilizing interactions that produce unfavorable entropic and enthalpic contributions to the Gibbs free energy. For instance, the sequestration of hydrophobic residues (hydrophobic effect) away from water is a major contributor to protein folding (Nikolic et al. 2011). In the protein's unfolded state, water molecules are released from their ordered state. Consequently, less ordering increases entropy and favorably contributes to the Gibbs free energy of folding. Moreover, the formation of stabilizing electrostatic interactions and hydrogen bonds produces a favorable enthalpic contribution to the overall free energy. A general inference can be drawn that proteins in their native (biologically active) state are marginally stable. Proteins have evolved to have their native states marginally stable, because living cells need to rapidly synthesize and degrade proteins for the physiological needs of the cell.

## Theory of Protein Folding

Proteins modulate their non-covalent interactions to affect entropic and enthalpic contributions enabling protein folding to be a thermodynamically favored process. In particular, the free energy is reduced as the protein transitions from unfolded to folded states. A typical folding reaction profile shows that the unfolded state approaches the folded state by way of intermediate transition states. For simplicity, the folding process can be described by a way of a two-state model. In the two state model, only the folded and unfolded states are identified, and the folding intermediates are presumed to have a negligible contribution (Baldwin and Rose 1999). Protein folding is a reversible reaction that can be described by the following equilibrium:

$$U \underset{k_2}{\overset{k_1}{\rightleftharpoons}} N \qquad (2)$$

where U represents the unfolded state and N the more stable native (folded) state. $k_1$ and $k_2$ are the rate constants associated with protein folding and unfolding respectively. These rates are related to the equilibrium constant ($K_{eq}$) governing the folding reaction.

$$K_{eq} = \frac{[N]}{[U]} \qquad (3)$$

$K_{eq}$ is related to the free energy associated with protein folding by the following equation:

$$\Delta G^{o} = -RT \ln K_{eq} \qquad (4)$$

where R is the gas constant and T is the absolute temperature in kelvins. If $K_{eq} > 1$, $\triangle G^{o}$ is negative and the folding equilibrium will favor the folded native state. $\triangle G^{o}$ is a measure of the conformational stability of folded proteins.

*In vitro* studies have revealed that protein folding is a cooperative process that is a culmination of multiple interactions within the polypeptide chain (Kuwajima 1989). According to *in vitro* unfolding experiments, regions, of the polypeptide chain, that are partially unfolded contribute to the instability of the remaining structure. Proteins with multiple domains have a tendency to deviate from the two-state folding model because protein folding is a hierarchic process. Simulations have provided additional evidence in favor of hierarchical folding (Lazaridis and Karplus 1997). For example, the burst phase is an early step in protein folding. During this phase, CD experiments confirmed the existence of an intermediate, with secondary structure, similar to the native state (Ptitsyn 1996). In this intermediate, referred to as the molten globule, the amino acid side chains are disordered and loosely packed. Furthermore, long range tertiary interactions are absent and it is during subsequent folding steps that subdomains appear. It has been proposed that molten-globule intermediates are part of a folding pathway toward the native conformation.

Cyrus Levinthal demonstrated that many combinations of dihedral angles are compatible with a protein's stable conformational state. If a protein randomly explored all conformations available, it would take an impossibly long time for the protein to fortuitously achieve its native state (Levinthal's paradox). To escape this paradox, Levinthal reasoned that proteins fold through an ordered set of pathways to attain the native state with the lowest free energy (Levinthal 1968). The concepts of thermodynamic and kinetic control evolved from Levinthal's paradox. Thermodynamic control describes how a protein attains its global energy minimum, in a folding pathway independent manner. Essentially, the conditions of denaturation do not determine final native structure, while kinetic control describes the physiological time scale of folding.

In this so called "classical view", the folding pathway is composed of discrete intermediate states. Intermediates were classified as on pathway or off pathway. On pathway intermediates pave the way to productive protein folding. All intermediates are assumed to be well defined and follow a sequential mechanism. There are three classical models: off-pathway, on-pathway, and sequential (Dill and Chan 1997). Each model is characterized by the following reaction schemes:

The off-pathway reaction scheme:

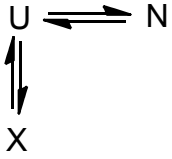


(5)

The on-pathway reaction scheme:

(6)

The sequential reaction scheme:

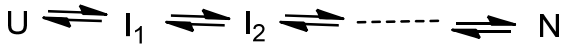

(7)

where N represents the native state, U the unfolded state, and X/I are intermediate states that have similar properties as the native and unfolded states. Each model demonstrates how different states are interrelated on a given protein folding pathway. The sequential model is commonly used to describe protein folding. This model suggests that folding occurs via a unique pathway of sequential intermediates (Baldwin 1995). The application of statistical mechanics and Monte Carlo simulations paved the way for a modern view of protein folding (Dobson and Karplus 1999; Dinner et al. 2000). The modern view replaces the folding pathway with energy landscape theory (Dill et al. 1995; Wolynes et al. 1995; Baldwin and Rose 1999). The energy landscape incorporates the free energy associated with each possible protein conformation. The energy surface is comprised of horizontal and vertical coordinates. The horizontal coordinates represent a particular protein conformation. Each horizontal coordinate is a direct reflection of the possible dihedral angles, along the protein backbone. Conformations that are similar in geometry are grouped closely to each other. Vertical coordinates represent the free energy associated with a particular conformation. The horizontal and vertical coordinates outline a funnel-shaped energy surface. The energy landscape contains hills, which are representative of high energy conformations.

The more favorable conformations are located within the valleys. The global free energy minimum is located at the bottom of the funnel and it corresponds with the native state.

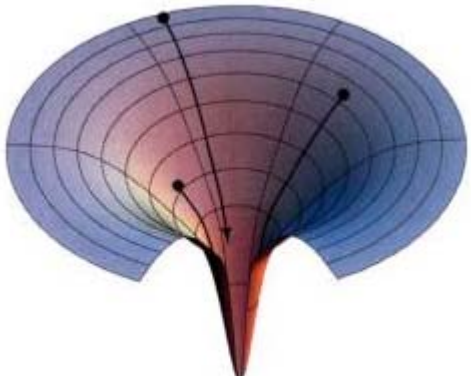

**Figure 1: Funnel-shaped energy landscape.** The native state (N) is located at the bottom of the funnel, and the native state is the global free energy minimum. The energy landscape suggests several routes for obtaining the native state with local energy minima existing along each pathway. This figure was adapted from Dill and Chen, 1997.

Now, the kinetic process of protein folding can be described by the energy landscape. As proteins fold, they change their conformations by reducing their free energy. The folding protein is constantly exposed to Brownian forces. Brownian motion causes the molecule to sample different conformations, and each conformation will have a different position along the funnel landscape. Individual conformations meander through hills and valleys on their way to the native state. Unfolded proteins follow different trajectories down the folding funnel to the global minimum (native state).

The folding funnel resolves Levinthal's paradox; in view of the fact that, the funnel shape guides all conformations toward the native state. The objective is to sidestep the random sampling of all possible conformations. For that reason, the restriction of the conformational space sampled by the protein leads to more rapid folding.

Nevertheless, the conclusion that a protein's primary sequence is the only director of the folding process toward the native conformation is a misleading assumption. In fact, proteins, *in vivo*, fold to their native conformation within a few seconds after translation. Efficient folding of proteins can occur because all cells contain accessory proteins that assist in the folding process toward the native conformation. The three types of accessory proteins are protein disulfide isomerase (PDI), peptidyl prolyl cis-trans isomerase (PPI), and molecular chaperones; each type of accessory protein performs a specific function in the pathway toward proper protein folding (Lorimer 1993; Hartl and Hayer-Hartl 2002; Young et al. 2004). For example, PDI catalyzes the formation of disulfide bonds, through disulfide bond shuttling, until native pairings are achieved. PPIs catalyze cis-trans isomerization of prolyl peptide bonds. Both PDI and PPI are of pivotal importance within the cell, because they catalyzed otherwise slow reactions greatly increasing folding efficiency.

In addition to PDI and PPI, molecular chaperones assist folding proteins in achieving their native conformation. Molecular chaperones are cytosolic proteins that prevent inappropriate interactions within nascent polypeptide chains.

These polypeptide chains have an abundance of solvent-exposed hydrophobic groups; consequently, newly synthesized polypeptide chains have a greater tendency to form aggregates which impair cellular function. Molecular chaperones bind unfolded or aggregated polypeptides thus shielding their solvent-exposed hydrophobic surfaces and inhibiting aggregation. Polypeptide release and binding occur repeatedly until proper folding and tertiary structure is achieved. The cellular system of molecular chaperones function at different stages in the protein folding network. Molecular chaperones play a pivotal role in protein quality control under normal and stressed conditions.

## Molecular Chaperones

As a counter measure to heat shock, oxidative, and osmotic stress, the cell responds by increasing the activation of 50 to 200 genes corresponding to heat shock proteins (Lindquist 1986; Parsell and Lindquist 1993; Richter et al. 2010). The majority of these genes are associated with molecular chaperones; since, the cell's first line of defense is to repair and refold proteins. Molecular chaperones are categorized into five families based upon molecular mass: Hsp100s, Hsp90s, Hsp70s, chaperonins, and small heat shock proteins (sHsps). These highly conserved families assist in the folding of nascent polypeptides while rescuing previously folded proteins from stress-induced unfolding.

Chaperones are capable of recognizing and binding patches of exposed hydrophobic amino acids; therefore, preventing the undesired intermolecular interactions which could result in protein aggregation (Bukau and Horwich 1998; Goloubinoff and De Los Rios 2007; Horwich et al. 2007; Saibil 2008; Richter et al. 2010).

The binding and release of substrate proteins, by molecular chaperones, is highly coordinated and controlled. ATP binding and hydrolysis is a key player in the affinity for binding between molecular chaperones and substrate. Due to diversity in function, molecular chaperones can be further categorized into foldases and holdases. The foldases are ATP-dependent, and these molecular chaperones have stress-inducible and constitutively expressed forms. The Hsp100s, Hsp90s, Hsp70s, and chaperonins are included in this category. sHsps are holdases which are ATP-independent and primarily expressed upon stress. The following subsections will provide a more detailed examination of the individual molecular chaperone families and their role in productive protein folding.

**Hsp100 family**

The Hsp100 family consists of the bacterial AAA ATPases ClpA, ClpB, ClpC, ClpE, ClpX, and ClpY (Sauer et al. 2004; Kirstein et al. 2009). Plants, mammals, yeast, and mitochondria contain homologues of the bacterial AAA ATPases.

All family members share a distinctive hexameric ring structure (Martin et al. 2005; Tomko Jr et al. 2010; Wang et al. 2011). Architecturally, these proteins form a hollow barrel with an internal proteolytic chamber (Effantin et al. 2010a). Within each ring, a narrow passageway provides access to the proteolytic active sites. The narrowness of this passageway serves as a gate keeper, because folded proteins are excluded due to their large size. Therefore, inadvertent contact between folded proteins with proteolytic active sites is prevented. For proteins targeted for proteolysis, ATP hydrolysis induces structural changes in the Hsp100/Clp protein resulting in transfer of substrate proteins into the proteolytic chamber (Kirstein et al. 2009). Hsp100/Clp family members are categorized into two classes based upon the number of nucleotide-binding sites per monomer (Sauer et al. 2004; Kirstein et al. 2009). Hsp100 proteins are characterized as disassembly chaperones, because they contain AAA+ protease activity. The dual nature of these proteins permits the efficient degradation of otherwise unfoldable substrates. For instance, *E. coli* has three discrete Hsp100/Clp proteolytic machines: ClpAP, ClpXP, and ClpYQ (HsIUV). Each proteolytic machine follows a similar mechanism (Effantin et al. 2010b; Rajendar and Lucius 2010; Aubin-Tam et al. 2011; Maillard et al. 2011). First, ClpX, ClpA, or HsIU recognize and bind substrate through unstructured peptide signals (chaperone activity). These peptide signals are categorized into two classes primary degradation tags and substrate tethers to the AAA+ ATPase. For example, the SsrA peptide signal functions as a degradation tag for nascent polypeptides.

The SsrA degradation tag is incorporated into the C-terminus of the nascent polypeptide, and it targets the polypeptide for degradation by either ClpXP or ClpAP (Maglica et al. 2008).

After substrate recognition and tethering, proteolytic machines utilize the energy from ATP hydrolysis to unfold their substrate (unfoldase activity) (Maillard et al. 2011). The unfolded substrate is translocated through the passageway of the internal proteolytic chamber of ClpP or HslV (Slack et al. 1995; Effantin et al. 2010b; Rajendar and Lucius 2010; Aubin-Tam et al. 2011). After translocation of substrate, proteolysis occurs at the proteolytic active site, and fragments from degradation diffuse out the proteolytic chamber. The intracellular levels of proteolytic machines increase in response to stress. Proteolytic machines (Hsp104/ClpB) act in concert with Hsp70 to break down protein aggregates (Ben-Zvi and Goloubinoff 2002; Liberek et al. 2008; Haslberger et al. 2010; DiSalvo et al. 2011). Consequently, these proteolytic machines are vital components of the cell's homeostatic mechanism.

**Hsp90 family**

Hsp90 is one of the most abundant proteins in the cytoplasm, where it constitutes about 2% of the total protein in the absence of stress (Li et al. 2011). Stress enhances the expression of Hsp90, and the Hsp90 gene is under the transcriptional control of heat shock factor 1 (HSF1).

The relationship between Hsp90 and HSF1 is peculiar in that HSF1 is sequestered within a complex between Hsp70 and Hsp90. In reaction to stress, HSF1 is released from this complex where it can activate Hsp90 transcription; therefore, Hsp90 can regulate its own transcription (Calderwood et al. 2009).

During environmental stress, Hsp90 can translocate from the cytoplasm to the nucleus. For instance, enhanced green fluorescence protein (EGFP) was fused with Hsp90$\alpha$ (EGFP-Hsp90$\alpha$), and heat stress caused EGFP-Hsp90$\alpha$ to translocate to the nucleus (Langer et al. 2003). In the absence of stress, EGFP-Hsp90$\alpha$ was localized predominantly in the cytoplasm, with no fusion protein detected inside the nucleus. These studies are evidence that Hsp90 is capable of being transported to multiple cellular compartments, where it performs discrete cellular functions. In eukaryotic cells, many genes encode compartment-specific Hsp90 proteins, which are highly conserved across multiple organisms (Chen et al. 2006; Taipale et al. 2010). The Hsp90 family is categorized into five families: Hsp90A-C, mitochondrial TNFR-associated protein (TRAP, Hsp75), and bacterial high temperature protein G (HtpG).

Hsp90A is a ubiquitous family that is present in the cytoplasm. Hsp90B, also known as GRP94 in humans, is localized to the endoplasmic reticulum (ER), where it is involved in ER protein homeostasis. Hsp90C proteins are present in chloroplasts; while TRAP proteins are found in the mitochondria. Expression of TRAP was found to protect cells from apoptosis after oxidative stress (Pridgeon et al. 2007). HtpG is present in bacteria and is not essential under non-stress conditions, in sharp contrast to eukaryotic Hsp90s (Taipale et al. 2010).

Members of the Hsp90 family are diverse in function, but structurally similar. All Hsp90 proteins are dimeric and share homology with the GHKL (DNA gyrase, histidine kinase, and MutL) superfamily of ATPases (Dutta and Inouye 2000). Likewise to GHKL, monomeric Hsp90 is divided into three separate domains: the amino terminal domain, middle domain, and carboxy-terminal domain.

Each domain takes part in the chaperone cycle; which is driven by the capacity to bind and hydrolyze ATP. Binding of ATP causes conformational changes in the amino terminal domain. The amino terminal domain contains two $\alpha$-helices and a loop region that form a lid covering the ATP binding site (Shiau et al. 2006). In the absence of ATP, the lid blocks the active site. A charged linker region, referred to as the SRC loop, connects the amino terminal domain to the middle domain. Hydrophobic residues of the middle domain are involved in Hsp90 client recognition (Shiau et al. 2006). The middle domain is connected to the carboxy terminal domain through a flexible tether. The carboxy terminal domain mediates both dimerization and co-chaperone interactions. The binding of co-chaperones to Hsp90 results in extensive conformational changes that regulate the open and closed states; therefore, affecting client protein binding (Picard 2002; Jascur et al. 2005; Taipale et al. 2010; Karagoz et al. 2011; Li et al. 2011). Many co-chaperones use their tetratricopeptide repeat (TPR) domains to bind Hsp90, a degenerate 34-amino acid consensus sequence (Young et al. 1998). The carboxy terminal domain, of Hsp90, contains five highly conserved residues referred to as the MEEVD motif.

Co-chaperones utilize their TPRs to bind the MEEVD motif of Hsp90. Each Hsp90 dimer contains a single TPR binding site. TPR containing co-chaperones have a fundamental role in coordinating the interaction of Hsp90 with other molecular chaperones, such as Hsp40 and Hsp70.

**Hsp70 family**

Members of the Hsp70 family are highly conserved from bacteria to humans (Craig et al. 1993). For example, *E. coli* DnaK shares about 50% sequence identity with its eukaryotic Hsp70 counterparts (Craig and Lindquist 1988). Even among the eukaryotic Hsp70s, sequence identity is as high as 98%. Hsp70 protein is present in the cytosol, and all major cellular organelles such as the mitochondria (Hsp75, Grp75, mortalin, TRAP-1) (Voos et al. 1999) and the endoplasmic reticulum (Grp78, BiP) (Munro and Pelham 1986). Hsp70 is also found in the chloroplasts of plants (ct-Hsp70) (Marshall et al. 1990). Eukaryotes are capable of producing Hsp70 homologs that are not regulated by environmental stress (Ingolia and Craig 1982). The constitutive form of Hsp70 is referred to as the 70-kDa heat shock cognate protein, Hsc70 or Hsp73. Hsc70 is present in the cytosol where it is involved in protein folding (Kazutoyo and Oike 2010). A role for Hsc70 (Hsp73) is to bind AU-rich elements (AREs) of mRNA to enhance their stability (Zimmer et al. 2001). Hsp70 proteins are responsible for numerous housekeeping functions within the cell.

These functions include: nascent polypeptide folding, protein translocation across membranes, and the assemblage of protein complexes for signal transduction (Ungewickell et al. 1995; D'Silva et al. 2004; Sharma et al. 2011).

Hsp70 acts in conjunction with numerous cofactors to construct an intricate chaperone machine (Bukau and Horwich 1998). In *Saccharomyces cerevisiae* there are several Hsp70 homologs: Ssa1-4, Ssb1-2, Pdr13 (Ssz1), Ksr2, Ssc1, SSq1, and Emc10 (Frydman 2001). The HSPA1-2, HSPA5-9, HSPA12A-B, and HSPA14 homologs exist in *Homo sapiens* (Kampinga and Craig 2010). The *Escherichia coli* homologue of Hsp70 is referred to as DnaK. DnaK acts in concert with two specific cofactors DnaJ/Hsp40 and GrpE; to form a chaperone machine that is capable of repairing proteins exposed to stress (Schroder et al. 1993; Mayer and Bukau 2005).

Hsp70 utilizes the energy of ATP hydrolysis to drive protein folding, unfolding, and translocation. The Hsp70 (Hsc70) protein is assembled from two functional domains. The first is an N-terminal nucleotide binding domain (NBD). The second is a C-terminal substrate binding domain (SBD); which has an $\alpha$ helical lid covering the binding pocket (Zhu et al. 1996; Chou et al. 2003). The opening and closing of the $\alpha$-helical lid is controlled by ATP hydrolysis, within the NBD. The C-terminal domain also contains an important substrate recognition $\beta$-sandwich subdomain. The $\beta$-sandwich recognizes extended regions of hydrophobic residues, commonly exposed on nascent polypeptide chains (Rudiger et al. 1997). Hsp70 in its ATP-bound state has its $\alpha$-helical lid in an open conformation, to facilitate polypeptide binding.

ATP hydrolysis results in α-helical lid closure, over the substrate binding pocket. DnaJ/Hsp40 has also been implicated in the direct binding of substrate and subsequent recruitment of Hsp70. Substrate is dissociated from Hsp70 by the action of NEFs, such as GrpE/Hsp110/Bag. NEFs catalyze the exchange of ADP for ATP, which opens the α-helical lid, and releases substrate.

**Chaperonins**

The chaperonins are large, cylindrical, multisubunit complexes that bind and encapsulate folding proteins. Encapsulation protects the folding protein from nonspecific aggregation, and the energy of ATP hydrolysis is used to drive the folding process. There are two groups of chaperonins (Horwich et al. 2007). Group I chaperonins include the bacterial GroEL, mitochondrial Hsp60, and Rubisco binding protein from the chloroplast (Georgopoulos et al. 1979; Hemmingsen et al. 1988; Cheng et al. 1989). Group II chaperonins include the archaebacterial Thermosome and the eukaryotic chaperonin-containing TCP-1 complex or tailless complex polypeptide-1 TCP-1 ring complex (CCT/TRiC) (Yaffe et al. 1992; Phipps et al. 1993).

Chaperonin family members differ in their structure and function. Stress induces the expression of GroEL, Hsp60, and the thermosome. However, CCT/TRiC is not induced after exposure to stress. GroEL and Hsp60 have 14 identical subunits arranged into two stacked rings of seven subunits each. Each GroEL subunit has an apical, intermediate, and equatorial domain (Braig et al. 1994).

GroEL and Hsp60 function with the cofactors GroES and Hsp10, to form a chaperone machine. GroES is a heptameric ring composed of identical 10 kDa subunits, and it forms a lid on top of the cis GroEL ring (Hunt et al. 1996). As a result, the GroEL cavity is sealed, and the folding substrate is enclosed inside of an “Anfinsen cage” (Saibil et al. 1993; Ellis 1994). The Thermosome and CCT/TRiC do not utilized an external lid structure to encapsulate their bound substrate; instead they utilize integrated protrusions (Klumpp et al. 1997; Ditzel et al. 1998; Pappenberger et al. 2002). The protrusion structures emerge from their apical domains. The extensively studied GroEL/GroES chaperone machine has significantly expanded our understanding of the action of chaperonins. There are at least 250 known GroEL/GroES substrates. In the presence of ATP, GroES binds to the cis ring of GroEL, which encapsulates the polypeptide substrate. Conformational changes cause the inner chamber walls to become hydrophilic and negatively charged. The change in chamber environment causes the folding substrate to bury its hydrophobic surface, while exposing its hydrophilic surface (Xu et al. 1997). ATP hydrolysis occurs within the GroES bound cis ring. Subsequently, ATP binds to the trans ring, of GroEL, which releases GroES and substrate. Both the released GroES and substrate are also capable of binding to the trans ring again, which initiates subsequent rounds of substrate folding. Therefore, the cis and trans rings of GroEL take turns nucleating a new folding active complex (Rye et al. 1999).

## Small heat shock proteins (sHsps)

### Distribution of sHsps among prokaryotes and eukaryotes

Among the molecular chaperones, small heat shock proteins (sHsps) are present in bacteria, archaea, and eukaryotes (de Jong et al. 1993; Parsell and Lindquist 1993; de Jong et al. 1998; Franck et al. 2004). It is interesting to note, that not all organisms contain sHsps. For example, *Mycoplasma genitalium* lacks the genes coding for sHsps (Fraser et al. 1995). The absence of sHsp genes is a common attribute of organisms with small genomes, ranging from 0.58 to 2.27 Mb (Narberhaus 2002). More significant than genome size is the temperature and environment, in which the organism lives. The genomes of *Rickettsia* and *Chlamydia* encode a single sHsp gene. These organisms are parasites, and they are dependent upon a mutual relationship with insect, human, and animal hosts (Andersson et al. 1998; Read et al. 2000; Shigenobu et al. 2000). Most bacteria and archaea have genomes that encode a small number of sHsps. For instance, *Methanococcus jannaschii*, *Thermotoga maritima*, and *Synechococcus vulcanus* each contain a single sHsp gene (Bult et al. 1996; Roy and Nakamota 1998; Nelson et al. 1999).

Subsequent evolution to eukaryotes with multiple copies of sHsps genes allows for greater adaption to a variety of stressful stimuli. In particular, plants are exposed to a variety of abiotic stresses such as drought, salinity, and heat. Thus there are six families of plant sHsps. Families I, II, and III are cytosolic.

Families IV, V, and VI are localized to the chloroplast, mitochondria, and endoplasmic reticulum, respectively. Plant sHsps are unique, because they have both cytosolic and organellar isoforms. This is a sharp contrast to other eukaryotes which have primarily cytosolic isoforms. Therefore, diversification of sHsps in plants is an indicator that reflects adaption to stresses unique to plants (Waters 1995). Having abundant small heat shock proteins is not just limited to plants. For example, *Caenorhabditis elegans* has eighteen sHsp genes (Aevermann and Waters 2008). The zebrafish *Danio rerio* has thirteen sHsps, *Drosophila melanogaster* has seven, and *Homosapiens* have ten sHsps, HSPB1-10 (Kappe et al. 2003; Taylor and Benjamin 2005; Elicker and Hutson 2007; Frydenberg et al. 2010). Multiple stress genes permit an increasingly adaptable response to changing environmental conditions.

**Sequence diversity in small heat shock proteins**

Among the molecular chaperones, small heat shock proteins (sHsps) are the most evolutionarily divergent. Most sHsps are characterized by a conserved sequence of ~90 residues referred to as the $\alpha$-crystallin domain (Caspers et al. 1995). The N-terminal domain and C-terminal extension flanking the $\alpha$-crystallin domain are more divergent in sequence (Fig. 2). The C-terminal extensions of sHsps vary in length, but they all share the conserved I-X-I/V sequence (de Jong et al. 1998). This flexible extension is involved in both oligomer stability and solubility (Smulders et al. 1996; Kim et al. 1998; van Montfort et al. 2001).

The N-terminal domains of sHsps are the least conserved except for short hydrophobic sequences SRLFDQFF and F/WDPF both rich in phenylalanines (Crabbe and Goode 1994; Ehrnsperger et al. 1997a; Pasta et al. 2003). Small heat shock proteins, lacking the flanking N-terminal domain or C-terminal extension, have a tendency to form monomeric, dimeric, and tetrameric structures (Merck et al. 1992; Leroux et al. 1997; Kokke et al. 1998; van de Klundert et al. 1998; Lambert et al. 1999; Bova et al. 2000; Feil et al. 2001; Koteiche and Mchaourab 2002; Theriault et al. 2004). However, N-terminal domain deletion in Hsp16.5 does not produce a change in oligomer size or symmetry (Koteiche and Mchaourab 2002; Shi et al. 2006).


{----------N-TERMINAL REGION----------
Hsp16.9 1 MSIV.....RR.....TNVFDPFADLWADPFDTFRSIVPAISGGGS....
Hsp18.1 1 MSLIPSFFSGRR.....SNVFDPFSLDVWDPLKDFPFSNSSPSASFPR...
Hsp25 1 MTERRVPFSLLRSPSWEPFRDWYPAHSRLFDQAFGVPRLPDEWSQWFSAAGWPGYVRPLP
Hsp27 1 MTERRVPFSLLRGPSWDPFRDWYP.HSRLFDQAFGLPRLPEEWSQWLGGSSWPGYVRPLP
alphaA 1 MDIAIHHPWIRRP.FFPF..HSP..SRLFDQFFGEHLLESDLFP.TSTSLSPFYLR...
alphaB 1 MDVTIQHPWFKRT.LGPF..Y.P..SRLFDQFFGEGLFEYDLLPFLSSTISPYYR....
HSP16.3 1 MATTLPVQRHP.....RSLFPEFS.ELFAAFPSFAGLRPTFDTRLMR...
Hsp26 1 MSFNSPFFDFFDN....INNEVDAFNRLLGEGGLRGYAPRRQLANTPAKDSTGKEVARP
Hsp16.5 1 MFGRDPFDSLFER.....MFKEFFATPMTGTTMIQSSTGIQISGK.....
----------N-TERMINAL REGION----------}α-crystallin domain
Hsp16.9 37 .....ETAAFANARMDWKETPEAHVFKADLPGVKK
Hsp18.1 44 .....ENPAFVSTRVDWKETPEAHVFKADLPGLKK
Hsp25 61 AATAEGPAAV.....TLAAPAFSRALNRQLSSGVSEIRQTADRWRVSLDVNHFAP
Hsp27 60 PAAIESPA.....VAAPAYSRALSRQLSSGVSEIRHTADRWRVSLDVNHFAP
alphaA 51 .....PPSFLRAPS.WFDTGLSEMRLEKDRFSVNLDVKHFSP
alphaB 50 .....QSLFRT...VLDSGISEVRSDRDKFVIFLDVKHFSP
Hsp16.3 42 .....LEDEMKEGRYEVRAELPGVDP
Hsp26 56 NNYAGALYDPRDETLDDWFDNDLSLFPSGFGFPRSVAVPVDILDHDNNYELKVVVPGVKS
Hsp16.5 41 .....GFMPISIIEGDQHIKVIAWLPGVNK
----------α-crystallin domain----------
Hsp16.9 67 E.EVKVEVEDGN.VLVVSGER.TKEKEDKNDKWHRVERSSGKFVRRFRLL..EDAKVEEV
Hsp18.1 74 E.EVKVEVEDDR.VLQISGER.SVEKEDKNDEWHRVERSSGKFLRRFRLP..ENAKMDKV
Hsp25 111 E.ELTVKTKEG..VVEITG.....KHEERQDEHGYISR...CFTRKYTLP..PGVDPTLV
Hsp27 107 D.ELTVKTKDG..VVEITG.....KHEERQDEHGYISR...CFTRKYTLP..PGVDPTQV
alphaA 87 E.ELKVKVLGD..VIEVHG.....KHEERQDEHGFISR...EFHRKYRIP..ADVDPLTI
alphaB 83 E.DLTVKVQDD..FVEIHG.....KHNERQDDHGYISR...EFHRRYRLP..SNVDQSAL
Hsp16.3 63 DKDVDIMVRDG..QLTIKA.....ERTEQKDFDGRSEFAYGSFVRTVSLP..VGADEDDI
Hsp26 116 KKDIDIEYHQNKNQILVSGEIPSTLNEESKDKVKVKESSSGKFKRVITLPDYPGVDADNI
Hsp16.5 66 E.DIILNAVGD..TLEIRAKRSPLMITESERIIYSEIPEEEEIYRTIKLP..ATVKEENA
----------{C-TERMINAL EXTENSION----------}
Hsp16.9 122 KAGLEN.GVLTVTVPKAE...VKKPEVKAIQISG
Hsp18.1 129 KASMEN.GVLTVTVPKEE...IKKAEVKSIEISG
Hsp25 158 SSSLSPEGTLTVEAPLPK..AVTQSAEITIPVTFEARAQIGGPEAGKSEQSGAK
Hsp27 154 SSSLSPEGTLTVEAPMPK..LATQSNEITIPVTFESRAQLGGPEAAKSDETAAK
alphaA 134 TSSLSSDGVLTVNGPRKQ....VSGPERTIPITREEKPAV..TAAPKK
alphaB 130 SCSLSADGMLTFCGPKIQTGLDATHAERAIPVSREEKP....TSAPSS
Hsp16.3 114 KATYDK.GILTVSVAVSE....GKPTEKHIQIRSTN
Hsp26 176 KADYAN.GVLTLTVPKLKPQKDGKNHVKKIEVSSQESWGN
Hsp16.5 121 SAKFEN.GVLSVILPKAE.....SSIKKGINIE

**Fig. 2. Amino acid sequence alignment for representative bacterial, archeal, plant, and human sHsps.** The following sHsps were aligned: Hsp16.9 (wheat), Hsp18.1 (pea), Hsp25 (mouse), Hsp27 (human), alphaA (human αA-crystallin), alphaB (human αB-crystallin), Hsp16.3 (*Mycobacterium tuberculosis*), Hsp26 (yeast), and Hsp16.5 (*Methanococcus jannaschii*). Gray shaded regions represent conserved residues. The sequence alignment was generated with CLUSTAL W in the biology workbench program package. (Thompson et al. 1994; Subramaniam 1998)

**Structure of small heat shock proteins**

Since the α-crystallin domain is highly conserved, the variable N- and C-terminal sequences contribute to the structural diversity observed among sHsps (Merck et al. 1993; Berengian et al. 1999; Bova et al. 2000; van Montfort et al. 2001; Stromer et al. 2004; Mchaourab et al. 2009). sHsps assemble into large flexible oligomers of 4 to 40 subunits that vary in size from 200 to 800 kDa (de Jong et al. 1998; Arrigo and Muller 2002). Oligomeric assemblies vary substantially from the symmetric and monodisperse to the polydisperse oligomers which are capable of rapid subunit exchange (Haley et al. 1998; Kim et al. 1998; Bova et al. 2000). The dynamic nature of eukaryotic sHsp oligomers hinder their high resolution structural analysis; nevertheless, eight crystal structures have been determined for *Methanococcus jannaschii* Hsp16.5, *Triticum aestivum* Hsp16.9, *Taenia saginata* Tsp36, *Xanthomonas* XaHspA, N-terminal truncated mammalian Hsp20, Hsp27, αA-crystallin, and αB-crystallin (Kim et al. 1998; van Montfort et al. 2001; Stamler et al. 2005; Bagneris et al. 2009; Laganowsky et al. 2010; Baranova et al. 2011; Hilario et al. 2011). All of these structures show the α-crystallin domain dimer as the basic building block of the sHsp oligomer.

The α-crystallin domain monomer consists of seven β-strands arranged into two antiparallel sheets. In Hsp16.5 and Hsp16.9, two monomers assemble into a dimer by way of an extended loop and the exchange of a $\beta_6$ strand from a neighboring monomer (Kim et al. 1998; van Montfort et al. 2001). However, in mammalian sHsps, sequence divergence results in deletion of a beta strand involved in assembling the dimeric interface (Mchaourab et al. 1997a; Berengian et al. 1999). As a result, the dimerization interface is altered, which produces different oligomer symmetry for mammalian sHsps. Additionally, the mammalian sHsps Hsp27 and Hsp20 have a dimer interface that is generated by the symmetric pairing of two β7 strands (Baranova et al. 2011). Consequently, the β-sheet is extended on one face of the α-crystallin domain. The variability of this extended interface contributes to the polydispersity of sHsps (Mchaourab et al. 1997a; Berengian et al. 1999; Koteiche and Mchaourab 1999; Feil et al. 2001; Jehle et al. 2009).

Furthermore, packing of the α-crystallin domain dimers contribute to the structural diversity observed in sHsp oligomeric assemblies. The structure of the α-crystallin domain has hydrophobic grooves located along each edge. Multiple inter- and intra-molecular interactions occur between the hydrophobic α-crystallin domain edges and the N- and C-terminal extensions producing higher order oligomeric structures (Kim et al. 1998; van Montfort et al. 2001; Jehle et al. 2009; Chen et al. 2010).

For instance, Hsp16.5 assembles into a spherical oligomer comprised of 24 subunits, while Hsp16.9 is dodecamer of two stacked hexameric disks. The orientation of the Hsp16.9 C-terminal extension relative to the α-crystallin domain enables two different dimer packing arrangements; even though, the Hsp16.9 and Hsp16.5 α-crystallin domain folds are similar (van Montfort et al. 2001). The capacity to form higher order oligomers is further enhanced by patching hydrophobic grooves on the N-terminal edge of the α-crystallin domain (van Montfort et al. 2001). Also in the Hsp16.9 monomer, the N-terminal domains interact by forming loosely packed helical knots, which function to stabilize the dodecamer (van Montfort et al. 2001).

**Determinants of sHsp oligomer polydispersity**

As demonstrated by CryoEM, the α-crystallins and Hsp27 display particles with different sizes and symmetries (Haley et al. 2000). The fold of the α-crystallin domain is conserved in sHsps, but the variable N-terminal domain has evolved to control subunit packing and oligomer dynamics (Mchaourab et al. 2009). Mammalian sHsps, such as α-crystallin and Hsp27, readily exchange subunits between oligomers (Bova et al. 2000). The subunit exchange mechanism involves equilibrium dissociation and reassociation of small multimers. For example, N-terminal domain deletion in αA-crystallin and Hsp27 results in oligomer dissociation to dimers and tetramers that are incapable of further subunit exchange. These studies support a role for the N-terminal sequence elements in mammalian sHsp oligomerization and dynamics.

Moreover, N-terminal domain phosphorylation induces changes in oligomer size. For example, the N-terminal residues S15, S78, and S82 of Hsp27 and S19, S45, and S59 of αB-crystallin are phosphorylation sites for stress related MAPKAP kinases 2/3 (Stokoe et al. 1992; Clifton et al. 1996; Arrigo et al. 2007). Stress-induced phosphorylation of Hsp27 causes its oligomer to dissociate into dimers, but it is worth noting that dissociation to tetramers has also been reported in the literature (Rogalla et al. 1999). Unlike Hsp27, αB-crystallin does not dissociate into discrete dimeric or tetrameric species, but dissociation results in a continuum of small sized multimers (Ito et al. 2001). In contrast, plant sHsps are not phosphorylated in response to stress and no phosphorylation induced size changes are observed (Suzuki et al. 1998). In short, these results clearly show that N-terminal residues play an important role in sHsp oligomer plasticity.

Case in point, acidic residues such as $Glu^{41}$ which is highly conserved in Hsp27 and αB-crystallin modulate oligomer plasticity. In the E41C mutant of Hsp27, the large undissociated oligomer is stabilized on both wild-type and phosphorylation mimic (S15D, S78D, S82D) backgrounds (Shashidharamurthy et al. 2005). The effect of the E41C mutant in the phosphorylation mimic (S15D, S78D, S82D), where normally serine to aspartate substitutions enhance dissociation of Hsp27 is particularly intriguing. An N-terminal sequence alignment was performed in order to identify additional N-terminal residues associated with the dynamic behavior of the Hsp27 and α-crystallin oligomers.

The sequence alignment, of Hsp27 and lens αA- and αB-crystallin, revealed a unique peptide insertion (residues 58 to 70), referred to as the P1 peptide (Fig. 1) (Shashidharamurthy et al. 2005). The P1 peptide is composed of numerous redundant alanine and proline residues. Since the P1 peptide is unique to Hsp27, this sequence insertion was postulated to participate in oligomer dynamics. Similar to the E41C mutant, P1 peptide deletion, in both wild-type and phosphorylation mimic backgrounds, stabilizes the large undissociated oligomer. An N-terminal domain sequence insertion was also identified in *Saccharomyces cerevisiae* Hsp26. The N-terminal domain of Hsp26 was subdivided into two domains, the N-terminal domain (NTD) and middle domain (MD) (Haslbeck et al. 2004b; White et al. 2006). The MD of Hsp26 is comprised of a short glycine-rich sequence (residues 25 to 31). Deletion mutants cause the Hsp26 oligomer to dissociate into dimers. These results indicate that unique N-terminal sequence insertions (MD of Hsp26 & P1 peptide of Hsp27) are important for oligomer plasticity of both Hsp26 and Hsp27.


**Figure 3. An N-terminal sequence alignment for human αB-crystallin (hαB), αA-crystallin (hαA) and Hsp27.** The unique P1 peptide insertion of Hsp27 is highlighted in red. Gray shaded regions represent conserved residues. The sequence alignment was generated with CLUSTAL W in the biology workbench program package. (Thompson et al. 1994; Subramaniam 1998)

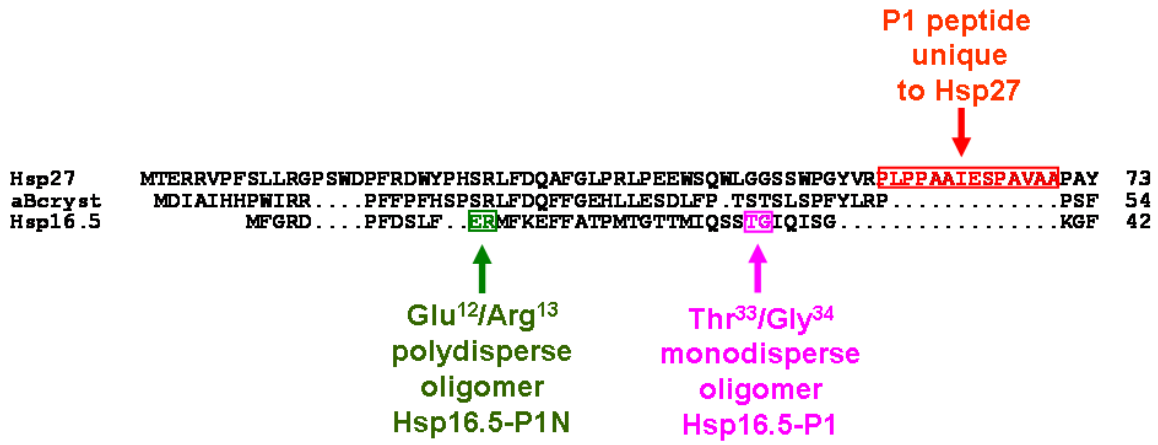


**Figure 4. The insertion of the P1 peptide from Hsp27 into the N-terminal domain of Hsp16.5.** An N-terminal sequence alignment for human Hsp27, αB-crystallin (aBcryst), and *Methanococcus jannaschii* Hsp16.5. The P1 peptide sequence insertion of Hsp27 is highlighted in red. The position of P1 to create Hsp16.5-P1N is highlighted in green and Hsp16.5-P1 in magenta. The sequence alignment was generated with CLUSTAL W in the biology workbench program package. (Thompson et al. 1994; Subramaniam 1998)

To further examine the role of the P1 peptide in oligomer plasticity, this sequence element was transposed into the rigid and monodisperse *Methanococcus jannaschii* Hsp16.5 (Shi et al. 2006). The P1 peptide was inserted at two positions within the N-terminal domain of Hsp16.5 (Fig. 2). The first insertion occurred between residues $Glu^{12}$ and $Arg^{13}$. As a result, the size of the oligomer increased from 410 to 650 kDa along with a concomitant increase in polydispersity. This polydisperse oligomer is referred to as Hsp16.5-P1N. The next position of P1 peptide insertion was between residues $Thr^{33}$ and $Gly^{34}$, which is located at the junction between the N-terminal and α-crystallin domains. A monodisperse oligomer was formed which was double the mass (~850 kDa) of wild-type Hsp16.5.

This monodisperse oligomer is referred to as Hsp16.5-P1. The Hsp16.5-P1 oligomer had 48 subunits, twice the number of subunits in wild-type Hsp16.5 (24 subunits). Site-directed spin labeling EPR and CryoEM show the two subunits in the dimeric building block are not equivalent (Shi et al. 2006; Mchaourab et al. 2009). Also, the position of the C-terminal extension changed creating new 4-fold openings. These new openings are not observed in wild-type Hsp16.5. The novelty of this experiment lies in the ability to transform a rigid monodisperse oligomer (wild-type Hsp16.5) to a polydisperse and dynamic species (Hsp16.5-P1N), by changing the N-terminal domain of Hsp16.5. As a result, the contact point between the C-terminal extension and the dimer interface changes, increasing oligomer plasticity. This speaks to biological relevance, because the mammalian sHsps Hsp27 and αA- and αB–crystallin are dynamic and polydisperse oligomers. This is in sharp contrast to the symmetric and monodisperse archael assembly. The N-terminal domains of mammalian sHsps have undergone extensive sequence divergence; while preserving the fold of the α-crystallin domain. This implies that the N-terminal domain has evolved to control the packing symmetry of subunits in order to create versatile oligomeric assemblies. Relative to wild-type, Hsp16.5-P1N and Hsp16.5-P1 have greater affinity for destabilized substrate (Shi et al. 2006). These results are evidence that oligomeric structure is related to chaperone activity.

**The mechanism of substrate recognition and binding in sHsps**

All molecular chaperones bind substrate proteins in their non-native state; however, individual families of molecular chaperones differ in their mechanism of substrate recognition and binding (Mchaourab et al. 2009). sHsps can bind substrate proteins, in their non-native state, without the input of ATP. The capacity for binding is one substrate protein per sHsp subunit of equal molecular mass (Horwitz 1992; Mchaourab et al. 2009). Small heat shock proteins form complexes with their substrate (Horwitz 1992; Ehrnsperger et al. 1997b; Lee et al. 1997). The release and refolding of substrate, from the complex, is the responsibility of Hsp70 (Lee and Vierling 2000). Therefore, the role sHsps, in the molecular chaperone network, is to create a reservoir of refoldable substrate (Arrigo and Muller 2002).

In order to understand the mechanism of sHsp chaperone function, the amount of light scattering that is produced by aggregating substrate proteins is measured after thermal or chemical denaturation (Horwitz 1992; Jakob et al. 1993; Lee et al. 1997; Pivovarova et al. 2005). Of primary importance is that model substrate proteins are exposed to conditions that promote unfolding, aggregation, and precipitation. The efficiency of sHsp chaperone activity is a function of the reduction in substrate light scattering in the presence of sHsp. These chaperone assays are often performed under nonequilibrium conditions (Sathish et al. 2003; Shashidharamurthy et al. 2005; Mchaourab et al. 2009).

The use of light scattering as the observable is a reflection of the kinetic partitioning of aggregated substrate and substrate bound to the sHsp (Mchaourab et al. 2009). Adequate determination of binding or structural parameters is hindered, because these assays are performed under strongly denaturing conditions. As a result, denaturing conditions promote the existence of heterogeneous ensembles of bound substrates that differ in conformation. Another complicating factor is that the chances of strongly denaturing conditions affecting the structural and functional integrity of the sHsps themselves are increased. Mutations in substrate proteins can shift the folding equilibrium toward non-native states. Many of these non-native states are structurally similar to the native state but differ in $\triangle G_{unf}$ (Mchaourab et al. 2002; Sathish et al. 2003). Therefore, under conditions that favor the native state, it is more physiologically relevant to have assays that detect excursions toward these non-native states (Mchaourab et al. 2009). Often these non-native states precede the nucleation of aggregation (Mchaourab et al. 2002). Based upon this reasoning, sHsp binding is induced by gradually reducing the equilibrium folding constant of the substrate until a sHsp/substrate complex is formed (Mchaourab et al. 2002).

With this in mind, a chaperone assay was developed, which utilized site-directed mutagenesis to produce incremental changes in protein stability of the model substrate T4 lysozyme (T4L). In this chaperone assay, a library of destabilized T4L mutants was constructed that differ in their $\triangle G_{unf}$ by 1 kcal/mol.

For instance, D70N has a free energy of unfolding of 5.1 kcal/mol, L99A has its free energy of unfolding at 6.4 kcal/mol, while L99A/A130S has its free energy at 7.7 kcal/mol. Each of these destabilized T4L mutants was structurally similar to wild-type T4L (Mchaourab et al. 2002). Within each mutant, a cysteine residue was introduced at a non-destabilizing solvent-exposed surface site. This site is for the attachment of a spin or fluorescence label, which is able to detect the sHsp/substrate complex. For example, the complex between αA-crystallin and spin labeled T4L was detected by analyzing changes in electron paramagnetic resonance (EPR) lineshape (Mchaourab et al. 2002). αA-crystallin binds more extensively to the destabilized T4L mutants. The αA-crystallin/T4L complex is formed when the free energy of binding to αA-crystallin is similar to the free energy associated with the transition from excited to native state.

Two distinct modes of binding were detected, and each mode was associated with the recognition of a different conformational state of T4L by αA-crystallin. The highly destabilized T4L mutants activate a low-affinity sHsp binding mode, in which each sHsp subunit binds a monomer of T4L (Mchaourab et al. 2009). The high affinity sHsp mode is characterized by four sHsps subunits binding a monomer of T4L (Mchaourab et al. 2009). Spin-labeled T4L mutants within the α-crystallin complex display increased inter-residue distances across the T4L active site interface (Claxton et al. 2008). The increase in the $i$, $i$ + 4 helical distances implies significant unfolding in α-crystallin bound T4L.

Two mode binding to destabilized T4L mutants was also observed with αB-crystallin, Hsp27, and Hsp16.5 (Koteiche and Mchaourab 2003; Sathish et al. 2003; Shashidharamurthy et al. 2005). Models for sHsp chaperone activity show that recognition and binding of substrate, in its non-native state, involves changes in the oligomeric state of sHsp. A coupled thermodynamic equilibrium describes the sHsp chaperone activity (Shashidharamurthy et al. 2005; Koteiche and Mchaourab 2006; Mchaourab et al. 2009). The minimalist model includes the substrate folding equilibrium (I) , sHsp oligomeric equilibrium (II), and the equilibrium binding between sHsp and substrate non-native states (III).

$$N \rightleftharpoons I_1 \rightleftharpoons \ldots \rightleftharpoons I_i \rightleftharpoons U \qquad \text{(I)}$$

$$\text{sHsp} \rightleftharpoons (\text{sHsp})_{\text{activated}} \qquad \text{(II)}$$

$$(\text{sHsp})_{\text{activated}} + \begin{pmatrix} I_1 \\ U \end{pmatrix} \rightleftharpoons \begin{pmatrix} C_1 \\ C_u \end{pmatrix} \qquad \text{(III)}$$

Equation (I) describes substrate in its native (N), partially unfolded intermediate ($I_1 \ldots I_i$), and fully unfolded states (U). Equation (II) describes the transition of the sHsp to its activated high affinity binding state. In the case of Hsp27, the activated state is the dimer. Both equations (I) and (II) are coupled to yield equation (III). Equation (III) describes the binding of the activated state of the sHsp to partially (I) or globally unfolded (U) states of the substrate. With age, mutations occur in the substrate, which shifts the equilibrium of equation (I) toward non-native states. There is an energetic preference of the substrate, in its non-native state, to bind with sHsps as oppose to folding to the native state N.

The equilibrium of equation (II) is shifted toward the activated state of the sHsp increasing its affinity for binding to substrate. Equation (II) represents dissociation of the sHsp (Hsp27) from a large oligomer to the dimer or expansion of the sHsp oligomer (Hsp16.5-P1). As a result, a sHsp/substrate complex is formed. Substrate binding sites have been reported in the N-terminal and $\alpha$-crystallin domains (Sharma et al. 1997; Stromer et al. 2004; Fu and Chang 2006; Ghosh et al. 2006; Shi et al. 2006; Jaya et al. 2009b). To access N-terminal substrate binding sites, structural rearrangements must take place within the sHsp oligomer. Substrate is capable of accessing binding sites by way of two possible mechanisms, static and dynamic (Mchaourab et al. 2009). In the static mechanism, as observed in the engineered variant Hsp16.5-P1, expansion occurs in the oligomeric assembly. Consequently, large openings appear in the outer shell of the oligomer, which facilitates substrate access to N-terminal binding sites (Shi et al. 2006). This transition to the activated high affinity state is accompanied by an increase in the apparent affinity for destabilized substrate as compared to wild-type Hsp16.5. Alternatively some sHsps, such as Hsp27, utilize a dynamic mechanism; in which signals from stress pathways result in equilibrium dissociation of its oligomer. The transition to the stress activated high affinity state results in increased apparent affinity for substrate (Shashidharamurthy et al. 2005). These mechanisms imply that sHsp oligomer is structurally flexible, serving as a switch activated by stress.

**The role of sHsps in disease**

Regulation of sHsp structural dynamics and substrate binding affinity is of critical importance in response to stress and aging. If this regulation is inhibited, marginally stable proteins can aggregate. In this event, the molecular chaperone and degradation machinery is overwhelmed, leading to disease state (Gidalevitz et al. 2006a). However, mutation of sHsps can cause a prolonged high affinity state which promotes equilibrium substrate unfolding. For instance, the hereditary cataract αA-crystallin R49C and R116C mutants have been reported to shift the T4L folding equilibrium in favor of non-native T4L intermediates (Koteiche and Mchaourab 2006). These gain of function type mutations, in sHsps, are associated with cataract, cardiaomyopathies, desmin-related myopathies, and Charcot-Marie-Tooth disease (Vicart et al. 1998; Evgrafov et al. 2004; Arrigo et al. 2007; Xi et al. 2008). Research in sHsps was stimulated by their role in the development of misfolding disorders such as Parkinson's, Alzheimer's, and Huntington's diseases (Sherman and Goldberg 2001; Wyttenbach et al. 2002; Muchowski and Wacker 2005). Since sHsps play a role in neurodegenerative disease, myopathies, cataracts, and cancer, extensive research has been aimed at therapeutic strategies for modulating sHsp expression and activation (Arrigo et al. 2007).

## Research Overview

Mammalian sHsps, such as Hsp27, form polydisperse and dynamic oligomers that readily undergo equilibrium subunit exchange (Bova et al. 2000). Hsp27 is unique in its ability to dissociate from an ensemble of oligomers to a dimer (Lambert et al. 1999; Theriault et al. 2004; Mchaourab et al. 2009). The dissociation of the Hsp27 oligomer is mediated by perturbation of relatively weak subunit contacts. N-terminal truncation studies in Hsp27 implicate the N-terminal domain in the global assembly of the oligomer from smaller multimeric units (Berengian et al. 1999; Bova et al. 2000). Phosphorylation of N-terminal $Ser^{15}$, $Ser^{78}$, $Ser^{82}$ destabilzes the Hsp27 oligomer, because the N-terminal domain is presumed to be located within the solvent shielded core of the Hsp27 oligomer. Therefore, in a low dielectric environment unpaired charges likely result in Hsp27 oligomer dissociation. The change in Hsp27 oligomeric state is important for substrate recognition and binding (chaperone activity) (Shashidharamurthy et al. 2005). The purpose is to transition the Hsp27 oligomer to a binding competent state (dimer); consequently, a change occurs in the accessibilty to N-terminal substrate binding sites. Studies from our laboratory utilized T4 Lysozyme (T4L) as a model substrate (Mchaourab et al. 2002; Sathish et al. 2003; Shashidharamurthy et al. 2005; Koteiche and Mchaourab 2006). These studies revealed that dissociation of the Hsp27 oligomer into dimers is accompanied by an increase in affinity for substrate (Shashidharamurthy et al. 2005).

Little is known about the structural changes and sequence determinants, in the N-terminal domain, that induce oligomer dissociation and underlie the increased affinity of Hsp27 dimers for substrate. In this dissertation work, N-terminal residues were mutated to cysteines and subsequently spin labeled with methanethiosulfonate (MTSSL) and 3-(2-Iodoacetamide)-proxyl (IAP). Electron paramagnetic resonance (EPR) studies determine the structure and environment of the N-terminal domain after dissociation from the large oligomers to the binding competent dimer. Cysteine mutagenesis identified residues that modulate the equilibrium dissociation of Hsp27. Motionally restricted EPR spectra were observed for N-terminal sites in the ensemble of large oligomers (Hsp27-WT). This EPR lineshape is consistent with a buried location, which is involved in extensive subunit contacts. EPR lineshapes, for the corresponding N-terminal residues in the dimer (Hsp27-D3), are less motionally restricted. The EPR data indicates that large segments of the N-terminal domain loose steric restriction, after oligomer dissociation to the dimer. Solvent accessibility, to nickel (II) ethylenediaminediacetate NiEDDA, was utilized to determine the environment of the N-terminal domain in the context of the large oligomers (Hsp27-WT) and after dissociation to the dimer (Hsp27-D3). NiEDDA is soluble in the aqueous phase and excluded from the sterically packed oligomer core of proteins (Altenbach et al. 2005). NiEDDA accessibility is significantly attenuated in Hsp27-WT, due to the buried location of the N-terminal domain. In contrast, a dramatic increase in NiEDDA accessibility was observed for Hsp27-D3.

The accessibility data shows that after dissociation the N-terminal domain transitions from its solvent shielded environment to a more exposed environment. Binding of the model substrate T4L causes Hsp27 dimers to reassemble into large oligomers; as a result, the N-terminal domain becomes sequestered within the Hsp27/T4L complex.

Mutagenic analysis revealed aspartate, glutamate, arginine, proline, glycine, and tryptophan residues that are capable of influencing the Hsp27 dissociation equilibrium. These residues may be involved in interactions that produce structural elements important for the stabilization of the large oligomer. The dissertation results define the structural role of the N-terminal domain in Hsp27 oligomer dynamics and chaperone activity.

# CHAPTER II

# ELECTRON PARAMAGNETIC RESONANCE SPECTROSCOPY (EPR)

## Theory of EPR

### Electron Spin State in a Magnetic Field

In an external magnetic field $H_o$, the electron has both a spin angular momentum S and a magnetic moment $\mu$. The vectors describing $\mu$ and S are related by the following equation:

$$\mu = -\gamma S \tag{1}$$

where $\gamma$ is the gyromagnetic ratio, an intrinsic property that determines the resonant frequency of the electron in $H_o$. The electron will precess about $H_o$ due to the torque generated by the interaction of $\mu$ with the magnetic field. $H_o$ is in the z-direction, and the components for the magnetic moment vectors are given by the following equations:

$$\frac{d\mu_x}{dt} = -\gamma H_o \mu_y \tag{2}$$

$$\frac{d\mu_y}{dt} = \gamma H_o \mu_x \tag{3}$$

$$\frac{d\mu_z}{dt} = 0 \tag{4}$$

According to the Larmor theorem, the angular frequency for precession of an electron about $H_o$ is represented by the equation:

$$\omega_o = \gamma H_o \tag{5}$$

$\omega_o$ is the characteristic Larmor frequency (Larmor 1900). If $\omega_o$ is substituted into equations 2, 3, and 4 then each equation is rewritten as,

$$\mu_x = \cos \omega_o t \tag{6}$$

$$\mu_y = \sin \omega_o t \tag{7}$$

$$\mu_z = \text{constant} \tag{8}$$

These equations state that a precessing magnetic moment in the z-directions has an angular momentum that is constant, but the x- and y- components of the angular momentum can not be precisely defined. Therefore, the x- and y-components will vary sinusoidally (Atherton 1973). By virtue of the fact that an electron has a primary spin quantum number of S = $\frac{1}{2}$ and two secondary spin quantum numbers $m_s = \pm \frac{1}{2}$, the magnetic moment will have two allowed orientations, each with a different energy (Fig. 1). Each orientation corresponds to the two spin states of an electron $\alpha$ ($E_\alpha = + \frac{1}{2} g_e \beta_e H_o$) and $\beta$ ($E_\beta = - \frac{1}{2} g_e \beta_e H_o$). The energy difference between $\alpha$ and $\beta$ is given by

$$\Delta E = h\upsilon = g_e \beta_e H_o \tag{9}$$

where h is the Planck's constant ($6.62607 \times 10^{-34}$ J • S), $\upsilon$ is the frequency of electromagnetic radiation applied perpendicular to the external magnetic field

($H_o$), $g_e$ is the Lande electron g-factor for an unbound electron which is 2.0023, and $\beta_e$ is the Bohr magneton with a value of 0.92 x $10^{-23}$ J/T.

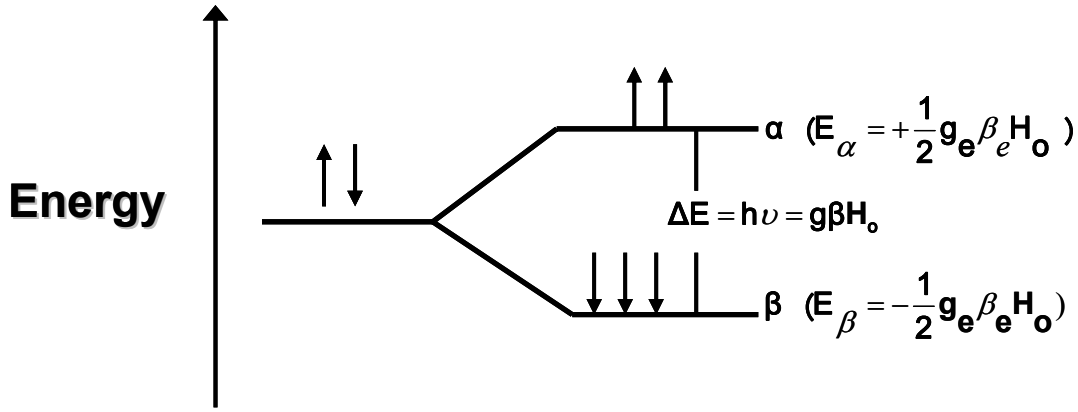


**Figure 5. An energy level diagram for an electron in an external magnetic field.** Electromagnetic radiation with energy proportional to △E induces transitions between the two energy states α and β.

Transitions between α and β are induced by electromagnetic radiation with the appropriate amount of energy that is proportional to the energy difference between the two spin states (△E = $g_e\beta_e H_o$). The measurement of this energy difference is the basis of the EPR experiment.

In a typical EPR experiment, an electron is precessing about $H_o$, and a second magnetic field $H_1$ is added to the system. $H_1$ is much weaker than $H_o$, and $H_1$ is rotating with an angular momentum ω in the xy-plane. $\omega_o$ is the frequency of electromagnetic radiation with an energy that corresponds to the energy difference between spin states α and β of an electron in a magnetic field. When ω is equal to $\omega_o$, then μ and $H_1$ will both be in phase.

As a result, the electron will be influenced by $H_1$ causing the downward movement of $\mu$. The projection of $\mu$ has changed from the +z direction to the –z direction, of $H_o$, by spiraling downwards through the xy-plane. Once the maximum value of -z is obtained the magnetic moment will spiral up towards the +z direction, of $H_o$. The magnetic moment of the electron will alternate between the +z and –z direction as long as $H_1$ is present (Atherton, 1973). During a transition between $\alpha$ and $\beta$, the electron is absorbing energy from $H_1$, and $\mu$ of the electron reorients itself in the magnetic field. This phenomenon is called the resonance condition in which energy is continually exchanged between the two spin states $\alpha$ and $\beta$ of the electron. The spin state with the lowest energy, $\beta$ corresponds to the magnetic moment which is parallel to the magnetic field. The energy difference between the electron spin states is in correspondence with magnetic fields in the microwave region. The most commonly utilized frequency is 9.8 GHz, which corresponds to an X-band spectrometer. Higher frequencies, such as Q-band (34 GHz), increase the sensitivity of the EPR experiment.

**Hyperfine Interactions**

In quantum mechanical terms, the energy associated with this interaction is described by the Zeeman Hamiltonian, $\hat{H}$.

$$\hat{H} = g_e \beta_e H_z S_z \qquad (10)$$

where g is the electron g-factor, $\beta$ is the Bohr magneton, $H_z$ is an external magnetic field along the z-axis, and $S_z$ is the electron spin operator.

The spin states of an electron influenced solely by the force of an applied magnetic field are described by equation (10). Nevertheless, this description is not completely true, because electrons in molecules are influenced by a variety of magnetic interactions. These interactions can increase the number of spin states and influence the lineshape of the EPR spectrum. To account for all of the magnetic interactions that can induce transitions between the spin states; additional spin operators are added to equation (10). In biological systems, nitroxide free radicals and transition metals are commonly employed in EPR experiments. These molecules are paramagnetic because they contain unpaired electrons. In the vicinity of the unpaired electron, there is an atomic nucleus which has a magnetic moment associated with it. The nuclear spin moment is described by a primary quantum number $I$, so there are $2I+1$ possible spin states for the nucleus. For example, $^{14}N$ has a primary spin quantum number $I = 1$; hence, $^{14}N$ will have three secondary spin quantum numbers $m_I = -1$, 0, and +1. The magnetic moment of $^{14}N$ is restricted to three possible orientations with respect to the magnetic field. Therefore, three nuclear spin states are possible each characterized by a nuclear Zeeman interaction energy of $\pm 1 g_n \beta_n H_z$ and $0 g_n \beta_n H_z$. For experiments involving nitroxide spin radicals, the magnetic moment of the electron can interact with the magnetic moment of the nitrogen. This interaction is referred to as the hyperfine interaction (Bersohn and Baird 1966). The energy associated with the hyperfine interaction is described in quantum mechanical terms by introducing additional spin operators into the Zeeman Hamiltonian.

$$\hat{H} = g_e\beta_e H_z S_z - g_n\beta_n H_z I_z + A_o S_z I_z \quad (11)$$

The subscripts e and n refer to nuclear and electron g-factors and Bohr magnetons. $I_z$ is the nuclear spin operator. The interaction energy between the unpaired electron and the nitrogen nucleus is described by the isotropic hyperfine coupling constant $A_o$. Essentially, $A_o$ describes the coupling of the electron and nuclear spin moments. As a direct result of the hyperfine interaction, the two spin states, $\alpha$ and $\beta$, of the electron are split into six additional spin states. The $\alpha$ spin state is split into $M_s = +\frac{1}{2}$, $M_I = \pm 1$, and $M_I = 0$, and the $\beta$ state is split into $M_s = -\frac{1}{2}$, $M_I = \pm 1$, and $M_I = 0$ (Fig. 2). The $M_s = -\frac{1}{2}$, $M_I = \pm 1$, and $M_I = 0$ spin states are lower in energy because the nuclear and electron moments are aligned parallel to the magnetic field. The resulting hyperfine spectrum originates from transitions between the six spin states (Smith et al. 1959). While a single line is observed when only an electron interacts with the magnetic field; the hyperfine interaction creates multiple lines. The number of transitions between the spin states is determined by selection rules due to the conservation of angular momentum (Bersohn and Baird 1966). The allowed transitions $M_s = \pm 1$ and $M_I = 0$ require absorption of energy and occur readily. The electron spin state and not the nuclear spin state can change. Thus, three lines of equal intensity are observed in the spectrum. The spacing of the three lines, which represent the allowed transitions, differs in energy by the amount of $A_o$.

There are two types of hyperfine interactions: Fermi contact and dipolar. The Fermi contact interaction describes the magnetic field of an unpaired electron in the region of the nucleus. This is a strong electrostatic interaction that is proportional to the delocalization of electron density at the nucleus. The Fermi contact interaction has no directionality because it is orientation independent; therefore, it is always isotropic. In equation (11), the Fermi contact term is $A_oS_zI_z$. The Hamiltonian representing the Fermi contact energy is expressed as,

$$\hat{H} = +\frac{8\pi}{3}\, g_e\beta_e g_n\beta_n \sum_{n,e}\delta(r_n - r_e) I_e S_z \qquad (12)$$

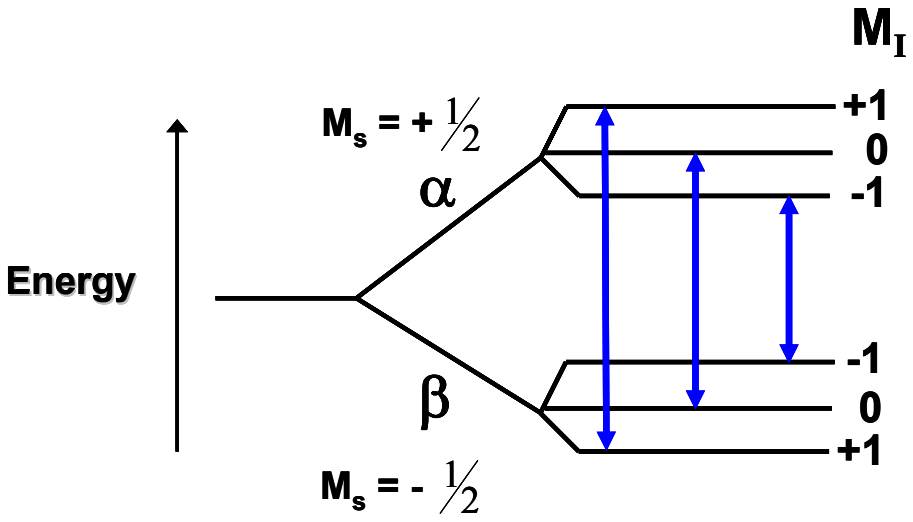


**Figure 6. An energy level diagram illustrating the effects of the hyperfine interactions on the magnetic energy of the electron.** The interaction between the magnetic moment of the electron and the $^{14}N$ nucleus increase the number of electron spin states. The blue vertical arrows indicate allowed transitions.

In most paramagnetic molecules, the size of the splitting of $A_o$ will vary because of the shape of atomic p orbitals, d orbitals, and $\pi$ molecular orbitals (Bersohn and Baird 1966).

These types of orbitals have very little electron density at the nucleus. However, s orbitals are spherical and more electron density is located at the nucleus. Essentially, an unpaired electron located within the orbital of one atom, in a paramagnetic molecule, can polarize the spins of another atom's orthogonal orbital (Drago 1992). The amount of electron density located at the nucleus contributes to the size of the $A_o$ splitting. The second type of hyperfine interaction is the dipolar interaction. This interaction is concerned with the magnetic field experienced by the electron due to vicinity of the nucleus. The dipolar interaction is represented by the following Hamiltonian:

$$\hat{\mathrm{H}} = \frac{-g_e \beta_e g_n \beta_n}{r^3}\left(I_z S_z - \frac{3(I_z r)(S_z r)}{r^2}\right) \qquad (13)$$

where r is radius vector from the nucleus to the electron. If the paramagnetic species tumbles rapidly, the dipolar interaction causes the magnetic field of the nucleus, at the electron, to average to zero. Therefore, the dipolar hyperfine splitting can only be measured in viscous solutions, where rapid tumbling of the paramagnetic species is reduced.

Hyperfine interactions are classified as isotropic and anisotropic. The concept of isotropic interactions was previously introduced during the discussion on Fermi contact interactions. In contrast to isotropic interactions, anisotropic interactions are dependent upon the orientation of the magnetic field with respect to the molecular axis. To understand the anisotropic nature of hyperfine interactions, a nitroxide spin label is placed at the center of a molecular coordinate system (Fig. 3). The nitroxide free radical was chosen as an example, because the unpaired electron is localized into a non-spherical orbital.

As a consequence, the electron g-factor and $A_o$ are orientation dependent within the external magnetic field. According to Figure 3, the unpaired electron is localized in an atomic p orbital along the z-axis, and the N-O bond is in the x-direction. The external magnetic field $H_o$ is normal to the plane and forms two angles θ and Φ (Fig. 3).

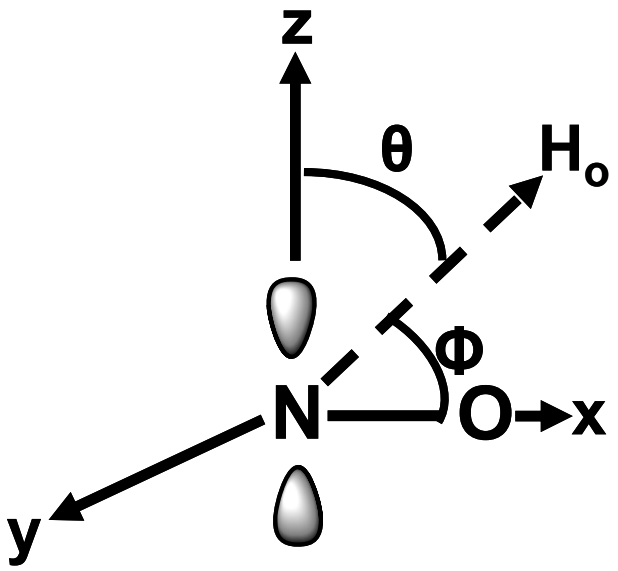


**Figure 7. The nitroxide spin label located within a molecular coordinate system.** The unpaired electron is localized with in a p orbital along the z-axis. The N-O bond is located along the x-axis. The external magnetic field $H_o$ forms two angles θ and Φ with the x- and y-axes.

The tensors g and A represent the electron g-factor and $A_o$, respectively. Due to the coupling of the spin angular momentum with the orbital angular momentum, the g-factor becomes anisotropic. The g-factors for bound electrons are different from free electrons due to the chemical environment of the paramagnetic molecule (Bersohn and Baird 1966). Therefore, the g-tensor is represented by the matrix,

$$g = \begin{matrix} g_{xx} & g_{xy} & g_{xz} \\ g_{yx} & g_{yy} & g_{yz} \\ g_{zx} & g_{zy} & g_{zz} \end{matrix} \qquad (14)$$

The x, y, and z components are defined within the laboratory frame, which is located along the axes of the molecular coordinate system.

For instance, the off-diagonal element $g_{zx}$ represents the contribution to g along the z-axis, when the field is applied along the x-axis (Drago, 1992). The diagnonalized g-tensor matrix is given by,

$$g = \begin{matrix} g_{xx} & 0 & 0 \\ 0 & g_{yy} & 0 \\ 0 & 0 & g_{zz} \end{matrix} \qquad (15)$$

and the three principle g-tensor components are $g_{xx}$, $g_{yy}$, and $g_{zz}$. If the g-tensor is written as a function of θ and Φ; then, the effective values of g are represented by,

$$g_{eff} = g_{xx}\sin^2\theta\cos\Phi + g_{yy}\sin^2\theta\sin^2\Phi + g_{zz}\cos^2\theta \qquad (16)$$

Similarly, the A-tensor is orientation dependent and can be represented by a 3 x 3 matrix, which is also diagonalized. There are three principle A-tensor components $A_{xx}$, $A_{yy}$, and $A_{zz}$. An effective value for the A-tensor which is a function of θ and Φ is represented by,

$$A_{eff} = [A^2_{xx}\sin^2\theta\cos^2\Phi + A^2_{yy}\sin^2\theta\sin^2\Phi + A^2_{zz}\cos^2\theta]^{1/2} \qquad (17)$$

Since the g-factor and $A_o$ are anisotropic, the observed spectrum is a function of the orientation of the nitroxide free radical in the magnetic field. To better understand this principle, it is best to begin with a crystal of nitroxide molecules each having the same orientation. It is important to assume the system is spin dilute; so, no interactions occur between spins.

If the crystal is crushed into a fine powder, the resulting spectrum will be representative of all molecular orientations (Millhauser et al. 1995). This type of spectrum is referred to as a powder pattern. It is only observed for randomly oriented nitroxides in the absence of molecular motion. The spectrum is so broad that only the $A_{zz}$ splittings are resolvable. In dilute solutions, the nitroxide molecules are capable of rapid molecular motion. The g- and A-tensors are averaged over time, in this fast motion regime. The average $g_{eff}$ and $A_{eff}$ anisotropy is determined from the following equations:

$$g_{eff} = (g_{xx} + g_{yy} + g_{zz})/3 \quad (18)$$

$$A_{eff} = (A_{xx} + A_{yy} + A_{zz})/3 \quad (19)$$

The g- and A- values become isotropic and independent of orientation. The spectrum will have three evenly spaced lines.

**Relaxation Phenomena and Lineshape**

An oscillating magnetic field $H_1$ can induce transitions from the lower energy state $\beta$ to the higher energy state $\alpha$. This transition involves the absorption of energy. An ensemble of electron spins can be divided into two populations. One population possesses energy in the $\alpha$ state and the other population in the $\beta$ state. When the $\alpha$ and $\beta$ state populations are equal, the amount of energy absorbed will equal the amount emitted. In this event, there is no energy difference between the $\alpha$ and $\beta$ state; therefore, no observable EPR signal is detected.

A resonance absorption signal can only be detected when the population of the lower energy $\beta$ state is larger than that of the higher energy $\alpha$ state. If an electron spin system is placed in a magnetic field at constant temperature and allowed to approach equilibrium, the resulting spin system is now at thermal equilibrium. At thermal equilibrium, the population in the upper state $\alpha$ relative to the population in the lower state $\beta$ is described by the Boltzmann distribution law (Bersohn and Baird 1966).

$$\frac{N(\alpha)}{N(\beta)} = e^{\frac{\Delta E}{kT}} \qquad (20)$$

where N($\alpha$) and N($\beta$) are the number of electron spins in each state, k is the Boltzmann constant (1.38 x $10^{-23}$ J/$K^{-1}$), T is the absolute temperature in kelvins, and $\triangle$E is the energy difference between the two states.

Changes in the strength of the magnetic field will shift the electron spin system from thermal equilibrium. An ensemble of electron spins, in a magnetic field, has a bulk magnetization, M. In the absence of a magnetic field, the electron spin states are degenerate, and M is equal to zero. However, at thermal equilibrium the spin system is dynamic and any given electron spin is rapidly changing its orientation with respect to the magnetic field. Electron spins are capable of interacting with their environment, which is referred to as the spin lattice. Fluctuating magnetic fields emanating from the spin lattice induce transitions between the $\alpha$ and $\beta$ energy states. Consequently, the population of spins in each energy state changes.

The spin system tries to restore thermal equilibrium by transferring energy between the lattice and spin system (Blumberg 1960). Spin-lattice relaxation is the process that restores the spin system to thermal equilibrium. Electron spins are also capable of interacting with each other; thereby, inducing transitions between the energy states $\alpha$ and $\beta$ (Solomon 1955). This process is referred to as spin-spin relaxation.

During the relaxation process, the bulk magnetization decays as a function of time. The decay of magnetization is a first order process which is described by two first order rate constants, $1/T_1$ and $1/T_2$. Relaxation times are the reciprocal of the rate constants. $T_1$ is the spin-lattice relaxation time (longitudinal relaxation time) and $T_2$ is the spin-spin relaxation time (transverse relaxation time). The Bloch equations describe the change in magnetization, as a function of time, during either $T_1$ or $T_2$ relaxation (Bloch 1966). In the presence of an external magnetic field $H_o$, the bulk magnetization aligns along the z-axis. An additional oscillating magnetic field $H_1$ is applied perpendicular to $H_o$, and the corresponding Bloch equations are:

$$\frac{dM_x}{dt} = \gamma\left(-M_x H_1 \sin\omega t + M_y H_1 \cos\omega t\right) + \frac{M_o - M_z}{T_1} \tag{21}$$

$$\frac{dM_x}{dt} = \gamma\left(-M_y H_o + M_z H_1 \sin\omega t\right) - \frac{M_x}{T_2} \tag{22}$$

$$\frac{dM_y}{dt} = \gamma\left(-M_z H_1 \cos\omega t + M_x H_0\right) - \frac{M_y}{T_2} \tag{23}$$

$M_o$ corresponds to the equilibrium value of the magnetization along the z-axis, $M_x$ is the component of the magnetization along the x-axis, and $M_y$ represents the magnetization component along the y-axis. $\omega$ is the frequency of the oscillating $H_1$ field. The steady state solutions to the Bloch equations are:

$$M_x = \frac{-M_0 \gamma H_1 T_2^2 (\omega_o - \omega_1)}{1 + T_2^2 (\omega_o - \omega_1)^2 + \gamma^2 H_{1_1}^2 T_1 T_2} \tag{24}$$

$$M_y = \frac{-M_0 (\gamma H_1 T_2^2)}{1 + T_2^2 (\omega_o - \omega_1)^2 + \gamma^2 H_{1_1}^2 T_1 T_2} \tag{25}$$

$$M_z = \frac{-M_0 (1 + (\omega_o - \omega_1)^2 T_2^2}{1 + T_2^2 (\omega_o - \omega_1)^2 + \gamma^2 H_{1_1}^2 T_1 T_2} \tag{26}$$

$\omega_o$ corresponds to the Larmor frequency, and $\omega_1$ is the angular frequency of $H_1$. Under steady state conditions, $H_1$ is weaker than $H_o$. When $\omega_1$ is close to $\omega_o$, the magnetization vector is tipped toward the y-axis (Bloch, 1946). Electron spins relax to equilibrium values along the z-axis and xy-plane at different rates. For instance, the magnetization relaxes along the z-axis at a rate of $1/T_1$ while relaxing along the xy-plane at a rate of $1/T_2$ (Bloch, 1946). The $T_1$ relaxation process restores z-axis magnetization by transferring energy between the spin system and the lattice; however, $T_2$ utilizes a different mechanism which is based upon phase coherence. Magnetic interactions occur at individual electron spins causing them to experience slightly different local magnetic fields. As a result, the frequency of each spin spreads out and must be gradually dephased. The dephasing process exponentially decays with a time constant $T_2$.

$T_1$ and $T_2$ processes affect the line width of the EPR signal. $T_2$ is experimentally determined from the line width and is related to the peak to peak first derivative line width $\triangle H$ (Farahbakhsh et al. 1992). In general if the $T_2$ process is long, the line width is narrow. Alternatively, if the $T_1$ process is short the line width is broad. EPR line widths are classified into the two classes: homogenously broadened and inhomogenously broadened. Spins within the same environment create homogenously broadened lines, because the energy absorbed from the microwave magnetic field is evenly distributed to all spins (Portis 1953). Therefore, thermal equilibrium must be maintained through resonance. Inhomogenously broadened lines are the result of spins in different environments. In this case, the line widths are the result of variations in local magnetic fields, and the energy absorbed is transferred to a subpopulation of spins. Only this subpopulation experiences fields which satisfy the resonance condition (Portis, 1953). A portion of the inhomogenously broadened line may be selectively saturated, and its EPR signal intensity is reduced. This event is referred to as burning a hole in the resonance line (Mims et al. 1961). On the other hand, if a portion of the homogenously broadened line is selectively saturated; then the EPR intensity of the whole line is reduced. A large increase in microwave power increases the line width of homogenously broadened lines. This effect is referred to as power broadening (Van Vleck 1948). Consequently, the spins spend a shorter time in each energy level; due to the increased number of transitions between the energy levels. The line width corresponding to a homogenously broadened line reflects the lifetime of a spin in each energy level.

The environment of the spin has an effect on the mechanism of relaxation. For example in the solid state, molecules of the crystal lattice are regularly ordered. The molecules of the crystal lattice are connected to one another and coordinately undergo vibratory motion. Each molecule's vibrations are quantized and referred to as a phonon (Standley and Vaughan 1969). The mechanism that causes changes in spin populations is the interaction between spins and phonons. This effect is referred to as spin-orbit coupling. In spin-orbit coupling, the magnetic field produced by the orbital of the electron interacts with the magnetic moment from the electron spin. Surrounding molecules within the lattice obstruct orbital motion; thereby, the magnetic field experiences oscillations. The relaxation process is temperature sensitive, and lower temperatures are favored in order to preclude the competing Raman process. In solids, dipolar interactions can occur between nuclear and electron spins (Leifson and Jeffries 1961). As a result, electron spins are out of phase with each other broadening resonance lines. This broadening effect is stronger in highly concentrated versus dilute paramagnetic samples.

In contrast, the liquid state lacks the regularity observed in solids. Relaxation occurs by modulating spin dipolar interactions. These interactions are effected by Brownian motion, introducing time dependence to these interactions. As a molecule tumbles, Fermi contact occurs between two electrons in close proximity to one another (Osheroff et al. 1972). Consequently, fluctuations occur in the magnetic field that produce transitions between electron spin states. When the spins rapidly tumble, $T_1$ is equivalent to $T_2$.

Increasing solution viscosity results in $T_1$ not being equal to $T_2$. In this regime, interactions occur between the paramagnetic species and either neighboring nuclear or electron spin dipoles (Osheroff et al. 1972). The lifetime of the spin in its spin state is decreased; therefore, spin exchange is capable of affecting the line shape. Lineshapes can be described as Lorentzian or Gaussian (Van Vleck 1948; Pake 1962). A Lorentzian lineshape arises when electrons are exchanged between paramagnetic species with their odd electrons in close proximity. The Gaussian lineshape is the result of a distribution of neighboring spin magnetic moments being influenced by a variety of magnetic fields. These field variations are the result of neighboring nuclei or electrons. Hyperfine structure influences the lineshape of a spectrum. The Fermi contact interaction predominates when molecules are rapidly tumbling. In rigidly immobilized molecules, Fermi contact and dipolar hyperfine interactions contribute to lineshape.

## EPR Spectroscopy Applications

### Site-directed Spin Labeling

The spectrum of a nitroxide spin label is sensitive to the local environment in the vicinity of the label (Hamilton and McConnell 1968; Todd et al. 1989; Hubbell et al. 1998; Czogalla et al. 2007). This is an extremely valuable tool for studying the structure and function of biological systems.

Site-directed spin labeling (SDSL) has emerged as an important technique for the study of water-soluble and membrane proteins (Altenbach et al. 1990; Mchaourab et al. 1996; Dong et al. 2005; Claxton et al. 2010). The general methodology of SDSL involves mutating all the reactive endogenous cysteines to non-reactive alanines or serines. The stratagem is to create a cysteine-free base mutant. Into this base mutant, the individual residue of interest is mutated via site-directed mutagenesis to a cysteine residue (Fig. 8). The cysteine residue is subsequently derivatized with a sulfhydryl specific nitroxide spin label (Fig. 8).

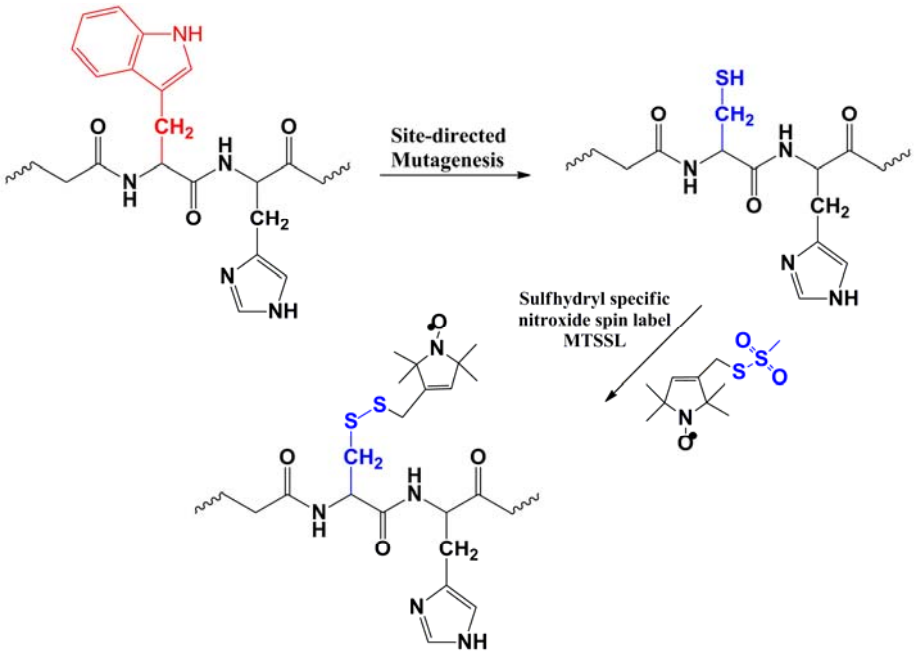


**Figure 8. The basic strategy of SDSL.** The tryptophan residue is mutated to a cysteine. The cysteine is derivatized with the MTSSL spin label. Consequently, the spin label is incorporated at the position of interest.

In theory, a nitroxide spin label can be positioned at any desired residue within the polypeptide chain. There are a variety of nitroxide spin labels such as 1-oxyl-2,2,5,5-tetramethyl-△3-pyrroline-3-methyl) methanethiosulfonate (MTSSL) and 3-(2-iodoacetamido)-PROXYL (IAP) (Fig. 9). The MTSSL spin labeling reaction product is a side chain designated as R1, and IAP produces the R2 side chain (Fig. 9). Analysis of the EPR spectra of both R1 and R2 provides information on the label environment by monitoring R1 and R2 mobility, solvent accessibility, polarity of the label's immediate environment, and the distance between individual labels or a paramagnetic metal ion (Hubbell et al. 2000).

That being the case, a set of sequentially labeled mutants provides a means to obtain global information on protein structure and dynamics (Hubbell et al. 2000).

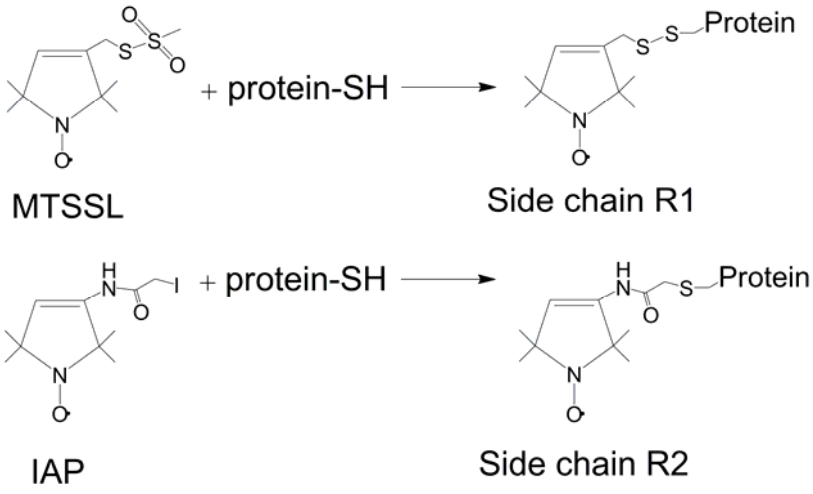


**Figure 9. The spin labeling reaction of MTSSL and IAP.** MTSSL produces a nitroxide side chain referred to as R1, while IAP produces the R2 side chain.

The mobility, polarity, and distance spectral parameters are inferred from the EPR spectral lineshape. Detailed information about these spectral parameters is obtained from spectral simulation (Freed 1976).

Experimentally, R1 and R2 mobility is measured by the inverse linewidth of the central resonance $\triangle H_o^{-1}$, and by the spectrum's inverse second moment $\langle H^2 \rangle^{-1}$ (Mchaourab et al. 1996). The polarity of the immediate environment, in the vicinity of the label, is proportional to the hyperfine splitting, $A_{zz}$ (Griffith et al. 1974). The distance between two nitroxide spin labels or a metal ion is determined by the static dipolar interaction. A qualitative characteristic, of the dipolar interaction, is the broadened EPR lineshape and reduction in spectral intensity. The separation distance, r between the paramagnetic centers is commonly determined by the deconvolution method (Steinhoff 2004). Longer distance ranges up to 80 Å are experimentally determined using pulse EPR techniques such as double electron-electron resonance (DEER) (Jeschke et al. 2004). The solvent accessibility of R1 or R2 is determined from the collision frequency with paramagnetic reagents Ni(II)ethylenediaminediacetate (NiEDDA) and molecular oxygen ($O_2$), which is expressed through the accessibility parameter $\Pi$ (Farahbakhsh et al. 1992). R1 and R2 collision frequency with these reagents reduces $T_1$, a parameter of saturation (Altenbach et al. 2005).

**Spectral Parameter: Nitroxide Side Chain Mobility**

The EPR spectrum is sensitive to the rotational motion of the nitroxide side chain. Spectra acquired with an X-band spectrometer display sensitivities to rotational motion in the range of 0.1 to 100 nsec time interval (Klug and Feix 2008). The rotational tumbling of a nitroxide in solution is governed by Brownian motion, which has a characteristic correlation time $\tau_R$ (Millhauser et al. 1995).

Rotational motion cause the magnetic fields experience by electron spins to fluctuate. As a result, anisotropy of the g and A tensor components influences the range of EPR lineshapes observed. This range is bound by two regimes motional narrowing and slow motion (Millhauser et al. 1995). At the motional narrowing limit ($\tau_R$=0.1 nsec), all g and A tensor components are averaged and three sharp lines of approximately equal amplitude are observed (Millhauser et al. 1995; Klug and Feix 2008). As the correlation time increases ($\tau_R$=5 and $\tau_R$=80 nsec), the rotational motion decreases broadening the lines and reducing their amplitude. These types of lineshapes are indicative of spectra with correlation times at the slow motion regime.

Rotational motion of the nitroxide is determined by three correlation time: $\tau_B$, due to the motion of the nitroxide relative to the $\alpha$-carbon backbone, $\tau_S$, reflecting the motion of the $\alpha$-carbon backbone, and $\tau_R$, which is attributed to the entire protein (Mchaourab et al. 1996). $\tau_R$ is affected by the size of the protein; for instance, protein complexes larger than 50 kDa will tumble very slowly. In this case, $\tau_R$ will have a lesser effect on spectral lineshape. The rotational diffusion of smaller proteins affects $\tau_R$, which influences the observed EPR spectrum (Klug and Feix 2008). To overcome this effect, EPR spectra is acquired in 30% sucrose solutions (Mchaourab et al. 1996). The addition of sucrose increases solution viscosity which attenuates the rotational diffusion of the protein (Klug and Feix 2008). Remarkably, the nitroxide's rotational motion remains mostly unaltered (Mchaourab et al. 1996).

The addition of bulky substituents, to the nitroxide spin label, can reduce $\tau_S$, due to $\alpha$-carbon backbone motion (Mchaourab et al. 1996; Columbus et al. 2001).

Of interest is the motion of the nitroxide side chain, because this motion is sensitive to tertiary contacts within the protein structure. The MTSSL side chain (R1) is composed of five bonds with corresponding dihedral angles ($\chi_1$, $\chi_2$, $\chi_3$, $\chi_4$, $\chi_5$) between the nitroxide ring and the attachment point on the protein backbone (Fig. 10). Facile rotation occurs about the two bonds associated with dihedral angles $\chi_4$ and $\chi_5$, with slow rotation about the disulfide bond $\chi_3$, and the interaction between $S_\beta$ and the $C_\alpha$ proton limit rotation about bonds associated with $\chi_1$ and $\chi_2$ (Langen et al. 2000; Czogalla et al. 2007; Klug and Feix 2008). Isomerization of the R1 side chain, of MTSSL, creates multicomponent EPR spectra.

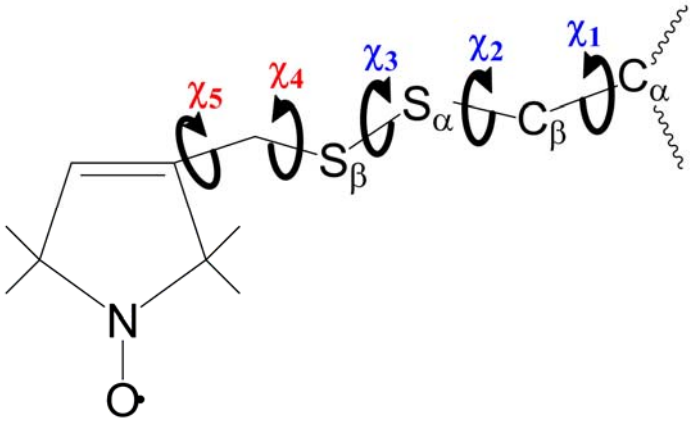


**Figure 10. The dihedral angles $\chi_1$-$\chi_5$ associated with the R1 side chain of MTSSL.** The two rotatable bonds are associated with angles $\chi_4$ and $\chi_5$ (red) and the $S_\beta/C_\alpha$ interaction precludes rotation about the bonds associated with $\chi_1$, $\chi_2$, and $\chi_3$ (blue).

For example, crystal structures of R1-labeled T4 lysozyme (T4L) mutants display two different components (Langen et al. 2000). These conformations are attributed to two distinct rotamers of R1 (Langen et al. 2000). Component $\alpha$ corresponds to a highly mobile population of R1 labels and $\beta$ is a population undergoing motional restriction (Langen et al. 2000).

Interesting spectral lineshapes are observed at sites where the nitroxide spin label is in tertiary contact with neighboring residues, as well as, buried sites within the protein core (Mchaourab et al. 1996; Mchaourab et al. 1997a; Koteiche and Mchaourab 1999). Based upon the extent of interaction, the mobility of a nitroxide spin label can be classified as mobile, weakly immobilized, and strongly immobilized. Spin label mobility varies with protein topography; therefore, regions along the protein fold are classified as buried, surface exposed, loops, and tertiary contact sites (Mchaourab et al. 1996; Hubbell et al. 1998). The EPR lineshapes can be qualitatively classified as broad or narrow based upon the separation between the outer hyperfine extrema ($2A_{zz}$) and the peak to peak width of the central line, $\triangle H_o$ (Fig. 11). Broad EPR spectra with widely spaced outer hyperfine extrema ($2A_{zz}$) indicate the spin label is immobilized (Fig. 11A). Spectra of this type is located within the protein interior (Mchaourab et al. 1996). Narrow EPR spectra have more closely spaced hyperfine extrema ($2A_{zz}$) indicative of highly mobile spin labels (Fig. 11B). Spin labels located within loops and on the protein surface display this type of spectra (Mchaourab et al. 1996).

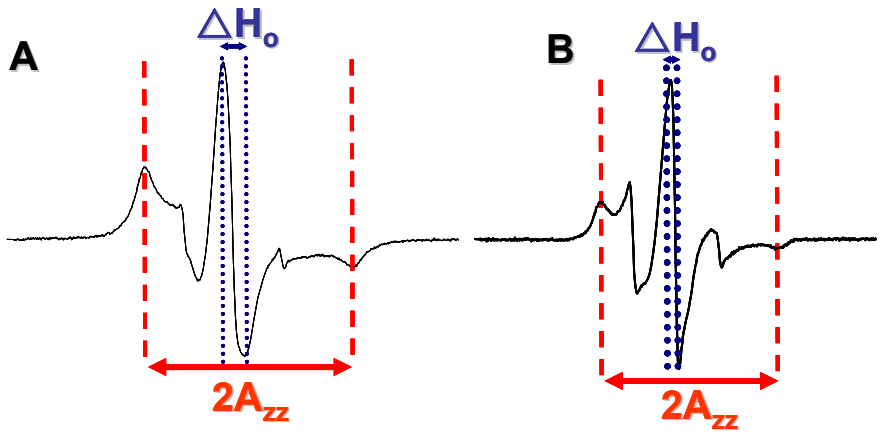


**Figure 11. The effect of spin label mobility on the outer hyperfine extrema $2A_{zz}$ (red dashed lines & double sided arrow) and the peak to peak central linewidth, $\triangle H_o$ (blue dashed lines & double sided arrow).** (A) Broad EPR spectral lineshape (B) Narrow EPR spectral lineshape

Empirical parameters, which describe spectral lineshape, provide a snapshot of the protein fold (Hubbell et al. 1996; Mchaourab et al. 1996; Czogalla et al. 2007). For example, the inverse of the peak to peak central line width ($\triangle H_o^{-1}$) can be plotted as a function of residue number. Plotting $\triangle H_o^{-1}$ reveals secondary structural elements through the periodic sampling of exposed, buried, or steric contact environments as R1 is scanned across the polypeptide chain (Mchaourab et al. 1996; Koteiche et al. 1998). A periodicity of 2 is consistent with $\beta$-strands, while 3.6 periodicity is consistent with $\alpha$-helical regions (Koteiche et al. 1998). Another empirical parameter is the inverse second moment $\langle H^2 \rangle^{-1}$ which describes the breadth of the spectrum (Mchaourab et al. 1996). A plot of $\langle H^2 \rangle^{-1}$ versus $\triangle H_o^{-1}$ indicates that protein side chains from different topographical regions cluster together into defined classes which represent mobilities consistent with portions of the protein fold. For instance, all buried sites are located at a region of the plot indicating low spin label mobility.

Characteristically, this is to be expected because buried sites are located within the sterically packed protein interior. In contrast, loop sites have the highest mobility indicating regions that lack steric restriction. Tertiary interaction and helix surface sites are located at regions of intermediate spin label mobility. The dynamics of the $\alpha$-carbon backbone contributes to regions of overlap between buried, tertiary, and helix surface sites (Mchaourab et al. 1996).

A quantitative understanding of EPR lineshape is obtained from simulations based upon dynamic models (Barnes et al. 1999; Borbat et al. 2001). EPR simulation is advantageous because it provides detailed information about the influence of protein structure adjacent to the site of spin labeling (Beier and Steinhoff 2006). The microscopic order macroscopic disorder (MOMD) model describes the motion of the nitroxide side chain using an order parameter and effective correlation time (Meirovitch et al. 1984). Simulating EPR spectra using the MOMD model allows for the determination of isotropic or anisotropic motion from EPR lineshapes (Budil et al. 1996; Columbus et al. 2001). MOMD is also effective in detecting and characterizing multiple components in EPR spectra (Barnes et al. 1999; Columbus et al. 2001).

**Spectral Parameter: Nitroxide Side Chain Accessibility**

The direct collision of a paramagnetic species with a nitroxide spin label, referred to as Heisenberg exchange, is a tool for investigating both water soluble and membrane protein topography (Altenbach et al. 1989; Koteiche et al. 1998; Berengian et al. 1999; Altenbach et al. 2005).

Using membrane proteins as an example, it is possible to determine whether a label, at a particular site, is located within the membrane interior or within the aqueous phase (Altenbach et al. 1990; Farahbakhsh et al. 1992; Dong et al. 2005; Vasquez et al. 2008; Amadi et al. 2010; Claxton et al. 2010). The capacity for Heisenberg exchange with fast relaxing paramagnetic species results in changes to the spin label's $T_1$ relaxation time.

Continuous wave (CW) power saturation and saturation recovery (SR) are techniques for the determination of $T_1$ relaxation time (Altenbach et al. 2005; Pyka et al. 2005). The amplitude of the EPR spectrum increases linearly with the square root of the incident microwave power. As the microwave power increases, the spin system deviates from this linear relationship, and this phenomenon is referred to as saturation. At saturation, the rate of relaxation, to equilibrium, can not compete with the rate at which microwave power is absorbed by the spin system. $P_{1/2}$ is the amount of microwave power required to saturate the EPR signal to half its amplitude, in the absence of saturation (Altenbach et al. 1989; Farahbakhsh et al. 1992) . The rate of relaxation is measured by $1/T_1$, and a sample with a long $T_1$ will saturate easily and relax very slowly. In contrast, a sample with a short $T_1$ will relax quickly but take longer to saturate.

The direct collision of paramagnetic species with the spin label enhances the relaxation rate. As a result, the spin system can absorb more microwave power before saturation.

This process is a reflection of the Heisenberg exchange rate ($W_{ex}$) between the nitroxide spin label and the paramagnetic species (Altenbach et al. 2005). The Heisenberg exchange rate is described by the following equation:

$$W_{ex} = k_{ex}C_R \quad (27)$$

where $k_{ex}$ is the exchange rate constant and $C_R$ is the concentration of paramagnetic species chosen as an exchange reagent. $W_{ex}$ is a measure of the accessibility of the nitroxide spin label to the solvent containing the paramagnetic species. On that account, $W_{ex}$ is an important parameter for obtaining information about the label's immediate environment. An important assumption is that the Heisenberg exchange is at the strong exchange limit. At the strong exchange limit, the rate of Heisenberg exchange is primarily determined by diffusion. The exchange rate constant, at the strong exchange limit, is described by the following equation:

$$k_{ex} = P_{max}fk_D = P_{max}f4\pi(N_A/1000)(D_N + D_R)r_C \quad (28)$$

$P_{max}$ is a measure of the maximum exchange efficiency, and f is the dimensionless orientation dependent steric factor. $P_{max}$ approaches 1 in the strong exchange limit, where $T_1<\tau_C$. $\tau_C$ is the lifetime of the spin label/paramagnetic exchange reagent complex. $K_D = 4\pi(N_A/1000)(D_N + D_R)r_C$ is the diffusion controlled rate constant, and $D_N$ and $D_R$ are individual diffusion rate constants for the nitroxide spin label and the paramagnetic exchange reagent (R). The collision radius, $r_c$ is the sum of the effective radii for the nitroxide spin label and the paramagnetic exchange reagent.

For a spin labeled protein, the diffusion constant for the nitroxide is negligible and $D_N + D_R \approx D_R$. An additional accessibility factor ρ accounts for the interaction of the nitroxide spin label with its environment. The value of ρ varies based upon the local protein environment. For instance, the value of ρ is zero for a label buried within the protein interior and one for a label located completely at an exposed surface site. The following equation is used to determine the accessibility factor of a nitroxide spin label at any site.

$$\rho = k^{p}_{ex}/k_{ex}\ [(DR + DN) / DR] \qquad (29)$$

where $k^{p}_{ex}$ is the exchange rate constant for a spin labeled protein in a solution containing a diffusing paramagnetic exchange reagent. A consequence of Heisenberg exchange is Lorentzian line broadening, which is measured from the first derivative peak to peak central linewidth ($\triangle H_{pp}$). In the presence of the paramagnetic exchange reagent, the collisions rate with the nitroxide spin label is related to the change in $\triangle P_{1/2}$.

$$\triangle P_{1/2} = P_{1/2} - P^{o}_{1/2} \qquad (30)$$

$P_{1/2}$ and $P^{o}_{1/2}$ are values in the presence and absence of paramagnetic exchange reagent. The $\triangle P_{1/2}$ is proportional to the Heisenberg exchange rate $W_{ex}$, and is dependent upon the properties of the resonator. As a consequence, the dimensionless accessibility parameter ($\Pi$) is defined.

$$\Pi = \left[ \frac{\frac{\Delta P_{1/2}}{\Delta H_{pp}}}{\frac{P_{1/2}}{\Delta H_{pp}}} \right]_{reference} \qquad (31)$$

The factor $[P_{1/2}/\triangle H_{pp}]_{reference}$ corresponds to reference compounds, such as 2,2-diphenyl-1-picrylhydrazyl (DPPH) and T4 lysozyme (T4L) , which account for variations in the resonator. The accessibility parameter is proportional to $W_{ex}$.

$$\Pi = \alpha W_{ex} \quad (32)$$

Molecular oxygen ($O_2$), Ni(II)ethylenediaminediacetate (NiEDDA), Ni(II)acetonylacetonate (NiAA), and chromium oxalate (CROX) are paramagnetic exchange reagents. Each reagent has specific physical and chemical properties making them ideal choices for a wide variety of applications. For example, molecular oxygen is hydrophobic with a small molecular volume. This property allows $O_2$ to be soluble within the protein interior. NiEDDA and NiAA are aqueous soluble, both display a limited capacity for partitioning into the protein or membrane interior. NiEDDA is neutral, while NiAA has a tendency to be charged at pH extremes (Altenbach et al. 1994). CROX is negatively charged restricting it only to the aqueous phase. The relative collision frequency, between the label and exchange reagent, is a source of information on the environment of the spin label site. Therefore, it is possible to distinguish between sites located within the lipid bilayer, protein interior, and solvent exposed surfaces.

Accessibility experiments are typically performed by placing spin labeled protein samples into gas permeable (TPX) tubes. The sample is equilibrated in 20% oxygen or nitrogen ($N_2$).

Nitrogen equilibration allows for the determination of spin label relaxation rate in the absence of paramagnetic exchange reagent (nitrogen control). The amplitude of the central line ($m_I$ = 0) is measured at a series of increasing microwave powers. NiEDDA, NiAA, or CROX are added to the spin labeled protein solutions prior acquiring measurements. The $P_{1/2}$ value is determined from the power saturation curve. Each $P_{1/2}$ value is subtracted from the nitrogen control to obtain the corresponding $\triangle P_{1/2}$ value. The $\Delta P_{1/2}$ (NiEDDA) value is high for solvent exposed sites and low for sites located within the protein interior or at the center of the lipid bilayer. In contrast, the $\Delta P_{1/2}$ ($O_2$) value is high for these sites. Secondary structural information is obtained from the study of a series of consecutive sites, within a protein or peptide. Accessibility values are plotted against residue number, and the resulting periodicity can distinguish between $\alpha$-helical, $\beta$-strand, and unstructured regions. The $\alpha$-helix has a periodic pattern of 3.6 to 4, a periodicity of 2 for $\beta$-strands, and unstructured regions lack no regular periodic pattern. This method is based upon the intrinsic asymmetry in the environment surrounding the secondary structural element (Hubbell et al. 1998). For a water soluble protein, a $\alpha$-helix has one of its surfaces solvent exposed, while the other is facing the interior of the protein. In this case, all paramagnetic exchange reagents will have $\Pi$ values with the same period and phase. For a $\alpha$-helix located within a membrane protein, one surface is aqueous solvated; while the other is in contact with the lipid bilayer. In this instance, the $\Pi$ values will have the same period but differ in phase by $180^o$.

The depth parameter (Φ) is a measure of the immersion depth of a spin label within the membrane bilayer (Altenbach et al. 1994).

$$\Phi = \ln\left[\frac{\Delta P_{1/2}(O_2)}{\Delta P_{1/2}(NiEDDA)}\right] \quad (33)$$

The concentration of $O_2$ is highest at the center of the membrane bilayer and progressively decreases toward the membrane surface (Altenbach et al. 1994). Conversely, the concentration of NiEDDA is highest at the membrane surface and negligible at the center of the bilayer (Altenbach et al. 1994).

**Spectral Parameter: Spin-spin Interactions**

The ability to measure both intramolecular and intermolecular distances between two spin labels, in the same monomer or between multiple sites on different proteins, is an extremely powerful technique for determining protein structure and dynamics (Beth et al. 1984; Voss et al. 1995; Hustedt et al. 1997; Koteiche and Mchaourab 1999; Liu et al. 2001; Eaton et al. 2002; Xiao et al. 2002; Steinhoff 2004; Zou et al. 2009; Amadi et al. 2010; Claxton et al. 2010). For SDSL based distance measurements, two sites are labeled with a nitroxide spin label, referred to as double site-directed spin labeling (DSDSL). The basis of distance measurements is to observe the effects of magnetic dipole interactions between the unpaired electrons of two nitroxide spin labels. The magnetic field from one electron's spin produces a force on the magnetic dipole of the second electron's spin (Eaton et al. 2002).

As a result, there will be a change in Zeeman energy, of one electron spin, due to the presence of the second electron spin. The interaction splits the resonance line, for the observed electron spin, into a doublet of lines.

The spin-spin interaction is described by the following spin Hamiltonian:

$$\hat{H} = \beta_e H_o g_1 S_1 + \beta_e H_o g_2 S_2 - \omega_n (I_{1z} + I_{2z}) + \gamma_e I_1 A_1 S_1 + \gamma_e I_2 A_2 S_2 + S_1 D S_2 + J S_1 S_2 \quad (34)$$

The two interacting nitroxide spin labels are referred to as 1 and 2, respectively. $\omega_n$ is the Larmor frequency associated with the nitrogen nucleus, and $\gamma_e$ is gyromagnetic ratio corresponding to the electron. J is a scalar quantity describing the interaction between the two electron spins. Orbital overlap produces J coupling, and it decreases exponentially with internitroxide distances greater than 10 Å (Hustedt and Beth 1999; Eaton et al. 2002). D is the dipolar coupling tensor that describes how two electrons spins, separated by the distance r, are coupled to one another. For a randomly oriented sample, the g-tensor values are isotropic, the value of D corresponds to the splitting observed in the Pake pattern (Rabenstein and Shin 1995). The dipolar interaction energy is proportional to $1/r^3$, and represented by the following equation:

$$E_{dipolar} = \frac{\mu_1 \mu_2}{r^3}\left(1 - 3\cos\ \theta\right) \quad (35)$$

Θ is the angle between the magnetic field and the interspin vector. The interaction energy is dependent upon the orientation of the electron spins in a magnetic field, and this interaction becomes zero at the magic angle $54.7^o$.

For distances in the range of 15 to 20 Å, line broadening is observed in the CW-EPR spectrum. Broadened spectra display a decrease in EPR signal amplitude, and spectra normalized to the same spin concentration is a qualitative indicator of spin-spin interaction (Mchaourab et al. 1997a; Klug and Feix 2008). EPR methods have been developed to measure dipolar interactions and obtain distances between nitroxide spin labels, in a variety of samples at various conditions. For example in an immobilized sample, the dipolar interaction can be determined for two slowly relaxing spins. In this case, it is assumed that there is only a single unique distance between the nitroxide spin labels. The hyperfine splittings are anisotropic, which is an indicator that there is a unique orientation of the interspin vector relative to the magnetic axes. If the dipolar splitting (D) is larger than the linewidth of the EPR signal observed in the CW-EPR spectrum, then the spectral lineshape must be analyzed by computer simulation. A caveat to analyzing spectral lineshape by computer simulation is that the dipolar splittings need to be well resolved; otherwise it is impossible to obtain a unique simulation for the corresponding spectrum.

In this case, two spectral simulation methods based upon deconvolution were developed. Both methods assume that there is enough conformation flexibility in the bonds tethering the labels to the protein; that there is a random distribution of orientations for the interspin vector, relative to the magnetic axes. In these methods, the EPR spectra for the two non-interacting spin labels (sum of singles) are compared with the spectrum corresponding to the interacting spin labels (doubly labeled mutant).

Essentially, it is assumed that the spectra displaying dipolar interaction is a convolution of non-interacting spectra. Another method uses Fourier deconvolution, and the alternative method uses a broadening function to deconvolute the EPR spectra to obtain distances from the dipolar interaction (Rabenstein and Shin 1995; Mchaourab et al. 1997b; Steinhoff et al. 1997). An additional method for simulating EPR spectra from dipolar coupled nitroxides is based upon the tether-in-a-cone model (Hustedt et al. 2006). In this model, the unpaired electron is situated at the end of a tether within a cone, allowing the electron to sample a multitude of angles dictated by the position of the tether (Hustedt et al. 2006). The model produces a distribution of distances. The relative orientation of the labels is extrapolated from various parameters such as: tether length, cone width, and the angle that defines the orientation of the tether with the magnetic axes (Hustedt et al. 2006). Other methods utilize the ratio of peak heights ($d_1/d$) as an estimation of the internitroxide distance; only if $T_1$ relaxation is slow and dipolar splittings are unresolved (Kokorin et al. 1972). Alternatively, the distance between the two spins is determined from the intensity of the half-field transition (Eaton and Eaton 1982). The half-field intensity measurement is applicable for short distances, less than 8 Å. However, the measurement is further complicated by a contribution from anisotropic exchange, which reduces both the resolution and precision of the distance measurement (Eaton and Eaton 1982).

All CW techniques are highly dependent upon the observation of spectral broadening. The degree of broadening is an indicator of the strength of the dipolar interaction, which is a function of the interspin distance. When the interspin distance is in the range of 20 to 80 Å, broadening of the spectral lineshape, due to dipolar interactions, become less significant. Pulse techniques are ideal, in this case, because the width of the spin packets are generally smaller than the broadened CW linewidth (Eaton et al. 2002). Pulse techniques require the perturbation of the spectral region of one nitroxide spin label by a pulse. Consequently, the time-dependent response in the spectral region of the other nitroxide spin label is observed. The timing of the pulse creates oscillations of spin echo intensity; that is a function of the dipolar interaction. The frequency of the oscillations is a characteristic signature of the interspin distance. There are several types of pulse EPR techniques, each characterized by a different pulse sequence. Examples of the pulse techniques are 3-pulse (electron-electron double resonance) ELDOR or PELDOR, 2 + 1 sequence, 4-pulse DEER (double electron-electron resonance), and double-quantum coherence (DQC) (Saxena and Freed 1997; Astashkin et al. 1998; Milov et al. 1999; Pannier et al. 2000; Jeschke 2002; Jeschke and Polyhach 2007).

The emphasis is on the 4-pulse DEER technique. The pulse pattern and absorption profile for the 4-pulse DEER experiment are shown in Fig. 12 (Pannier et al. 2000). In a spin system, there are two populations of electron spins $S_A$ and $S_B$.

The $S_A$ spin population has a microwave resonance frequency of $\upsilon_A$, while population $S_B$ has a resonance frequency $\upsilon_B$. At first, all spins have their magnetic moments aligned along the z-axis producing a bulk magnetization. A $\pi/2$ pulse is turned on, at time (t=0) and the frequency of the pulse corresponds to $\upsilon_A$ "observe frequency". Therefore, the $S_A$ spins experience a torque along the x-axis, which tips their magnetization into the xy-plane. Hyperfine interactions result in inhomogeneous broadening which causes each spin to experience slightly different local magnetic fields. The loss of spin coherence causes gradual dephasing of magnetization in the xy-plane. A $\pi$ pulse is turned on, at time ($t = \tau_1$) which flips the magnetization of $S_A$ by $180^o$. Spin coherence is restored at time ($t = 2\tau_1$), and a spin echo is formed. In order to study the dipolar interaction between spin populations $S_A$ and $S_B$, a $\pi$ pulse is turned on at resonance frequency $\upsilon_B$ "pump frequency". This $\pi$ pulse is inserted between the two $\pi$ pulses at irradiation frequency $\upsilon_A$ "observe frequency". The resonance frequencies $\upsilon_A$ and $\upsilon_B$ do not have overlapping excitation bandwidths; therefore, the $\pi$ pulse, at pump frequency $\upsilon_B$, will excite the $S_B$ spin population. Since $S_B$ is dipolar coupled to $S_A$, the local magnetic field experience by $S_A$ is altered. However, the magnetization of $S_A$ can not be fully refocused, so another $\pi$ pulse is turned on, at observe frequency $\upsilon_A$, resulting in a refocused echo at time ($t = 2\tau_1+2\tau_2$).

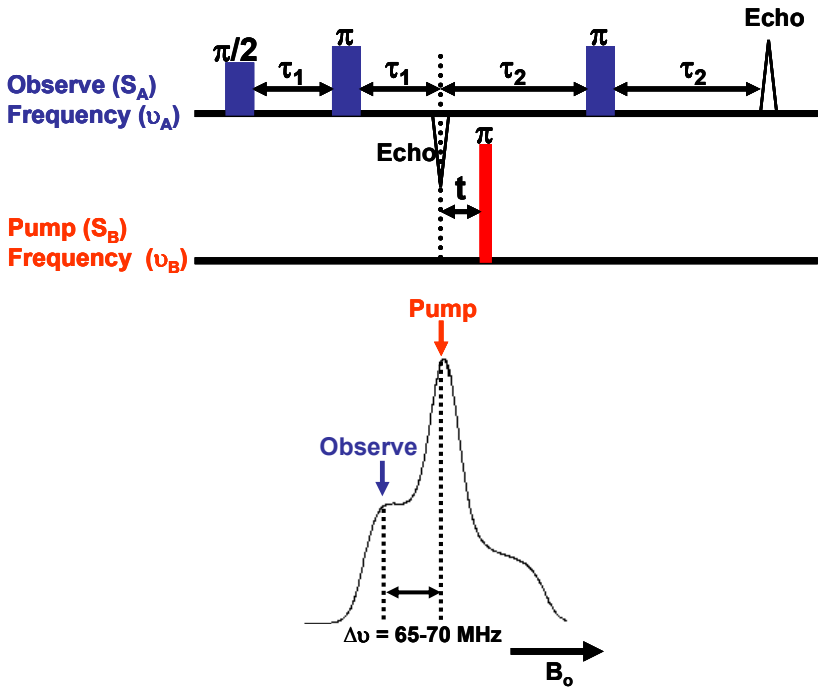


**Figure 12. Pulse sequence for the four-pulse DEER experiment and its expected excitation profile.** In a DEER experiment, there is a population of observing spins which are resonating at frequency $\upsilon_A$ (red). A second population of pumping spins is resonating at $\upsilon_B$ (blue). A pumping $\pi$ pulse, at frequency $\upsilon_B$, cause flipping of the pump spins. The pump spins are dipolar coupled to the observe spins, leading to alterations in the local magnetic field of the observe spins. Another $\pi$ pulse, at resonance frequency $\upsilon_A$, refocuses the observe spins creating a refocused echo.

Unlike the first echo at time ($t=2\tau_1$), this refocused echo is our observable. The $\pi$ pulse, at pump frequency $\upsilon_B$, is applied at a variable time t modulating the intensity of the refocused echo. The spin system is described by a Hamiltonian, which is a function of the angular frequencies, $\omega_A$ and $\omega_B$, associated with $S_A$ and $S_B$.

$$\hat{H} = \omega_A S_A + \omega_B S_B + \omega_{AB} S_A S_B \qquad (36)$$

The dipolar coupling $\omega_{AB}$ is described by the following equation

$$\omega_{AB} = \omega_{dip}(3\cos^2\theta_{AB} - 1) \quad (37)$$

where $\omega_{dip}$ is the dipolar coupling. The intensity of the refocused echo is described by equation

$$I = I_o\cos(\omega_{AB}t) \quad (38)$$

where $I$ and $I_o$ are initial and final states of the refocused echo intensity, because $S_A$ spins experience a different magnetic environment before and after the pump $\pi$ pulse. $t$ represents the time modulation of the dipolar coupling as a function of the pump $\pi$ pulse. The intensity of the refocused spin echo is plotted as a function of $t$. The stronger the dipolar coupling; the more oscillations are observed in the DEER signal. However, the DEER signal is attenuated by phase memory time $T_m$ or the transverse relaxation time $T_2$. The effects of relaxation decay are reduced by decreasing the absolute temperature to approximately 80 K (Eaton et al. 2002). Distance information is obtained through the Fourier transformation of the dipolar Pake spectrum. The relationship between experimental DEER time domain data and the corresponding distance distributions between spins is described by a Fredholm integral equation, which must be approximated through Tikhonov regularization (Weese 1992; Banham et al. 2008). The Tikhonov regularization method requires the appropriate regularization parameter, in order to obtain a unique fit for the data. Otherwise, the distance distributions will contain spurious peaks corresponding to unrealistic distances.

# CHAPTER III

# EXPERIMENTAL METHODS

## Hsp27 Gene Cloning and Site-directed Mutagenesis

The cDNA of human HSP 27 was obtained from Enzo Life Sciences (Plymouth Meeting, PA). The cDNA of HSP 27 was cloned into the NdeI and XhoI sites of the pET20b+ expression vector (Novagen, California, USA). Wild-type HSP 27 has a native cysteine at residue 137 which was substituted by alanine using the QuikChange Mutagenesis Kit (Stratagene, La Jolla, CA). The new construct containing the C137A substitution is referred to as HSP 27_WT*. The phosphorylation mimic of HSP 27 has three serine residues that were substituted for aspartates using the QuikChange Mutagenesis Kit. The resulting construct is referred to as HSP 27_D3*. Seven clusters of residues were chosen for analysis: cluster 1 (residues 2-6), cluster 2 (residues 16-23), cluster 3 (residues 24-35), cluster 4 (residues 36-40), cluster 5 (residues 50-55), cluster 6 (residues 52-67), and cluster 7 (residues 73-80). Single cysteine mutants were made for all residues within each cluster utilizing either Hsp 27_WT* or Hsp 27_D3* as backgrounds. All cysteine mutants were confirmed by sequencing at the Vanderbilt DNA Sequencing Facility.

**Protein Expression and Purification**

The plasmids containing HSP 27 cysteine mutants were transformed into BL21 Gold (DE3) E. coli competent cells (Stratagene, La Jolla, CA). HSP 27 mutants were overexpressed by autoinduction (Studier 2005). A single colony was inoculated into 2mL of minimal non-inducing medium (MDG) (1M $MgSO_4$, 40% glucose, 25% aspartate, 50mM $PO_4$, 50mM $NH_4Cl$, 5mM $Na_2SO_4$, 1M Citrate, 0.1M $FeCl_3$) and incubated for 8 hours at 37$^oC$ with shaking at 300rpm. MDG was inoculated into ZYM medium (1M $MgSO_4$, 0.5% glycerol, 0.05% glucose, 0.2% $\alpha$-lactose, 50mM $PO_4$, 50mM $NH_4Cl$, 5mM $Na_2SO_4$, 1M Citrate, 0.1M $FeCl_3$) and incubated overnight at 30$^oC$ with shaking at 300rpm.

Cells were harvested by centrifugation at 4000 x g for 20 minutes. The cell pellets were resuspended in lysis buffer (20mM Tris, 75mM NaCl 1mM EDTA, 0.02% azide) supplemented with 10mM DTT, 10$\mu$M PMSF, and 0.05% polyethyleneimine. The cells were sonicated and the lysates were centrifuged at 12,000 x g for 20 minutes. Mutants were purified by anion exchange chromatography and eluted with a NaCl gradient. For Hsp27_D3 mutants ammonium sulfate was added to each eluted fraction to yield a final concentration of 0.5M. Each Hsp27 protein sample was injected onto a Hi Trap phenyl HP column (GE Healthcare Life Science, Piscataway, NJ, USA) and eluted with a gradient of 0.5M to 0M ammonium sulfate.

All protein samples were further purified by size exclusion chromatography (SEC) on a Superose 6 column (GE Healthcare Life Science, Piscataway, NJ, USA) (Fig. 13). Each sample was incubated with 10-fold molar excess of either 1-oxyl-2,2,5,5-tetramethyl-△3-pyrroline-3-methyl-methanethiosulfonate (Toronto Research Chemicals, Ontario, Canada) or 3-(2-Iodoacetamide)-proxyl spin label (Sigma-Aldrich, St. Louis, MO, USA). The spin labeling reaction was allowed to proceed for 2 hours at room temperature with subsequent completion overnight at 4$^{o}$C. Excess label was removed by desalting on a Hi Trap desalting column (GE Healthcare Life Science, Piscataway, NJ, USA).

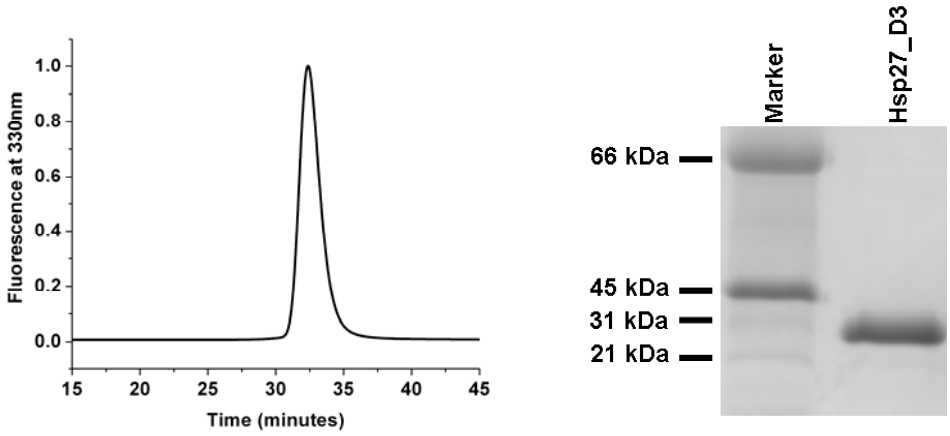


**Figure 13: Purified Hsp27_D3.** Left panel is the gel filtration profile. The right panel is the SDS-PAGE gel of purified Hsp27_D3 stained with comassie blue.

**Electron Paramagnetic Resonance (EPR)-Continuous Wave (CW)**

X-band (9.8 GHz) CW-EPR spectra was acquired on a Bruker EMX spectrometer equipped with a super High Q cavity (Bruker Biospin, Billerica, MA) at room temperature. Spin labeled samples of 1mM to 10μM concentrations were prepared in 9/6-buffer (9mM Mops, 6mM Tris, 50mM NaCl, 0.1mM EDTA, 0.02% Azide) at pH 7.2. Samples were inserted into round 25μL or 50μL glass capillaries (VWR, West Chester, PA) and sealed with Cha-seal (Chase Scientific, Rockwood, TN). EPR spectra were acquired with a magnetic field sweep width of either 150 or 200 Gauss and 5mW incident power. The Zeeman modulation amplitude was 1.6 G. The spectra was analyzed and processed with the WinEPR program (Bruker, Biospin, Billerica, MA) and HMEPR version 4 written by Richard Stein (Vanderbilt University).

**Power Saturation Measurements**

Spin labeled Hsp27 mutants, 50 μM and 25 μM concentration, were loaded into gas-permeable TPX capillaries (Medical Advances, Wisconsin, USA). Power saturation measurements were performed on a Varian E102 spectrometer (Varian, Palo Alto, CA) equipped with a two-loop one gap resonator. The field scan of the central resonance line for each sample was carried out at 20 Gauss.

The amplitude of the central resonance line was obtained with the following microwave powers: 1, 2, 3, 4, 9, 16, 25, 36, 49, 64 mW. The measurements were done under nitrogen, in the presence of 20% molecular oxygen or 3 mM NiEDDA. The experimental data was collected and analyzed by non-linear curve-fitting software (OriginLab Corporation, Massachusetts, USA) to obtain the spectral amplitude (A) versus the square root of the microwave power

According to the following equation (Altenbach et al., 2005)

$$A = \frac{I\sqrt{P}}{\left(1 + \frac{\left(2^{\frac{1}{\varepsilon}} - 1\right)P}{P_{1/2}}\right)^{\varepsilon}}$$

where A is the peak-to-peak amplitude of the central line; $I$ and $\varepsilon$ are adjustable parameters; $P_{1/2}$ is the half-saturation power; and P is the power of the incident electromagnetic wave. The NiEDDA and oxygen accessibility ($\Pi$) were calculated by the following equation:

$$\Pi = \frac{\left(\frac{\Delta P_{1/2}}{\Delta H_o}\right)}{\left(\frac{P_{1/2}^{\mathrm{T4L}}}{\Delta H_o^{\mathrm{T4L}}}\right)}$$

where P is the accessibility, $\triangle P_{1/2}$ is the difference of the half saturation power in the presence and absence of paramagnetic reagents (3mM NiEDDA or 20% molecular oxygen).

$P_{1/2}^{T4L}$ is the T4L half saturation power in the absence of paramagnetic reagent. T4L served as a reference for normalization due to variations in the resonance frequency, and $\triangle H_o$ is the central line width.

**Size Exclusion Chromatography (SEC)**

Analytical SEC was performed on a Superose 6 column (GE Healthcare Life Sciences, Piscataway, NJ) with a separation range of 5 kDa to 5000 kDa. The Superose 6 column was connected to an Agilent 1100 chromatography system with scanning fluorescence and absorption detectors. The column was equilibrated in 9/6-buffer (9mM Mops, 6mM Tris, 50mM NaCl, 0.1mM EDTA, 0.02% Azide) at pH 7.2. Samples were prepared at 1 mg/mL, .05 mg/mL, 15 μg/mL concentrations with 100μL injected at 0.5 mL/min. Absorbance was recorded at 280 nm. Tryptophan fluorescence was detected at an excitation wavelength of 280 nm and an emission wavelength of 330 nm. For molar mass determination, a multi-angle laser light scattering detector (Wyatt Technologies, Santa Barbara, CA) was connected in line with the absorption detector. The signal at the 90° angle was analyzed to obtain molar mass values.

**Binding of Destabilized T4L Mutants to the Phosphorylation Mimic of Hsp27**

For binding experiments, 50μM or 25μM spin labeled Hsp27 on the phosphorylation mimic background was incubated with 25μM or 12.5μM T4L (Hsp27:T4L ratio of 2:1) or (Hsp27:T4L ratio of 1:1) at 37°C for 2 hours.

Binding experiments were carried out in SEC buffer at pH 7.2. Hsp27:T4L complexes were both monitored and purified by SEC on a Superose 6 column. This SEC purification step ensured the removal of uncomplexed Hsp27 and T4L. Purified complexes were concentrated to 50μL for further analysis. CW-EPR spectral analysis was performed on a Bruker EMX spectrometer and power saturation experiments were performed on a Varian E102 spectrometer in the presence of 3mM NiEDDA. Following EPR analysis, further confirmation of complex formation was carried out by SDS-PAGE on a 15% acrylamide gel which was stained with Coomassie Blue.

**Fluorescence Binding Measurements**

Samples for binding reactions contained 6μM of bimane-labeled T4L-D70N mutant. The T4L-D70N mutant was labeled at residue 151. Hsp27_D3 and Hsp27_TR mutants, with varying concentrations over the 180μM to 1μM range, were incubated at 37$^{o}$C for 2 hours. Fluorescence intensity was measured by a Photon Technology International (PTI) L-format spectrofluorometer. The spectrofluorometer has a RTC2000 temperature controller with a sample holder controlled by a Peltier heater/cooler. Fluorescently labeled binding reactions were excited at 380 nm, and the resulting fluorescence emission spectra were recorded over a 420 nm to 500 nm range. The binding isotherms were analyzed using Origin 7.5 (OriginLab Corporation, Massachusetts, USA). The Levenberg-Marquart method was used for non-linear least-square fits.

# CHAPTER IV

## The Role of the N-terminal Domain in Hsp27 Oligomer Assembly and Dissociation

### Rationale

Mammalian sHsps exhibit distinctive structural and dynamic characteristics. In particular, Hsp27 forms polydisperse oligomers capable of equilibrium dissociation; in fact, Hsp27 readily exchanges its oligomeric subunits (Bova et al. 2000). This structural and dynamic behavior is correlated with the architecture of the $\alpha$-crystallin and N-terminal domains. The $\alpha$-crystallin domain specifies interactions capable of assembling dimers into the native oligomer (Merck et al. 1993; Berengian et al. 1999). Global dimer assembly and oligomer dynamics are under the control of the N-terminal domain (Berengian et al. 1999; Lambert et al. 1999). Studies in which the N-terminal domain was deleted provide further evidence in support of this model. Isolated $\alpha$-crystallin domains assemble into dimers incapable of further subunit exchange (Bova et al. 2000).

The polydispersity and dynamic nature of the Hsp27 oligomer is related to its chaperone activity (Shashidharamurthy et al. 2005). Hsp27 is regulated by N-terminal domain phosphorylation, which is important for its role in signal transduction (Stokoe et al. 1992; Yuan and Rozengurt 2008). Phosphorylation induces changes in the size and mass distribution of oligomers (Rogalla et al. 1999). Therefore, phosphorylation is an important modulator of Hsp27 chaperone activity (Theriault et al. 2004; Shashidharamurthy et al. 2005).

Since phosphorylation sites are located within the N-terminal domain, it stands to reason that this domain would be important for oligomer stability (Lambert et al. 1999; Theriault et al. 2004; Shashidharamurthy et al. 2005). The structural basis of this stability is not well understood. The dynamic nature of the Hsp27 oligomer is a major detriment to high resolution structural analysis.

A unique feature of Hsp27 is its ability to dissociate into discrete dimeric species at low protein concentrations. Phosphorylation shifts this concentration dependent dissociation equilibrium in favor of the dimer, over a range of protein concentrations (Shashidharamurthy et al. 2005). For instance, dissociation of the Hsp27 oligomer to the dimer is accompanied by an increase in affinity for destabilized substrate (Shashidharamurthy et al. 2005). In contrast, N-terminal mutations that stabilize the large oligomer reduce affinity for substrate (Shashidharamurthy et al. 2005). Hence, phosphorylation must produce conformational changes in the N-terminal domain that affect equilibrium dissociation to the binding competent dimer.

In this chapter, the structural role of the N-terminal domain in oligomer assembly and the phosphorylation induced conformational changes that result in oligomer dissociation were analyzed by site-directed spin labeling EPR. Seven clusters of residues along the N-terminal domain of Hsp27 were selected for analysis of EPR lineshapes (Fig. 14). Cluster 1 includes residues 2-6, cluster 2 residues 16-23, cluster 3 residues 24-29, cluster 4 residues 30-41, cluster 5 residues 50-55, cluster 6 residues 61-67, and cluster 7 residues 73-80.

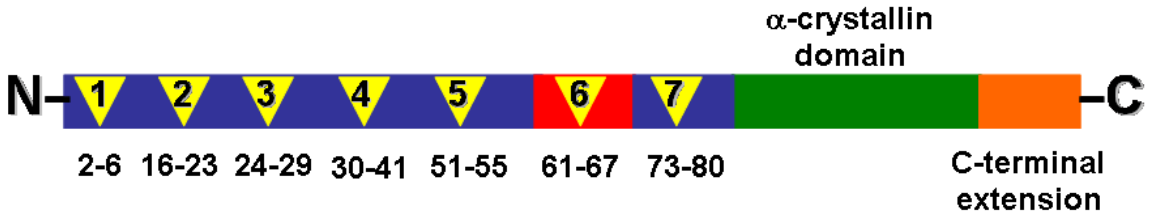


**Figure 14. The seven clusters of N-terminal residues chosen for EPR analysis.** The residues are represented underneath the corresponding triangles. The N-terminal domain is in blue, the P1 peptide (residues 58-70) is represented by the red box, the α-crystallin domain is in green, and the orange box represents the C-terminal extension.

Each cluster was selected to sample different regions along the N-terminal domain in both the native oligomer (wild-type background) and the phosphorylation mimic (where the S15D, S78D, and S82D mutations are present). The environment of the N-terminal domain was determined by analyzing spin labeled mutants for changes in EPR lineshape and solvent accessibility.

### The N-terminal Domain of Hsp27 is Important for Substrate Binding

The polydisperse Hsp27 oligomer undergoes equilibrium dissociation from an ensemble of oligomers with an average molecular mass of 426 kDa to a dimer. High protein concentrations shift the concentration-dependent equilibrium in favor of the large ensemble of oligomers (Shashidharamurthy et al. 2005). On the other hand, phosphorylation favors dissociation to the dimer. To study the effect of phosphorylation, the phosphorylatable serines 15, 78, and 82 were substituted by negatively charged aspartate residues (Rogalla et al. 1999; Shashidharamurthy et al. 2005).

The molecular mimicry approach stabilizes the dimeric form to minimize the heterogeneous nature of the phosphorylation reaction. This phosphorylation mimic is referred to as Hsp27-D3. Based upon structural and biophysical studies with Hsp16.5 and Hsp16.9, the N-terminal domain is located within a relatively solvent-inaccessible environment (Kim et al. 1998; van Montfort et al. 2001; Koteiche et al. 2005; Shi et al. 2006a). It is likely that in this low dielectric environment, unpaired charges will destabilize sHsps oligomers. At comparable protein concentrations, wild-type Hsp27 (Hsp27-WT) assembles into an ensemble of large oligomers while Hsp27-D3 is a dimer.

Based upon extensive binding studies with destabilized T4L mutants, the minimalist model describes the chaperone activity of Hsp27 (Fig. 15) (Shashidharamurthy et al. 2005; Koteiche and Mchaourab 2006; Mchaourab et al. 2009).

$$\mathbf{N \rightleftharpoons I_1 \rightleftharpoons \ldots\ldots \rightleftharpoons I_i \rightleftharpoons U} \quad (1)$$

$$\underset{\text{Oligomer}}{\text{Hsp27}} \rightleftharpoons \underset{\text{Competent Dimer}}{\text{Binding}} \quad (2)$$

$$\underset{\text{Competent Dimer}}{\text{Binding}} + \begin{pmatrix} I_1 \\ \vdots \\ U \end{pmatrix} \rightleftharpoons \begin{pmatrix} C_1 \\ \vdots \\ C_U \end{pmatrix} \quad (3)$$

**Figure 15. The minimalist model of Hsp27 binding to substrate.** Equation (1) describes the unfolding equilibrium for the substrate in the partially (I) and globally unfolded (U) states. Equation (2) is the activation equilibrium describing the dissociation of the Hsp27 oligomer to the binding competent dimer. It is worthy to note that equation (2) is modulated by protein concentration and phosphorylation. Equation (3) describes the subsequent reassembly to a Hsp27/substrate complex (C), following the binding of partially (I) and globally unfolded substrate (U).

The model couples three thermodynamic equilibria that describe the unfolding of the substrate (1), the dissociation of the Hsp27 oligomer to binding competent dimers (2), and the binding of the dimer to partially or globally unfolded states (3). Substrate binding results in reassembly to an Hsp27/substrate complex. Experiments in favor of this model confirm that a shift in the equilibrium toward the dimer (equation 2) enhances the apparent affinity for destabilized T4L mutants (Shashidharamurthy et al. 2005). The direct detection of the Hsp27/substrate complex by SEC is a measure of further confirmation of substrate binding.

In order to determine the role of the N-terminal domain in substrate recognition and binding, the affinity of Hsp27-D3 was compared with the dissociated form of Hsp27, lacking an N-terminal domain (Fig. 16). Residues 2 to 87, of the N-terminal domain of Hsp27, were deleted to form Hsp27-trunc. A crystal structure of an N-terminal truncation of Hsp27 was recently determined (Baranova et al. 2011). Hsp27-trunc is a tetramer that is in concentration-dependent equilibrium with smaller species. The masses of Hsp27-D3 and Hsp27-trunc are similar. This contribution is independent of their oligomeric state. The destabilized mutant T4L-D70N was used as a model substrate, for comparison of binding characteristics of Hsp27-D3 and Hsp27-trunc. The D70N mutant has the $Asp^{70}$ replaced by an $Asn^{70}$, and the $\triangle G_{unf}$ for D70N is reduced relative to wild- type T4L (Mchaourab et al. 2002). The T4L-D70N mutant has a $Cys^{151}$ where a bimane label was attached.

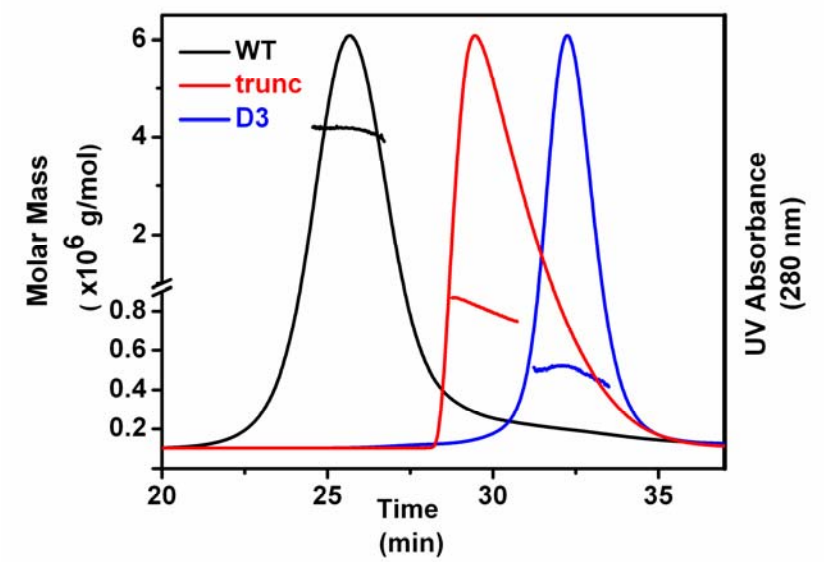


**Figure 16. The distribution of molar mass and the UV absorption profile corresponding to Hsp27-WT (WT, black), Hsp27-trunc (trunc, red), and Hsp27-D3 (D3, blue).** All molar mass values are indicated as solid lines across the UV absorbance peaks

The change in intensity of the bimane label is a reflection of binding. It has been previously reported in the literature that Hsp27-D3 had a significantly higher apparent affinity for T4L-D70N than Hsp27-WT (Shashidharamurthy et al. 2005). According to the binding isotherms shown in Figure 17, truncation of the N-terminal domain attenuates binding to T4L-D70N. Therefore, dissociation of the large oligomer is necessary for substrate binding.

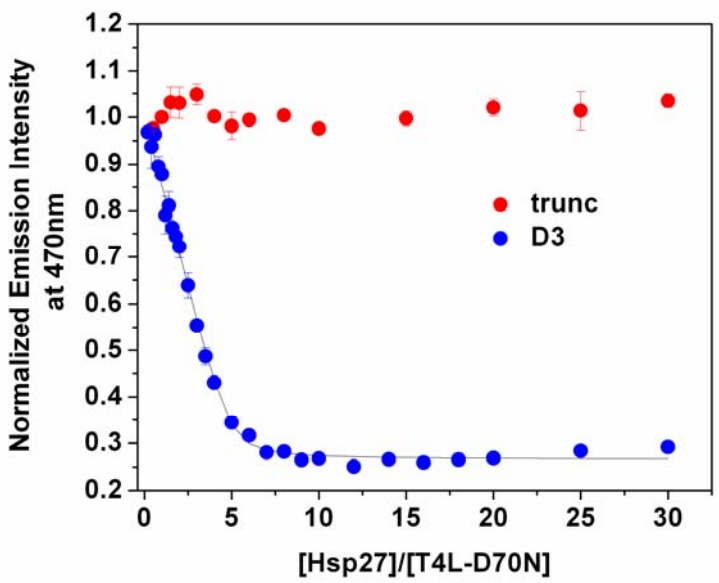


**Figure 17. Isotherms for binding of Hsp27-trunc and Hsp27-D3 to T4L-D70N.** The concentration of bimane labeled T4L-D70N was 6 μM. Non-linear least squares fits to the data are represented by solid lines. The Hsp27-D3 binding parameters are n = 0.20 ± 0.02 and $K_D$ = 0.07 ± 0.04 μM where n is the number of binding sites and $K_D$ is the apparent dissociation constant. Each isotherm was generated at pH 7.2 and 37°C.

### Phosphorylation induces exposure of the N-terminal domain

Since the N-terminal domain is important in substrate binding, this domain must undergo a structural change after the transition from the large ensemble of oligomers to the dimer. To determine the structural consequence of dissociation, spin labels were introduced within the seven clusters along the N-terminal domain (Fig. 14). Each cluster contains a single cysteine substitution in both the wild-type (Hsp27-WT) and phosphorylation mimic (Hsp27-D3) backgrounds.

For representative sites, EPR spectra in the large ensemble of oligomers (Hsp27-WT) were compared to spectra in the dimer (Hsp27-D3) (Fig. 18, Appendix A1-A9).

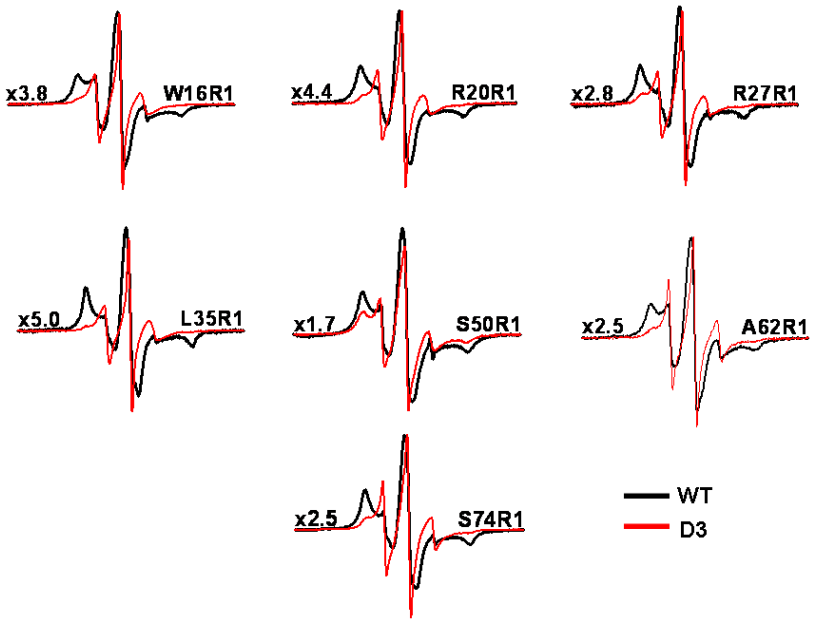


**Figure 18. Representative EPR spectra for spin labeled N-terminal Hsp27-WT and Hsp27-D3.** Spectra in black traces are spin labeled Hsp27-WT residues acquired at 100 μM concentration, while spectra in red are the corresponding spin labeled Hsp27-D3 residues at 50 μM concentration. The spectra of the Hsp27-WT mutants were scaled by the factor to the left of the spectrum for ease of presentation.

In the black trace, EPR lineshapes are characterized by dominant spectral component indicative of slow spin label motion. This type of lineshape is observed at sites buried within the protein's hydrophobic core or at subunit interfaces (Mchaourab et al. 1996). The occurrence of motionally restricted spectra is an indicator that the N-terminal domain is located in a buried environment. Furthermore, the N-terminal domain is involved in extensive subunit contacts within the large oligomer.

On the other hand, EPR lineshapes from spin labels at the equivalent sites in Hsp27-D3 have features indicative of less restricted spin label motion (Fig. 18, red traces). These spectra are similar to those observed at protein surface sites (Mchaourab et al. 1996). Therefore, dissociation to the dimer attenuates the steric restriction (observed in the large oligomer) over large segments of the N-terminal domain.

For spin labeled residues 61-67 and 73-80 in Hsp27-D3, the width of the central resonance line is an indicator of large amplitudes of motion in the backbone (Fig. 19). This lineshape is similar to that observed for unfolded proteins or short unstructured peptides (Mchaourab et al. 1996). The corresponding EPR spectra in the WT background indicates highly restricted motion of the spin labels consistent with a buried environment in the large oligomer. Figure 20 displays EPR spectra for representative residues 62, 63, 74, and 76 in Hsp27-WT. The corresponding EPR spectra in the WT background displays more restricted motion of the spin labels consistent with a more buried environment in the large oligomer. Comparison of Figures 19 and 20 implies that after dissociation, the backbone loses ordered secondary structure and becomes highly flexible. This result supports previous data from our laboratory, where residues 58-70, also referred to as the P1 peptide, are implicated in the dynamic dissociation of Hsp27 (Shashidharamurthy et al. 2005). When the P1 peptide is deleted, the large oligomer is stabilized and affinity for T4L is reduced (Shashidharamurthy et al. 2005)

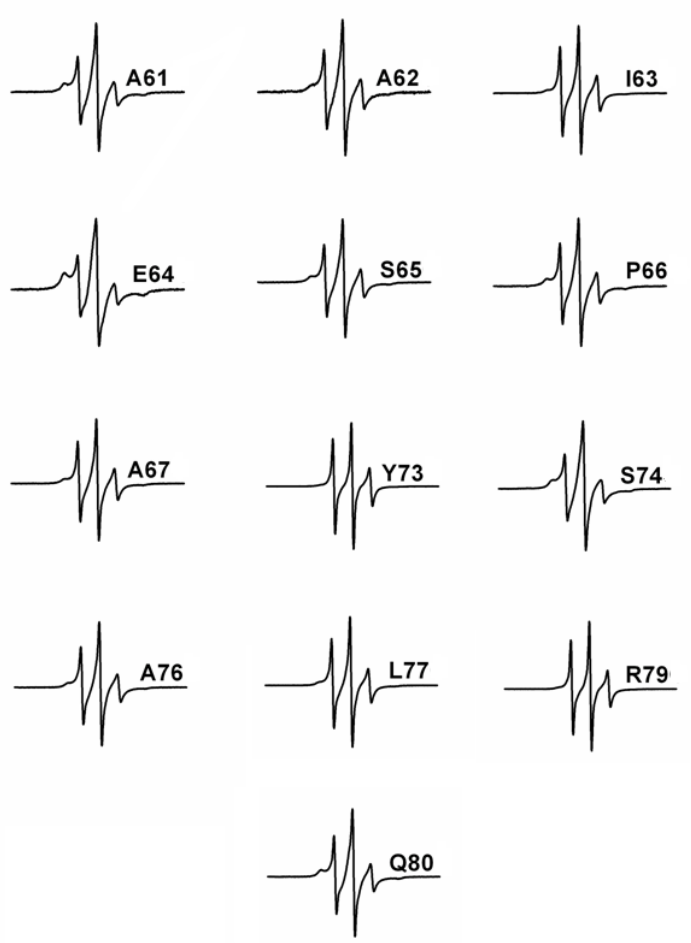


**Figure 19. Spectra for spin labeled residues 61 to 67 and 73 to 80 on Hsp27-D3 at 50μM concentration**


**Figure 20. Spectra for spin labeled residues 62, 63, 74, and 76 on Hsp27-WT at 100μM.**

The spectral features observed in the Hsp27-D3 background indicate significant conformational changes occur in the N-terminal domain after oligomer dissociation. The spectral lineshape can be partially or completely reversed by increasing the protein concentration. For instance, increasing the protein concentration selectively enhance the spectral component corresponding to restricted motion of the spin label (Fig. 21 and Appendix A11-A16). At intermediate Hsp27-D3 concentrations, the EPR lineshapes reflect at least two components. One of these components is motionally restricted (immobilized) and the other is mobile, which reflects the equilibrium between oligomers and dimers respectively (Fig. 21, Equation 2 of Fig. 15). In addition, changing the pH from 7.2 to 6.5 shifts the equilibrium toward the large oligomers (decreasing pH promotes oligomer reassembly in Hsp27-D3) (Appendix A17-A20).

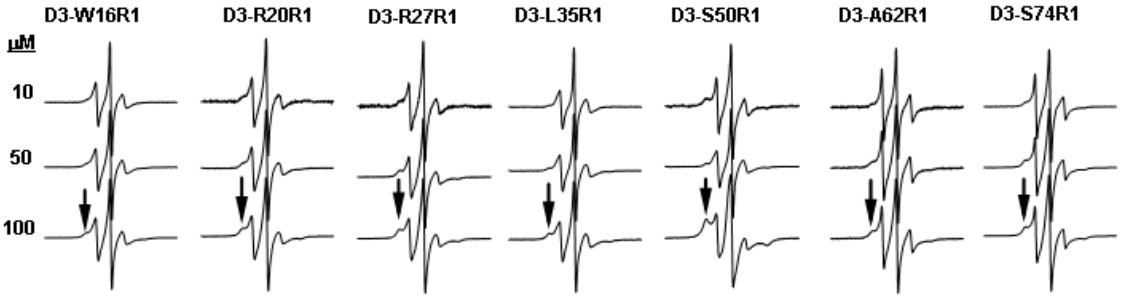


**Figure 21. Representative spin labeled Hsp27-D3 residues displaying the concentration dependence of the EPR lineshape.** The motionally restricted component represents dimer reassembly into the large oligomer (arrow).

The fraction of oligomers or dimers was plotted by measuring the amplitude of the immobile (representative of oligomeric population) and mobile (representative of dimeric population) spectral components over a 1600 μM to 10 μM concentration range (Fig. 22).

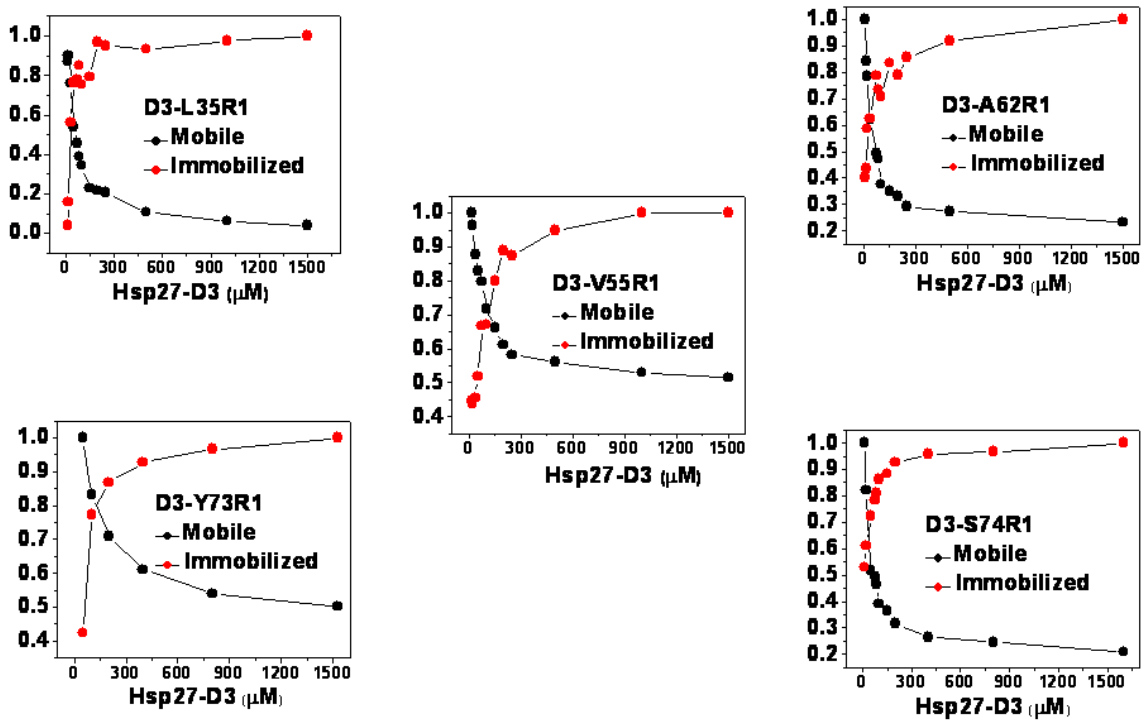


**Figure 22. Titration curves displaying the fraction of mobile (dimer) and immobile (oligomer) components as a function of protein concentration.**

All the titration curves show dimer reassembly into the larger oligomers; however, the titration curves are shifted relative to each other. There are two possible reasons for this shift: substitution of the original residue by cysteine and the attachment of spin label at that specific residue position. Taken together these results indicate that the dissociation equilibrium can be recapitulated in the phosphorylation mimic (Hsp27-D3). A distinct advantage to the phosphorylation mimicry approach is that phosphorylation-mimicking mutations shift the transition between the large oligomer and the dimer, into a concentration range that can be studied by EPR.

### Dissociation Does Not disrupt the α-crystallin Domain Dimer

The structural changes observed in the N-terminal domain were revealed through changes in spin label mobility (Figs. 18, 19, 20, and 21). In variance with the N-terminal domain, EPR lineshapes at selected residues in the α-crystallin domain remain unchanged between Hsp27-WT and Hsp27-D3. The α-crystallin domain dimer interface, which encompasses residues 135-144, was previously identified by spin labeling and confirmed by crystal structures of αB-crystallin, Hsp20, and Hsp27 (Berengian et al. 1999; Bagneris et al. 2009; Baranova et al. 2011). In the phosphorylation mimic (Hsp27-D3), this dimer interface remains intact. Dipolar broadened EPR lineshapes are observed, along the dimer interface, in Hsp27-WT. This type of spectral feature indicates that spin labels located across the interface are less than 8Å apart (Berengian et al. 1999). $Cys^{137}$ is a residue located within the dimer interface, and spin labeling this residue shows dipolar broadening remains in Hsp27-D3 (Fig. 23). Additionally, the dipolar broadened lineshape observed in Hsp27-D3 is not concentration-dependent (Fig. 23). Hence, dissociation disrupts interfaces in the N-terminal domain, but the α-crystallin domain dimer interface remains intact. A crystal structure of the Hsp27 α-crystallin domain was recently determined (Baranova et al. 2011). The seven β-strand fold previously identified in structures of truncated lens sHsps, αA- and αB-crystallin is conserved as expected based on the high sequence similarity between mammalian sHsp (Bagneris et al. 2009).

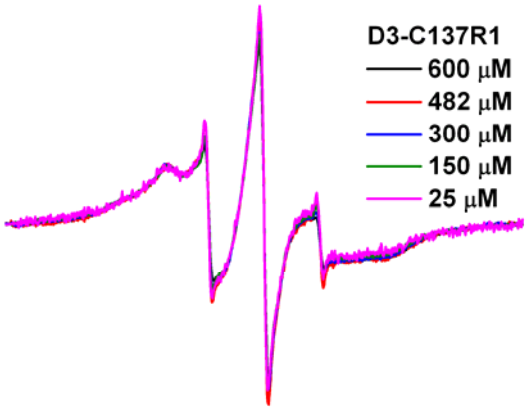


**Figure 23. EPR spectrum of spin labeled Cys$^{137}$ in Hsp27-D3.** Dipolar broadening is the result of spin-spin interactions across the α-crystallin domain dimer interface.

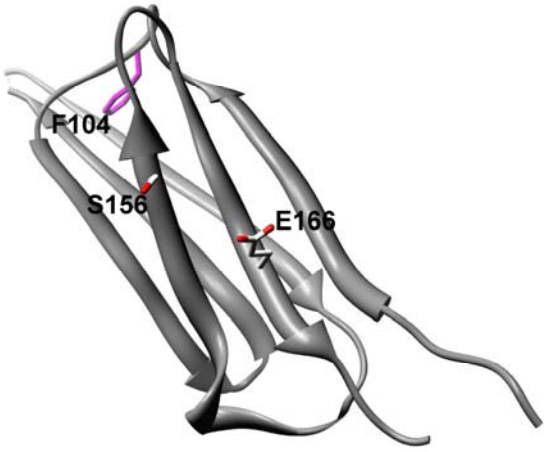


**Figure 24. Ser$^{156}$, Glu$^{166}$ and Phe$^{104}$ mapped on the recently determined α-crystallin domain crystal structure of Hsp27 adapted from Baranova et. al. 2011**

The residue pair Ser$^{156}$ and Glu$^{166}$ was spin labeled, in order to obtain information about the proximity of two β-strands within the α-crystallin domain (Fig. 24). In the spin labeled Ser$^{156}$/Glu$^{166}$ double mutant, dipolar broadening indicates that Hsp27 oligomer dissociation to the dimer does not alter the fold of the α-crystallin domain.

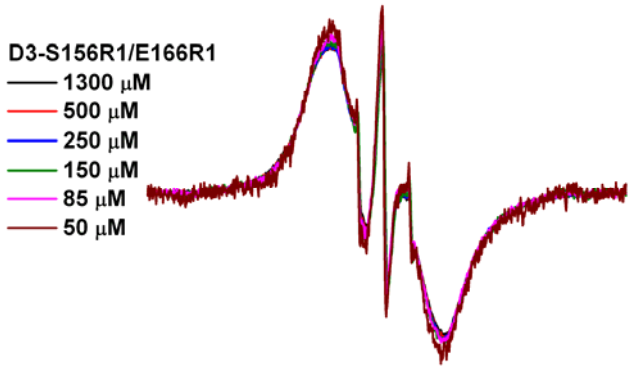


**Figure 25. Dipolar broadening of the spin labeled Ser$^{156}$/Glu$^{166}$ double mutant.** The broadened lineshape indicates that spin labels are located on two β-strands which are in close proximity. The scan width was 250 G.

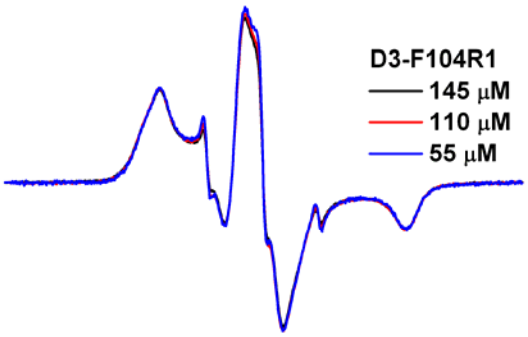


**Figure 26. Spin labeled Phe$^{104}$ with an immobilized lineshape over both high and low concentration.**

Phe$^{104}$ is located within the α-crystallin domain core with an immobilized EPR lineshape, regardless of concentration (Figs. 24, 26). The EPR data provides further evidence that dissociation causes structural changes within the N-terminal domain that are not propagated to the C-terminus.

**Substrate-induced reassembly of Hsp27-D3 sequesters the N-terminal domain**

As reported by the EPR lineshape data, phosphorylation induced dissociation causes the N-terminal domain to transition to a less sterically restricted environment. The spectra of residues spin labeled in Hsp27-D3 show increased backbone dynamics accompany dissociation to the dimer. Additional insight into the environment of the N-terminal domain after dissociation was obtained by measuring the collision frequency between the spin label and paramagnetic reagent NiEDDA. Direct collision between the spin label and NiEDDA reduces the spectral amplitude, which is correlated with a reduction in spin label relaxation time (refer to power saturation section of EPR chapter). NiEDDA is soluble in the aqueous phase with little solubility in the hydrophobic core of proteins (Altenbach et al. 2005). At representative sites within the N-terminal domain, oligomer dissociation results in an increase in NiEDDA accessibility (Fig. 27). The accessibility values are in correspondence with those observed for spin labels on the exposed surface of monomeric water soluble proteins (Altenbach et al. 2005). Spin label accessibility of NiEDDA varies with local environment of the spin labeled site, presumably due to steric restraints imposed by neighboring residues. Increasing Hsp27-D3 protein concentration from 25 μM to 50 μM reduced NiEDDA accessibility, which suggests an increase in the population of large oligomers (Fig. 28). Spin label accessibility is also a function of the amount of NiEDDA with increasing concentrations producing greater effects (Appendix, A10).

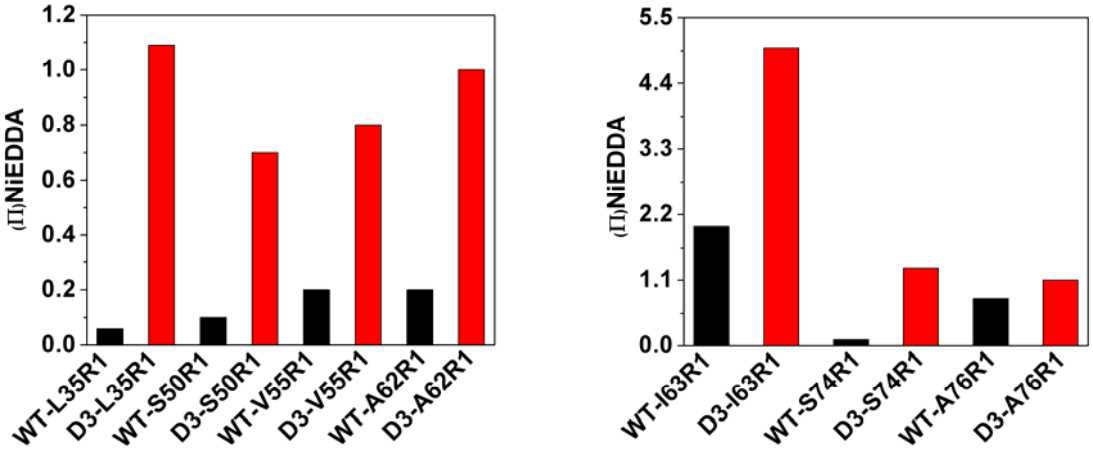


**Figure 27. The accessibility of spin labeled sites to NiEDDA in both Hsp27-WT (black) and Hsp27-D3 (red).** The protein concentration was 25 μM except for S50R1 which was 50 μM. The concentration of NiEDDA was 3 mM except for I63R1 which was acquired at 10 mM.

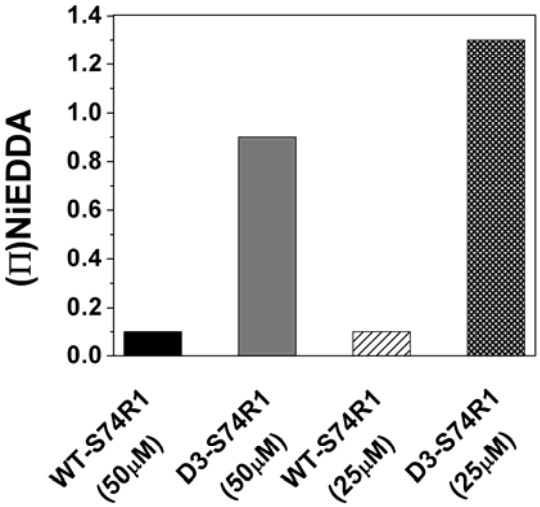


**Figure 28. The effect of increasing concentration on NiEDDA accessibility.** The concentration of NiEDDA was 3 mM.

SEC shows substrate binding causes Hsp27-D3 to reassemble into the large oligomer (Shashidharamurthy et al. 2005). Spin labeled Hsp27-D3 mutants were incubated with T4L-L99A/A130S, a destabilized mutant of T4L, in order to determine the environment of the N-terminal domain in the chaperone/substrate complex. T4L-L99A/A130S has been shown to bind in both low and high affinity modes (Mchaourab et al. 2002; Shashidharamurthy et al. 2005). EPR analysis shows that binding of destabilized T4L mutants to Hsp27-D3 results in spectral lineshapes indicative of steric restriction (Fig. 29).

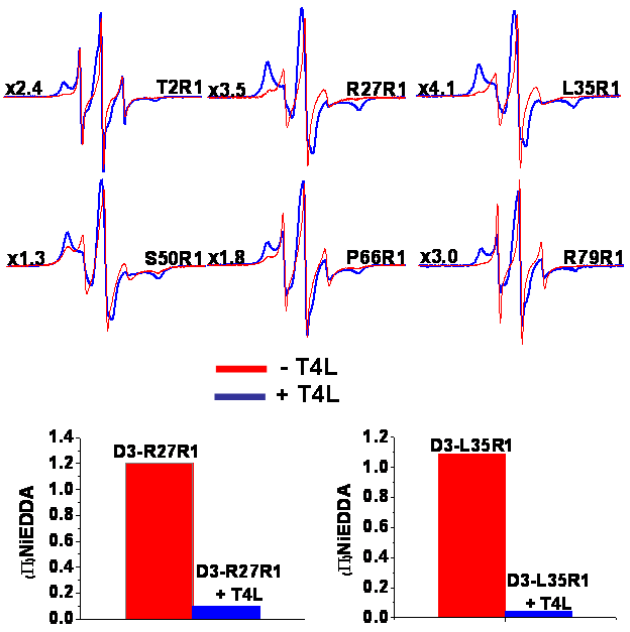


**Figure 29. EPR spectra and NiEDDA accessibility after binding T4L to spin labeled Hsp27-D3.** An increase in spin label mobility and NiEDDA accessibility is observed prior to T4L binding (red). After T4L binding, spin labeling motion is restricted and NiEDDA accessibility is reduced. The spectra were scaled by the factor to the left of the spectrum for ease of presentation.

Binding of T4L to spin labeled T4L mutants was confirmed by SEC and SDS-PAGE (Appendix, A21 & A22). These lineshapes are similar to ones previously observed for spin labeled Hsp27-WT mutants (Figs. 18, 20). However, subtle changes in spin label mobility are a reflection of the local environment of the spin label site, within the Hsp27/T4L complex. Concurrent to the lineshape change, after destabilized T4L mutant binding, the accessibility of NiEDDA is decreased (Fig. 29). Therefore, binding of T4L shifts the thermodynamic equilibrium of Hsp27-D3 in favor of oligomer reassembly into an Hsp27/T4L complex.

**N-terminal sequence determinants of equilibrium dissociation.**

The substitution of the endogenous residue for a cysteine or the incorporation of a spin label can shift the Hsp27 oligomer equilibrium (Fig. 22). There are spin labeled residues such as $Asp^{17}$, $Asp^{21}$, $Pro^{24}$, $Ser^{26}$, $Asp^{30}$, $Pro^{36}$, $Arg^{37}$, $Leu^{37}$, $Pro^{39}$, $Glu^{40}$, and $Glu^{41}$, in the Hsp27-D3 background, where the EPR lineshape shows restricted spin label motion regardless of concentration. Figure 30 shows EPR spectra at representative sites. This type of lineshape is similar to that observed for spin labeled residues in Hsp27-WT. In these residues, (spin labeled Hsp27-D3 mutants that display restricted spin label motion) it is apparent that the cysteine substitution and subsequent labeling favor the large oligomeric species.

These results are particularly puzzling, because the S15D, S78D, and S82D mutations, in the phosphorylation mimic background (Hsp27-D3), normally favor dissociation of the oligomer to the dimer. In general, reassembly of Hsp27-D3 to the large oligomer occurs at high protein concentrations. Therefore, it is apparent that these results highlight residues or structural elements important in stabilizing the large oligomer.

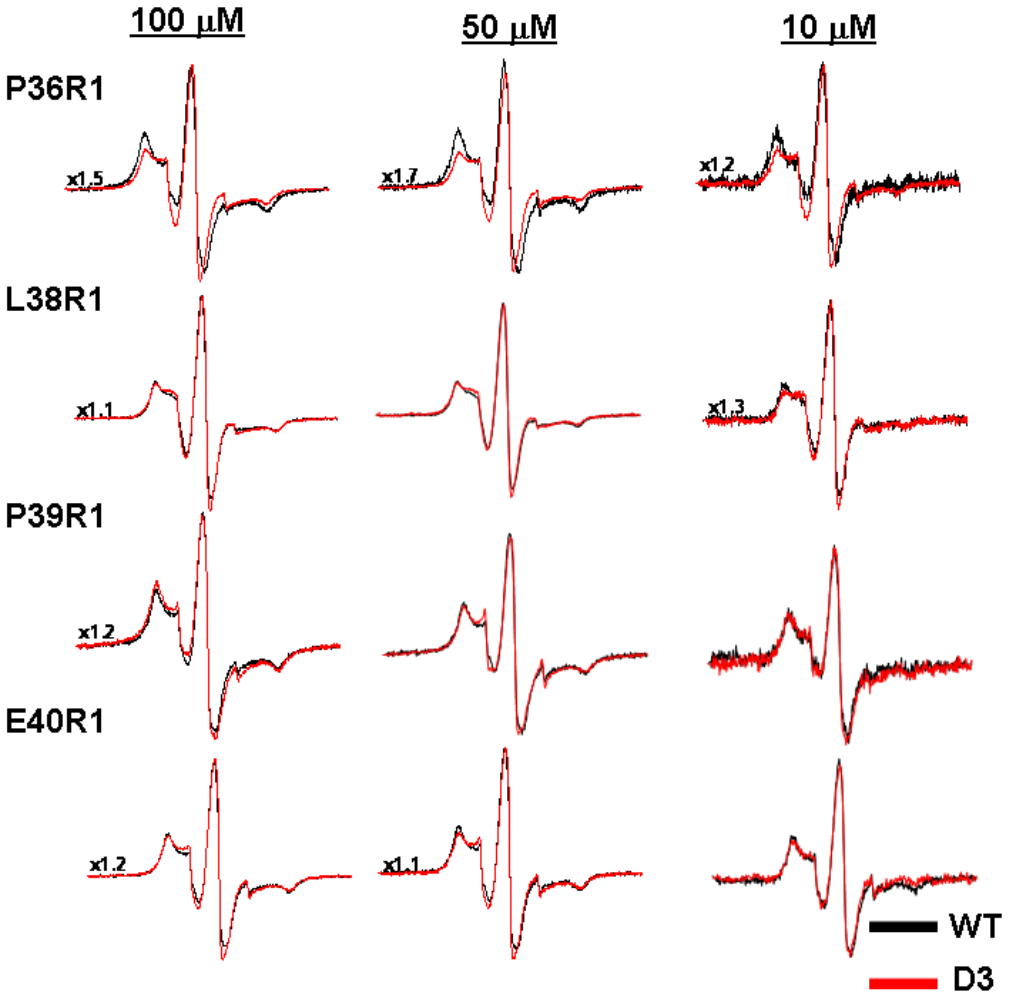


**Figure 30. Spin labeled mutants that display restricted spin label motion in both the wild-type and phosphorylation mimic backgrounds.** EPR spectra corresponding to the spin labeled Hsp27-WT mutants are displayed in black and Hsp27-D3 mutants in red. The spectra were scaled by the factor to the left of the spectrum for ease of presentation.

To further examine both the role of the chemical identity and structural context of these residues in the equilibrium dissociation of Hsp27, cysteine mutants and their corresponding spin labeled counterparts were analyzed by EPR and SEC (Appendix, A11-A16 & A23-A35). The MTSSL label (incorporates an R1 side chain) is hydrophobic; consequently, the spin label 3-(2-Iodoacetamide)-proxyl (IAP) which has an amide bond in its linking arm was utilized (Fig. 18, refer to EPR chapter). The IAP label incorporates an R2 side chain. The strategy is to incorporate a label with a more polar linking arm to destabilize the oligomer, promoting dissociation to the dimer. EPR lineshapes for IAP labeled Hsp27-D3 reflect equilibrium between motionally restricted and mobile spin label populations. R2 increases the mobile spin population to a greater extent than R1. The tendency of R2 to favor the dimer is also evident in EPR lineshapes in the WT background where a mobile component was consistently observed. However, EPR lineshapes are similar in the L38R2, P39R2, and E40R2 in both wild-type and phosphorylation mimic backgrounds. P36R2 is the only R2-labeled mutant in which lineshapes between wild-type and the phosphorylation mimic differ. Proline normally produces bends in the polypeptide chain, and substituting with R2 might change the local structure. Consequently, R2 is less immobilized resulting in a lineshape change. This effect is position specific for residue 36, because no change in lineshape is observed for L38R2, P39R2, or E40R2.

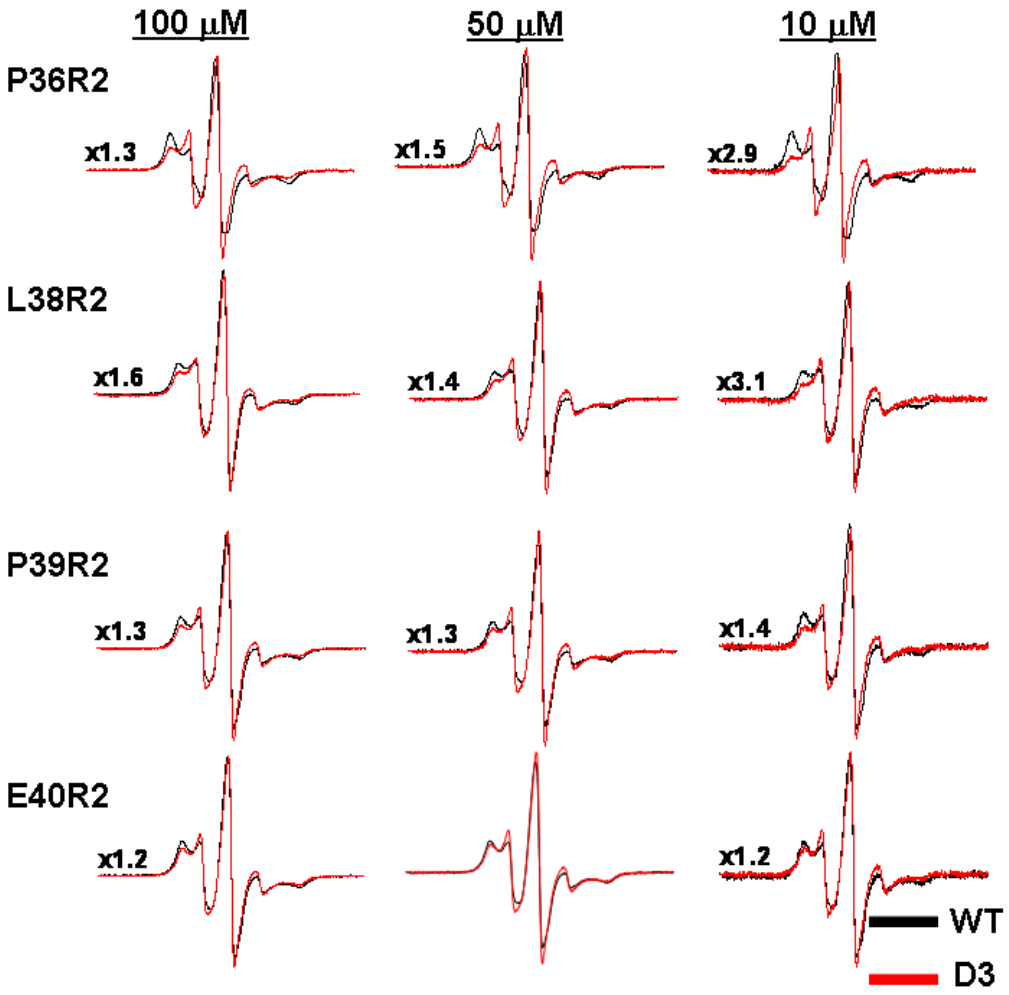


**Figure 31. IAP (R2) labeled mutants on both the wild-type and phosphorylation mimic backgrounds.** EPR spectra corresponding to the spin labeled Hsp27-WT mutants are displayed in black and Hsp27-D3 mutants in red. The spectra were scaled by the factor to the left of the spectrum for ease of presentation.

Based upon SEC analysis, there are two categories of residues capable of modulating the Hsp27 oligomer dissociation equilibrium. In the first category, the substitution of the original residue by a cysteine shifts the equilibrium in favor of the ensemble of large oligomer.

Figure 32 shows SEC chromatograms for representatives of this first category. These residues are primarily acidic or aromatic. Given the buried location of the N-terminal domain, in the context of the native oligomer, acidic residues not involved in salt bridges are likely to destabilize the large oligomer. It is interesting to note that D21C and D30C mutants in Hsp27-D3 predominantly form a dimer at 1 mg/mL. The D17C mutant, in contrast, remains assembled at concentrations as low as 15 μg/mL (Fig. 33). The mechanism by which other residues in this category stabilize the large oligomer is less clear. For residues 37-41 and 51-54, substituting the endogenous residue by cysteine shifts the Hsp27 dissociation equilibrium in favor of the large oligomer (Fig. 34). These residues include arginines as well as prolines, glycines and tryptophans.

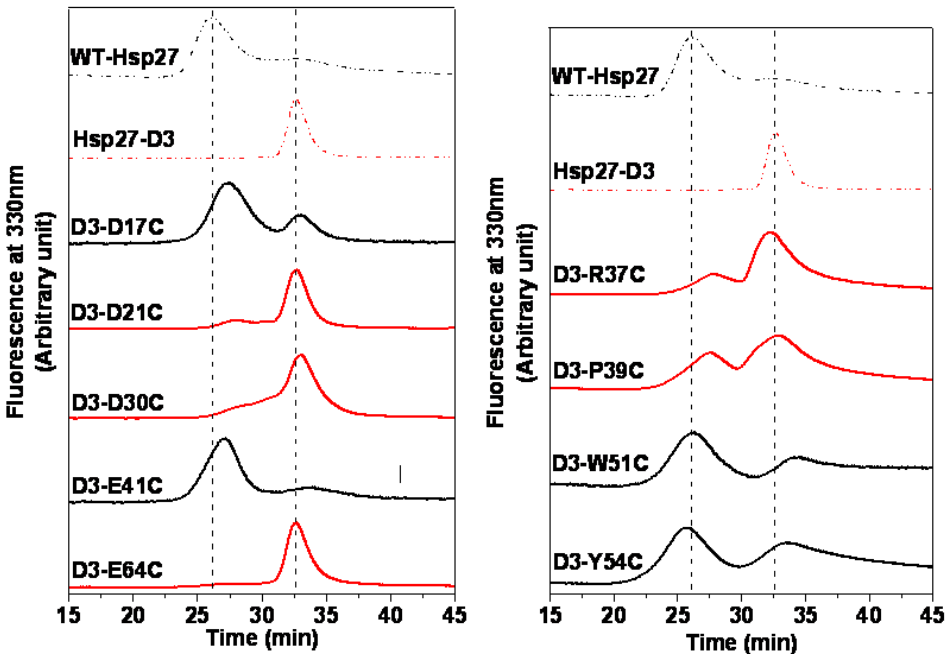


**Figure 32. Size exclusion chromatograms for N-terminal residues that modulate the Hsp27 dissociation equilibrium.** The red traces represent residues where the dissociation equilibrium is shifted in favor of the dimer, while the black traces show residues which favor the large oligomer. The protein concentration was 0.05 mg/mL for D3-D17C, D3-D21C, D3-D30C, D3-E41C, and D3-E64C. The protein concentration was 0.1 mg/mL for D3-R37C, D3-P39C, D3-W51C, and D3-Y54C.

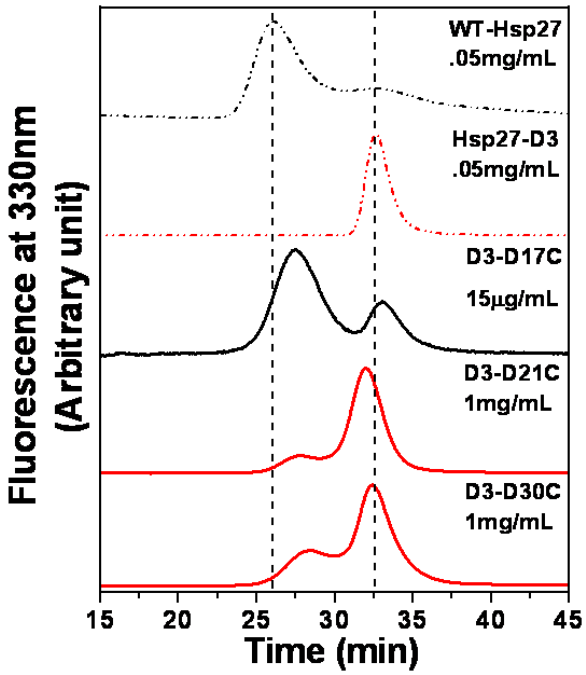


**Figure 33. SEC chromatograms for cysteine mutants D17C, D21C D30C in Hsp27-D3.** The red traces represent residues where the dissociation equilibrium is shifted in favor of the dimer, while the black traces show residues which favor the large oligomer.

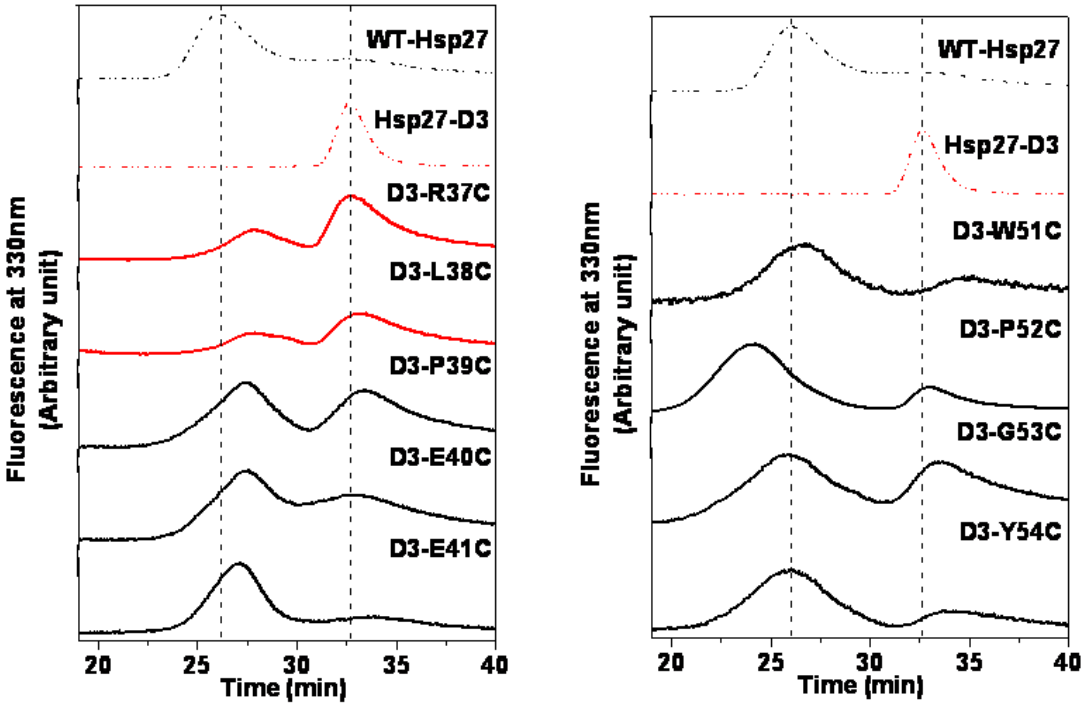


**Figure 34. SEC chromatograms for residues 37-41 and 51-54, in Hsp27-D3, that shift the Hsp27 dissociation equilibrium in favor of the large oligomer.** The red traces represent residues where the dissociation equilibrium is shifted in favor of the dimer, while the black traces show residues which favor the large oligomer. The protein concentration was 0.05 mg/mL.

The SEC data suggests that either the local structure is important for dimer stabilization, or that these residues are implicated in repulsive interactions that would destabilize the native oligomer. Sequence analysis shows conservation of these residues in the Hsp27 superfamily (Fig. 35).


**Figure 35. A sequence alignment for the N-termini of mammalian sHsp homologs αB-crystallin (αB), αA-crystallin (αA), and human Hsp27.** Grey residues are conserved, while conserved residues in Hsp27 homologs are highlighted by the red box. Two red + indicate residues that shift the dissociation equilibrium in favor of the oligomer reassembly, and the single black + indicate residues that partially dissociate the oligomer.

Nevertheless, the homologous α-crystallins often contain non-conservative residue substitutions. Sequence analysis further validates the conclusion of a critical role for the N-terminal domain in the modulation of equilibrium dissociation. This distinctive characteristic distinguishes Hsp27 oligomer dynamics from other mammalian sHsp homologs.

In the second category of residues, the incorporation of the R1- or R2-labels is capable of shifting the dissociation equilibrium. In spin labeled mutants such as D21R1, D21R2, P24R1, and P24R2, the hydrophobicity of R1 favors larger oligomer. In contrast, the more polar R2 stabilizes the dimer and destabilizes the oligomer (Fig. 36). EPR lineshapes are consistent with the trend observed by SEC. For instance, R1 displays a more immobilized EPR spectrum, and R2 shows an enhancement in the contribution of the mobile component.

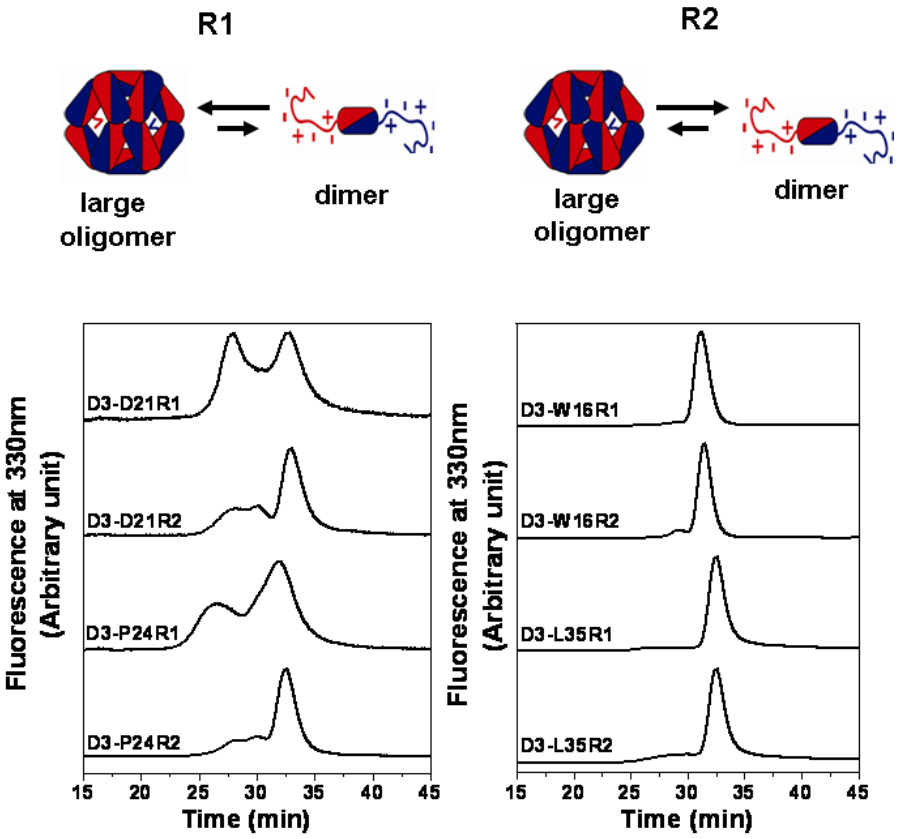


**Figure 36. SEC analysis displaying the effect of either R1 or R2-labels on the Hsp27 dissociation equilibrium.** The protein concentration was 0.05 mg/mL.

These results reveal that regardless of the identity of the original residue the dissociation equilibrium can be modulated by the polarity of the introduced side chain. However, not all residues stringently follow the R1/R2 rule (Fig. 36). For example, in D21C the negative charge is important for destabilizing the large oligomer (Fig. 33). Labeling with R2 shows that the label's contribution to the dissociation energetics is insufficient to overcome the stabilizing effect of the large oligomer. A similar effect is observed with the P24R2 mutant. On the other hand, at residues $Trp^{16}$ and $Leu^{35}$ neither R1 nor R2 is capable of modulating the Hsp27 dissociation equilibrium. In these mutants, the dimer consistently dominates.

## Discussion

In sHsps, the most sequence divergence occurs in the N-terminal domain. The length of the N-terminal domain varies from 32 amino acids, in the *archeal* Hsp16.5, to 87 amino acids in *human* Hsp27. In contrast to the α-crystallin domain, the structure and function of the N-terminal domain has not been extensively investigated. The role of the N-terminal domain in sHsp oligomer architecture and chaperone activity remains largely enigmatic. The literature does show strong evidence in support of a direct role for the N-terminal domain in oligomer stabilization and subunit exchange in both α-crystallin and Hsp27 (Bova et al. 1997; Bova et al. 2000; Koteiche et al. 2005; Shi et al. 2006). For example, deletion of the N-terminal domain results in dissociation of αA-crystallin into both dimers and tetramers (Bova et al. 1997). Also, these smaller multimeric units were incapable of further subunit exchange (Bova et al. 1997). Although N-terminal domain deletion in Hsp16.5 results in assembly into an intact oligomer; protein engineering in Hsp16.5 has revealed a pivotal role of the N-terminal domain in oligomer plasticity (Koteiche and Mchaourab 2002; Shi et al. 2006). Moreover, the insertion of the peptide P1 from Hsp27 within the N-terminal domain of Hsp16.5 induced an oligomeric transition from a 24- to a 48-subunit oligomeric species (Shi et al. 2006). The P1 peptide of Hsp27 is highlighted by the blue box in figure 22. Apart from the putative structural role, N-terminal sequences within plant sHsps and α-crystallin were identified as contact sites for bound substrate.

These studies strongly indicate an N-terminal domain contribution to the chaperone activity of sHsps (Giese et al. 2005; Ghosh et al. 2006; Jaya et al. 2009).

A mechanistic correlation can be envisaged between the dynamic Hsp27 oligomer and *in vitro* chaperone activity. The minimalist model of figure 15 illustrates this point in equations 1 and 3. According to the model, dissociation of Hsp27 into dimers is an important step in substrate binding (Fig. 37). As a result, the binding competent dimer, with its N-terminal domain solvent exposed, interacts with destabilized substrate with high affinity. Substrate binding causes reassembly of the N-terminal domain into a solvent shielded environment with its substrate sequestered on the inside of the Hsp27/substrate complex. The fast rate of Hsp27 subunit exchange and the concentration dependence of Hsp27 equilibrium dissociation strongly suggest that there is a relatively small energetic balance in favor of the large oligomer in Hsp27-WT (Bova et al. 1997; Bova et al. 2000). Additionally, a direct correlation was demonstrated, using T4L as a model substrate, between propensity for dissociation and substrate affinity (Shashidharamurthy et al. 2005).

On the sequence level, a thorough mutagenic analysis reveals two important motifs that modulate dissociation. Acidic residues in the N-terminal domain favor the large oligomer to the extent that substitution of a single residue such as $Asp^{17}$ or $Glu^{41}$ reverses the dissociation induced by the three phosphorylation mimicking aspartates.

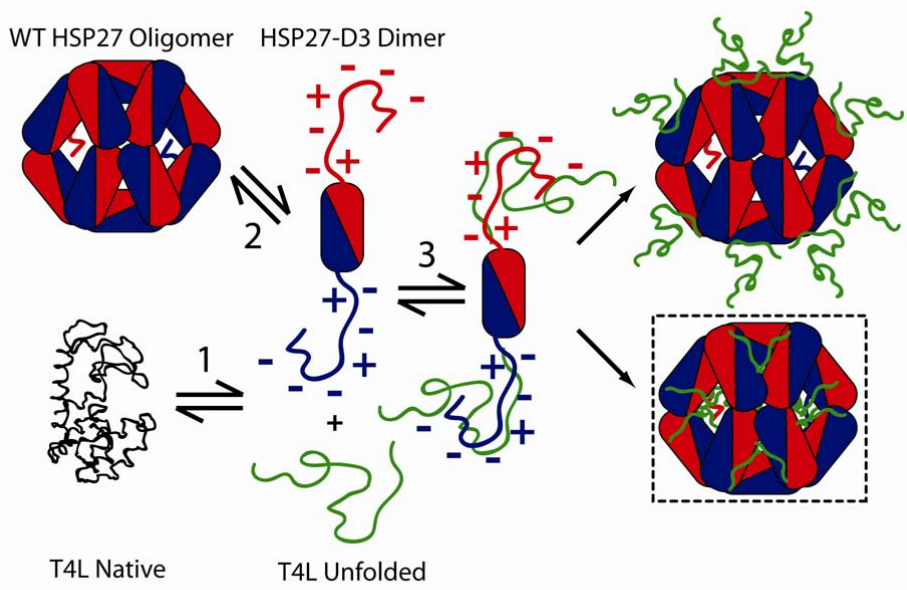


**Figure 37. The model illustrating substrate binding to Hsp27.** The model focuses on the role of the N-terminal domain in the three coupled equilibria of Figure 2. Initially the N-terminal domain is unfolded and solvent exposed in the dimer, and monomer contacts within each dimer occur along the $\alpha$-crystallin domain. After binding destabilized T4L, the oligomer reassembles into a Hsp27/substrate complex. The T4L substrate is sequestered within the inside of this complex which is shown with a dashed square (high affinity mode). Additionally there is also a low affinity binding mode which involves T4L binding to the surface of the Hsp27 oligomer. (Figure created with the assistance of Sanjay Mishra)

The origin of this effect appears to be the energetic costs of excluding N-terminal charges from the aqueous phase. However, the contribution of these acidic residues is not uniform most likely reflecting interactions of these residues with neighboring side chains. Presumably some of the negative charges are not ion paired while others such as $Asp^{21}$ and $Asp^{30}$ may be involved in salt bridges that reduce the energetic penalty associated with their transfer into a buried environment.

A second unexpected yet important finding is the identification of consecutive residues whose substitutions stabilize the large oligomers. In addition to being contiguous, the chemical properties of these amino acids are diverse suggesting that the origin of their effects on the dissociation equilibrium is primarily structural. Notably, most of these residues are conserved in the Hsp27 family but not in the $\alpha$-crystallin subfamily of sHsp. This conservation pattern is consistent with a critical role in the dynamics of oligomer dissociation characteristic of Hsp27.

The EPR data complements the mutagenic analysis of oligomer stability by revealing the structural aspect of oligomer dissociation. Transition to a dimer does not perturb the $\alpha$-crystallin domain fold or its dimer interface. Structural rearrangements occur primarily in the N-terminal domain where extensive subunit contacts are disrupted exposing this domain to the solvent. Analysis of N-terminal domain dynamics and environment suggests a structural contribution to the dissociation energetics. For residues where either cysteine substitution or spin label incorporation did not drastically affect the equilibrium, the R1- and R2-labels report a transition to a more water-exposed environment. The lineshapes are uniformly mobile suggesting the lack of a packed core in this domain. For residues 60-80, EPR lineshapes in the dimer suggest an unstructured backbone. The P1 peptide (residues 58-70) is included in this region and their deletion stabilizes the native oligomer (Shashidharamurthy et al. 2005). Native oligomers assembly sequesters the N-terminal domain away from the aqueous solvent, as demonstrated by the dramatically reduced NiEDDA accessibility.

Therefore, either the N-terminal domain will form regular secondary structure or it will be buried without satisfying the hydrogen bonding requirements of the backbone or the interaction potential of side chains. The latter is energetically unfavorable while the former's net energetic contribution is reduced by loss of conformational entropy. As a result, N-terminal sequence and structural elements contribute to the energetic modulation of the dissociation equilibrium.

The fact that substrate binding induces oligomer reassembly supports the fact that important interactions occur between the substrate and N-terminal sequences. These interactions are capable of neutralizing negative charges and inducing conformational changes. The purpose is to reduce the unfavorable energetics of oligomer assembly. However, spin labels are motionally restricted in the native oligomer; therefore, the ability to use EPR lineshape or accessibility to NiEDDA to identify residues in direct contact with the substrate is hindered. The evolution of mammalian sHsp ensures binding promiscuity to a wide variety of substrates, while allowing for dynamic regulation of substrate affinity. There is increasing evidence that correlates the dynamics of Hsp27 oligomer dissociation to its physiological role (Abisambra et al. 2010). The data presented provides definitive evidence that N-terminal domain sequence divergence contributes to the structural and dynamic properties that distinguish mammalian sHsps from their *archeal* counterparts. EPR and SEC data clearly demonstrate how the marginal stability of the native oligomer functions as a switch allowing single amino acid substitutions to modulate the Hsp27 dissociation equilibrium.

# CHAPTER V

## Summary and Future Perspectives on the Mechanism of sHsp Chaperone Activity

### Overview

It is well documented that mammalian small heat shock protein 27 (Hsp27) is capable of equilibrium dissociation from an ensemble of large oligomers to a dimer (Lambert et al. 1999; Bova et al. 2000; Theriault et al. 2004). Furthermore, Hsp27 exchanges subunits in a dynamic process, which involves equilibrium dissociation and reassembly (Bova et al. 2000). Consequently equilibrium dissociation, to the dimer, facilitates high affinity binding to destabilized substrate (Shashidharamurthy et al. 2005; Mchaourab et al. 2009). N-terminal substrate binding sites have been previously identified in other sHsps; however, the conserved architecture of sHsps, such as Hsp16.5 and Hsp16.9, places the N-terminal domain within the core of the sHsp oligomer (Kim et al. 1998; Haley et al. 2000; van Montfort et al. 2001; Haslbeck et al. 2004a; Basha et al. 2006; Shi et al. 2006; Jaya et al. 2009a). Since the N-terminal domain is not readily accessible, substrate binding requires sHsp oligomer dissociation (van Montfort et al. 2001; Haslbeck et al. 2004a; Giese et al. 2005; Shashidharamurthy et al. 2005). Unfortunately, the structural contribution of the N-terminal domain to both Hsp27 oligomer dynamics and chaperone activity is not well understood.

This is a direct consequence of the refractory nature of mammalian sHsps, such as Hsp27, to high resolution structure determination. The work presented in this dissertation describes the N-terminal conformational changes that accompany Hsp27 oligomer dissociation, and examines the role of N-terminal sequence elements in equilibrium dissociation.

**N-terminal domain dynamics and environment suggests a structural contribution to dissociation energetics**

By means of systematic spin labeling and subsequent analysis of EPR lineshapes, the environment of the N-terminal domain in the native oligomer (Hsp27-WT) as well as in the phosphorylation mimic (Hsp27-D3) was examined. Motionally restricted EPR spectra are observed in Hsp27-WT, indicating that the N-terminal domain is located in a buried environment and involved in extensive subunit contacts. The conclusion drawn, for Hsp27-WT, was further confirmed by the dramatic reduction in NiEDDA accessibility. In contrast, for the corresponding spin labeled residues, in Hsp27-D3, there were less restricted spin label motion observed. Therefore, dissociation to the dimer causes large portions of the N-terminal domain to loose the steric restriction observed in the native oligomer. Furthermore, an increase in NiEDDA accessibility implies that the N-terminal domain has transitioned to a more exposed aqueous environment. Now, these lineshape and accessibility features, in Hsp27-D3, indicate significant conformational changes, in the N-terminal domain, have taken place after oligomer dissociation. Consequently, these conformational changes precipitate the dissociation of the Hsp27 oligomer.

The EPR results indicate that a relatively small energetic balance favors the ensemble of large oligomers, and this balance is disrupted by structural changes in the N-terminal domain. As a result, oligomer dissociation, to the dimer (chaperone activated state), is promoted and substrate binding affinity is enhanced.

Since cells must rapidly respond to stress, sHsps such as Hsp27, have a remarkable propensity to sense changes in cellular environment (Craig and Lindquist 1988; Parsell and Lindquist 1993). For that reason, the architecture of the Hsp27 oligomer serves as a switch that can be readily activated during stress. The conformational changes within the N-terminal domain control the switch; therefore, Hsp27 shifts from an inactive to chaperone ready state. In the cell, molecular chaperones assist in protein folding thereby, preventing non-specific protein aggregation (Hartl and Hayer-Hartl 2002; Haslbeck et al. 2005; Buchberger et al. 2010). For many molecular chaperones, with the exception of sHsps, binding and release of substrate is regulated by ATP binding and hydrolysis (Bukau and Horwich 1998; Richter et al. 2010). However, persistent stress may contribute to periods of non-productive ATP-dependent cycling; as a result, the ATP-dependent molecular chaperone machinery becomes overwhelmed. The consequence of this event is the release of misfolded proteins which is detrimental to cell survival. sHsps act independently of ATP and are capable of forming stable substrate complexes with misfolded proteins. Thus, sHsps are ideal in the management of protein homeostasis during conditions of persistent stress.

It is readily apparent that a tightly regulated stress activated oligomeric switch would ensure instantaneous availability of sHsps according to cellular requirements.

**The influence of N-terminal sequence determinants in the modulation of Hsp27 equilibrium dissociation**

According to SEC and EPR analysis, a number of N-terminal aspartate, glutamate, arginine, proline, glycine, and tryptophan residues, in Hsp27-D3, have the propensity to modulate the dissociation equilibrium after cysteine substitution or incorporation of the spin label side chain (R1 and R2). The EPR lineshapes for these sites unexpectedly revealed restricted spin label motion, similar to that observed for the corresponding spin labeled Hsp27-WT mutants. Furthermore, these key residues show a shift in the dissociation equilibrium in favor of the large ensemble of oligomers. The significance of these results lies in part on the ability of these residues to effectively reverse the phosphorylation-induced dissociation, commonly observed in Hsp27-D3. That being so, these results identify residues that significantly stabilize the large ensemble of oligomers possibly via the formation of stabilizing interactions. These interactions include hydrogen bonds, salt bridges, and aromatic interactions (Brinda and Vishveshwara 2005). It has been previously reported that addition of extra hydrogen bonds and salt bridges enhances the energy of stabilization of oligomeric enzymes (Perutz and Raidt 1975; Walker et al. 1980; Vetriani et al. 1998). The general premise behind this stabilization is the formation of networks of structural elements, such as $\alpha$-helices, $\beta$-sheets, and turns.

It is worthy to note that the location and context of the structural elements are extremely important. Hence networks of structural elements serve to bring together clusters of interacting residues into close proximity (stabilizing interactions), while at the same time preventing other residues from interacting (destabilizing interactions). For example, $Asp^{17}$, $Glu^{41}$, $Trp^{51}$, and $Tyr^{54}$ may be involved in a network of salt bridges and hydrogen bonds. Cysteine mutagenesis serves to alter the local environment in the vicinity of these residues; consequently, the network of structural elements, in which these residues were originally involved, is now modified. Furthermore, consecutive clusters of residues, such as 36 to 41 and 51 to 54, are particularly intriguing, because their substitution to cysteine and subsequent spin labeling stabilizes the large ensemble of oligomers. The contiguous location of these residues is further evidence that they are involved in structural elements, within the N-terminal domain of Hsp27. Also, $Pro^{39}$ maybe involved in a $\beta$-turn within a cluster of these residues. Since, the N-terminal domains of Hsp16.5 and Hsp16.9 are predominantly $\alpha$-helical and involved in the interaction between subunits; it's entirely possible that the N-terminal residue $Pro^{39}$, of Hsp27, may serve to restrain the orientation of an $\alpha$-helix located at a subunit interface. However, different residues contribute to oligomer stability to varying extents. For instance, $Asp^{21}$, $Asp^{30}$, and $Glu^{64}$ residues, when mutated to cysteines, shift the Hsp27 dissociation equilibrium in favor of the dimer, due to the local nature of their chemical interactions.

As a result, $Asp^{21}$, $Asp^{30}$, and $Glu^{64}$ residues are critical for the stabilization of the dimer; at the same time, these residues are involved in repulsive interactions that act to destabilize the large oligomer. Therefore, the importance of these residues, in the modulation of the Hsp27 dissociation equilibrium, is illustrated by their strict conservation in Hsp27. Nevertheless, the stringent sequence conservation of these residues is not observed in the homologous αA- and αB-crystallins. Sequence conservation is consistent with a pivotal role for the N-terminal domain in the dynamics of Hsp27 oligomer dissociation.

Hsp27 oligomeric structure and dynamics are linked to chaperone activity, by the minimalist model (Shashidharamurthy et al. 2005; Koteiche and Mchaourab 2006; Mchaourab et al. 2009). In this model, the substrate folding, Hsp27 oligomeric, and reassembly to Hsp27/substrate complex equilibria are all coupled. According to the coupled equilibria, substrate binding is favored by the stability of the substrate; in which, the free energy of unfolding will favor the intermediate states. Furthermore, the population of chaperone in its activated state (dimer) also promotes substrate binding. In the case of mutations that stabilize the large oligomer, the Hsp27 dissociation equilibrium is shifted toward the large ensemble of oligomers (not the chaperone activated state). Therefore, there will be a reduction in the extent of substrate binding. It becomes evident how Hsp27 utilizes equilibrium dissociation to recognize and bind substrate in its non-native state. Dissociation to the dimer enables substrate access to N-terminal binding sites (Haslbeck et al. 2005; Shashidharamurthy et al. 2005; Mchaourab et al. 2009).

The modulation of the equilibrium is important for the physiological role of mammalian sHsps. Mutations in key residues that influence the dissociation equilibrium can alter the ability of sHsps to dynamically respond to changes in cellular protein folding. As a result, cellular proteostasis is altered, as in the case of stress, aging, and neurodegenerative disease (Hsu et al. 2003; Gidalevitz et al. 2006b; Mehta et al. 2009). There are numerous physiologically relevant examples where aberrant Hsp27 and αB-crystallin function have been associated with Alzheimer's disease, Alexander's disease, desmin related cardiomyopathies, neuropathies, and cataracts (Vicart et al. 1998; Evgrafov et al. 2004; Dierick et al. 2005; Muchowski and Wacker 2005; Liu et al. 2006).

**Future Perspectives**

The correlation between Hsp27 oligomeric structure, dynamics, and *in vitro* chaperone activity has been extensively studied (Berengian et al. 1999; Lambert et al. 1999; Rogalla et al. 1999; Theriault et al. 2004; Shashidharamurthy et al. 2005; Koteiche and Mchaourab 2006). However, details concerning chaperone function remain poorly understood. For instance, the N-terminal residues that directly contact substrate remain undefined. In the dissertation work, EPR lineshape and NiEDDA accessibility could not be used to accurately identify residues in direct contact with substrate. It is apparent that additional biochemical analysis is needed to identify Hsp27/substrate binding sites.

There are a number of crosslinking studies which have utilized the fluorescent dye 1-anilino-8-naphthalene sulfonate (ANS), 1,1'-bi(4-anilino)naphthalene-5,5'-disulfonic acid (bis-ANS), or aromatic molecules such as p-benzoyl-L-phenylalanine (Bpa) to photolabel and subsequently identify potential substrate binding sites in sHsps (Lee et al. 1997; Raman and Rao 1997; Sharma et al. 1997; Smulders and de Jong 1997; Fu and Chang 2006; Jaya et al. 2009a). In cross-linking studies, it is assumed that N-terminal residues that interact with both the label and substrate protein are identical. Therefore, the binding of label should reduce the chaperone activity of sHsps. It may be an important consideration for future work to apply crosslinking studies to identify potential N-terminal sites for substrate binding, in Hsp27-D3 (binding competent dimer). The identification of substrate binding sites in sHsps is fundamental to the understanding of their cellular function in eye lens transparency, thermotolerance, resistance to apoptosis, cytoskeleton modulation, protection against oxidative stress, and neurodegenerative disease (Waters et al. 1996; Brady et al. 1997; Graw 1997; Mehlen et al. 1997; Muchowski and Wacker 2005; Launay et al. 2006; Laskowska et al. 2010). Additional insight into the correlation between Hsp27 oligomer dynamics and its cellular function can be obtained by transfecting neuronal cells with cysteine mutants capable of modulating the Hsp27 dissociation equilibrium. Neuronal cells are ideal, because they are particularly vulnerable to the cytotoxic effects of misfolded protein aggregates (inclusions).

Mammalian sHsps, Hsp27 and αB-crystallin, are upregulated and accumulate into inclusion bodies in many neurodegenerative diseases (Muchowski and Wacker 2005). In neuronal disease models, the overexpression of Hsp27 has been protective against neuronal cell death (Wyttenbach et al. 2002; Zourlidou et al. 2004; Patel et al. 2005; Arrigo et al. 2007; Stetler et al. 2009). The dissociation equilibrium modulating Hsp27 cysteine mutants can be tested for their ability to inhibit the accumulation of abnormally folded proteins in the neuronal cell's nucleus or cytosol. It is beneficial to further study these cysteine mutants in model organisms such as zebrafish, Drosophila, *Caenorhabditis elegans*, and mice. The importance of these studies is to provide additional insight into the structure and mechanism of mammalian sHsps. A long term goal is to develop therapeutic strategies targeted at modulating the chaperone activity of mammalian sHsps in disease.

## APPENDIX

### Figure A1. Hsp27-D3 & Hsp27-WT EPR Spectra

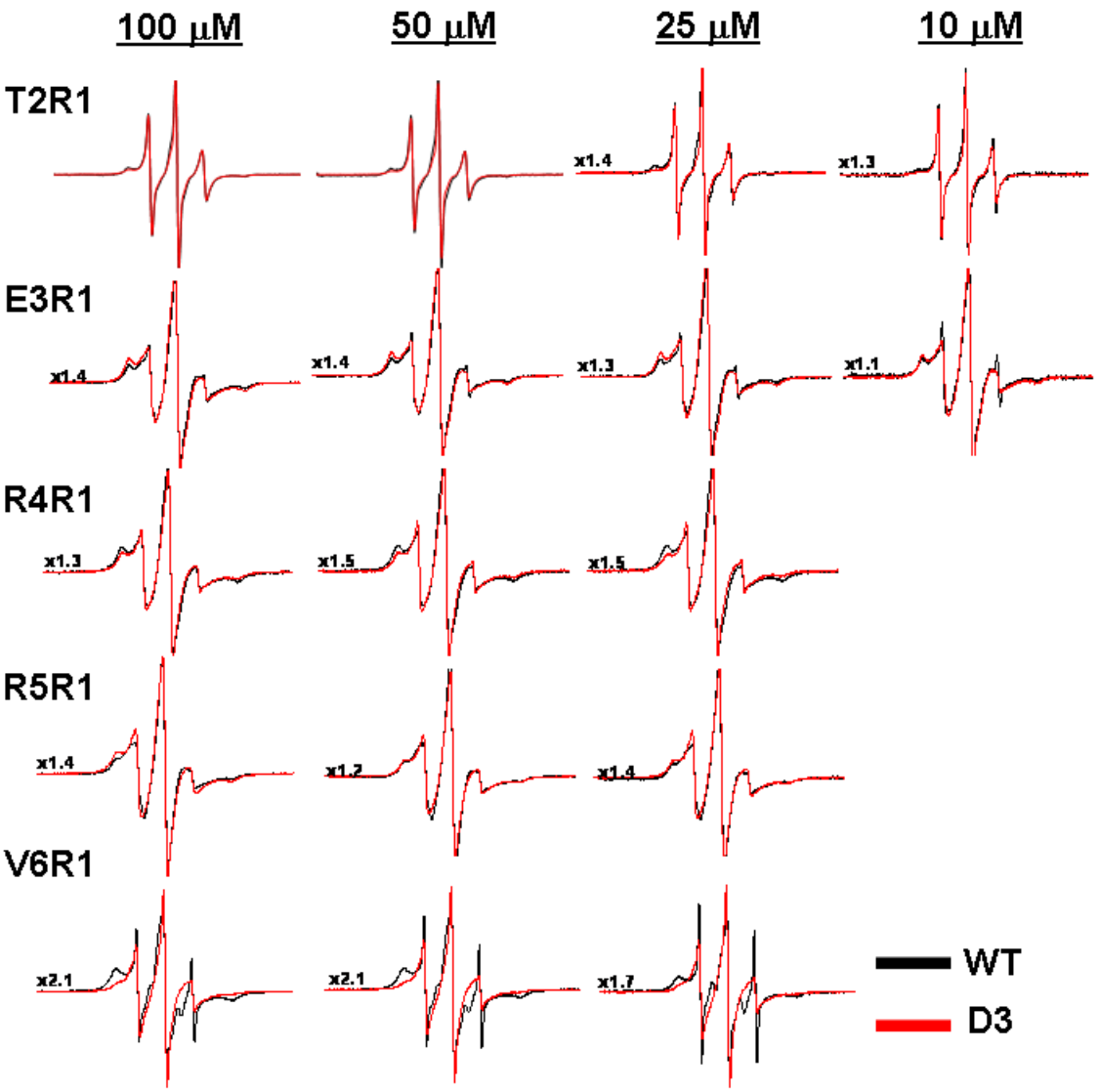


*The Hsp27-WT mutant spectra were scaled by the factor to the left of the spectrum for ease of presentation.

**Figure A2. Hsp27-D3 & Hsp27-WT EPR Spectra**

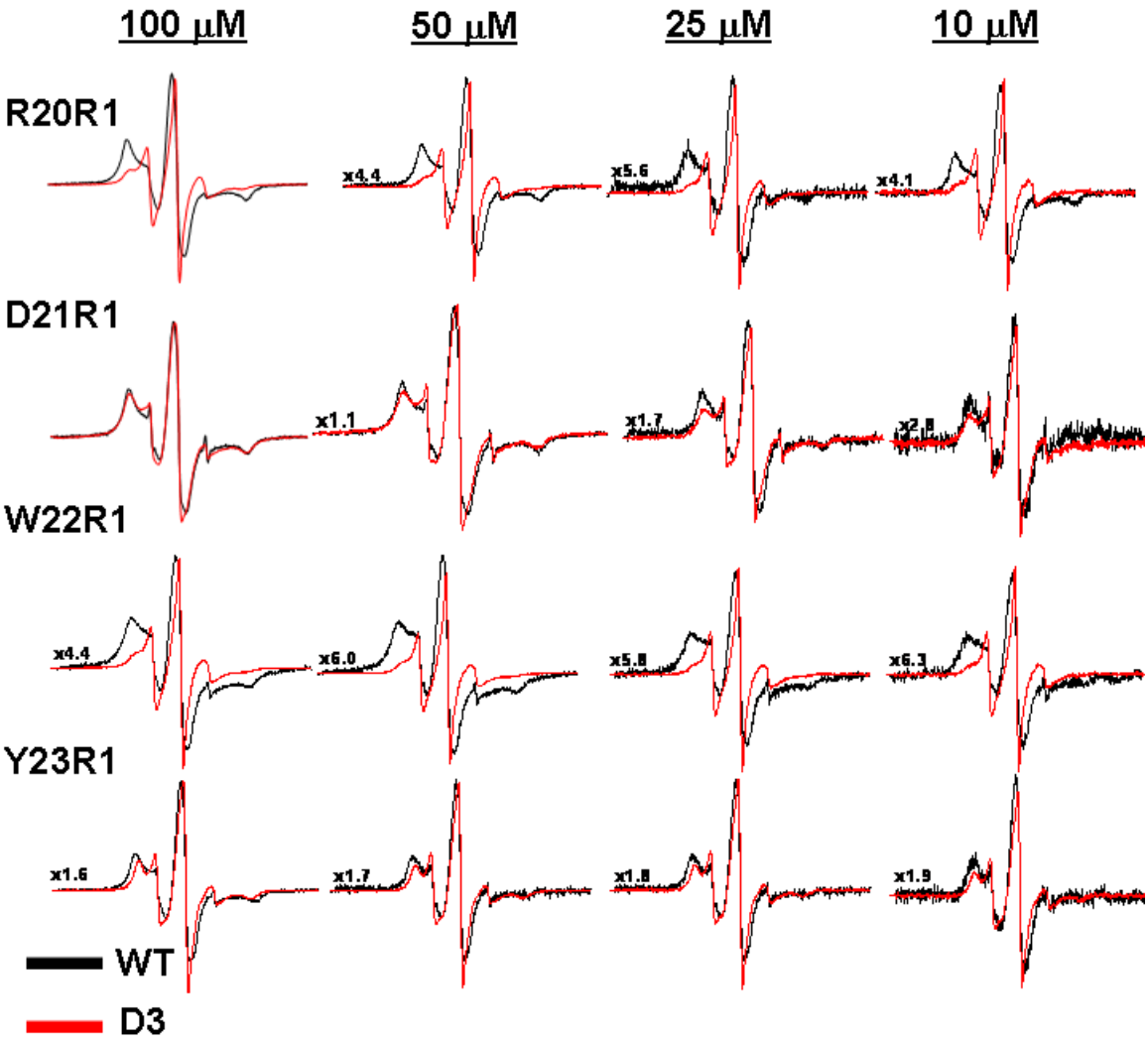


***The Hsp27-WT mutant spectra were scaled by the factor to the left of the spectrum for ease of presentation.**

**Figure A3. Hsp27-D3 & Hsp27-WT EPR Spectra**

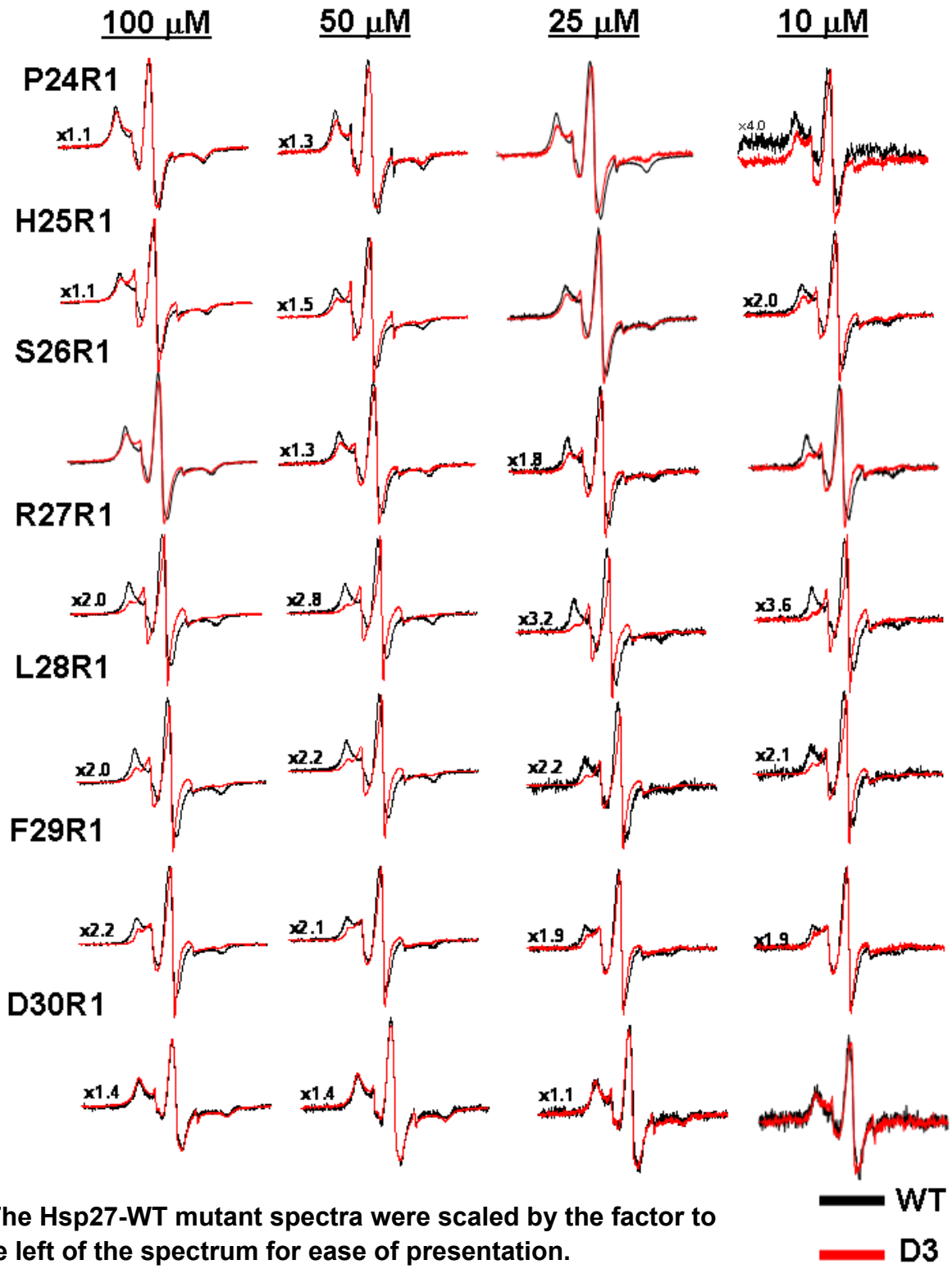


*The Hsp27-WT mutant spectra were scaled by the factor to the left of the spectrum for ease of presentation.

**Figure A4. Hsp27-D3 & Hsp27-WT EPR Spectra**

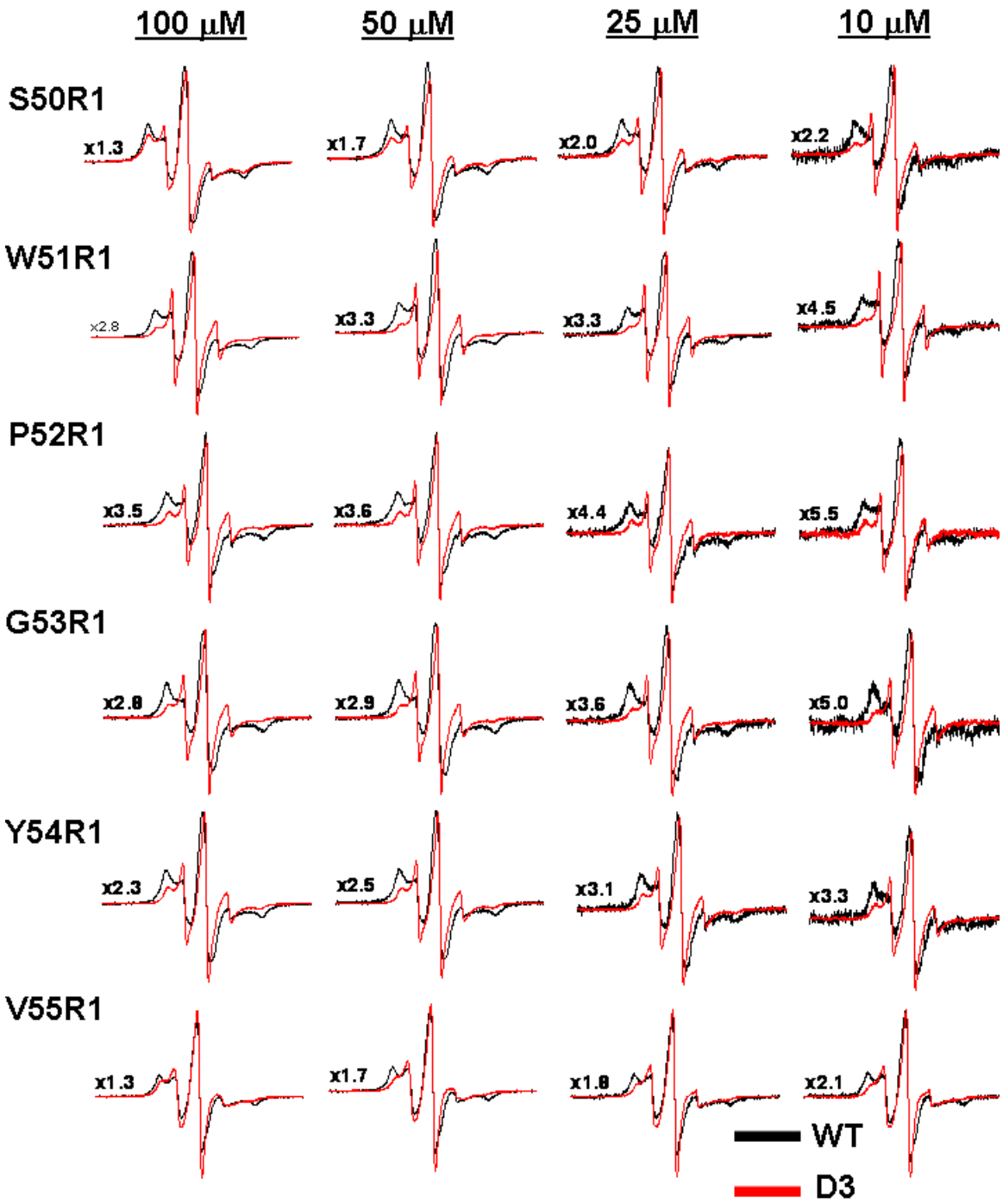


*The Hsp27-WT mutant spectra were scaled by the factor to the left of the spectrum for ease of presentation.

**Figure A5. Hsp27-D3 & Hsp27-WT EPR Spectra**

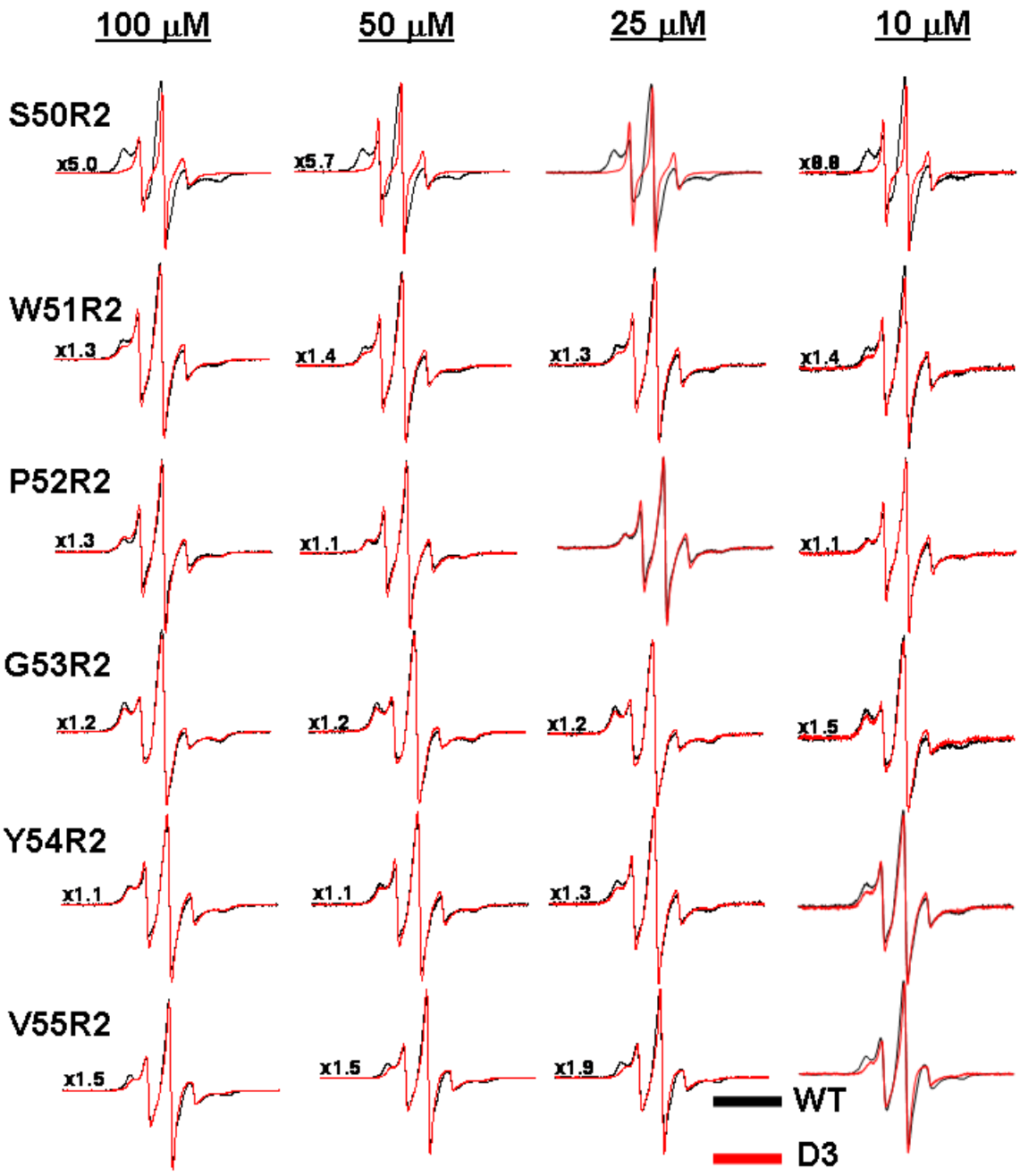


*The Hsp27-WT mutant spectra were scaled by the factor to the left of the spectrum for ease of presentation.

**Figure A6. Hsp27-D3 & Hsp27-WT EPR Spectra**

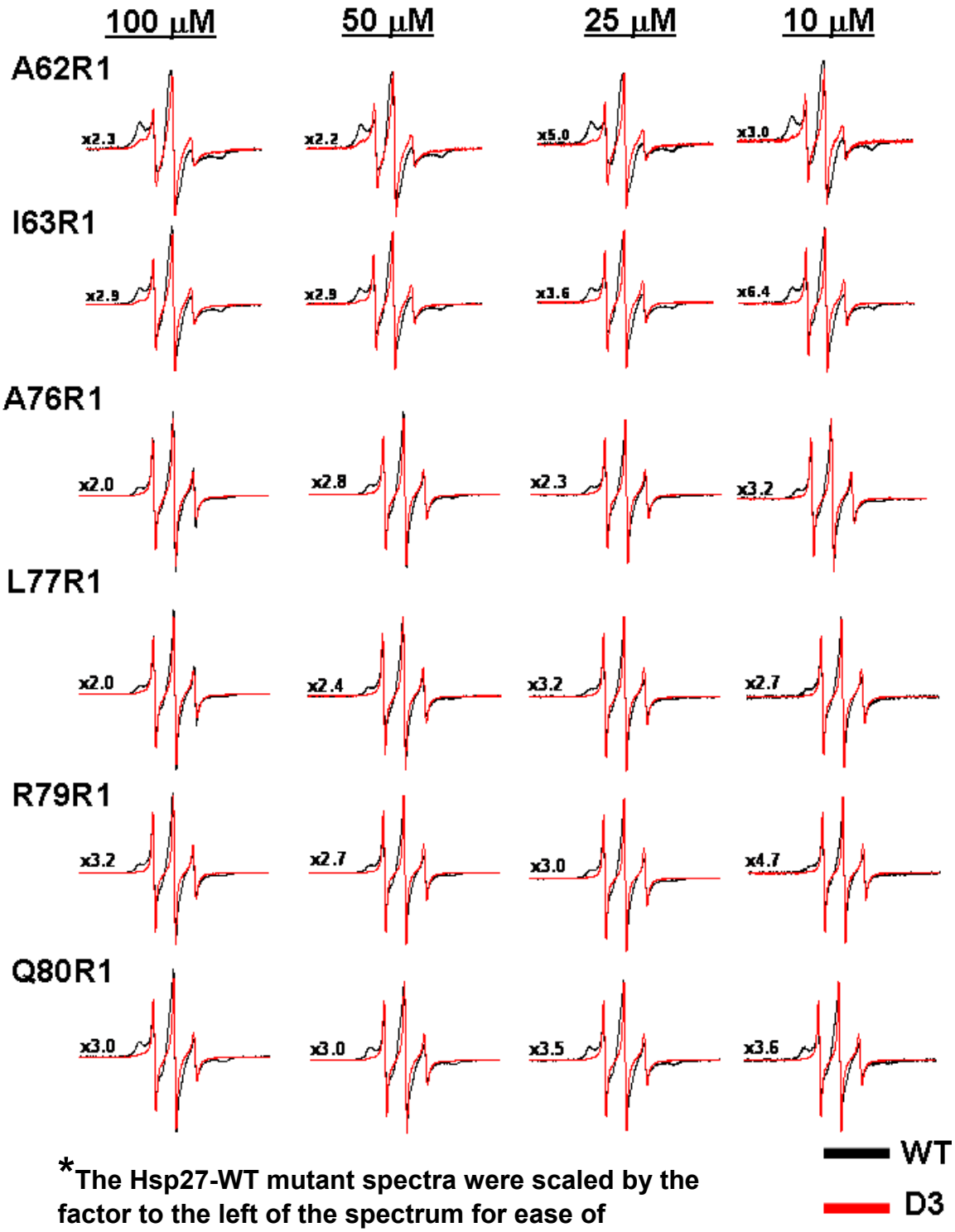


*The Hsp27-WT mutant spectra were scaled by the factor to the left of the spectrum for ease of presentation.

**Figure A7. Hsp27-D3 & Hsp27-WT EPR Spectra**

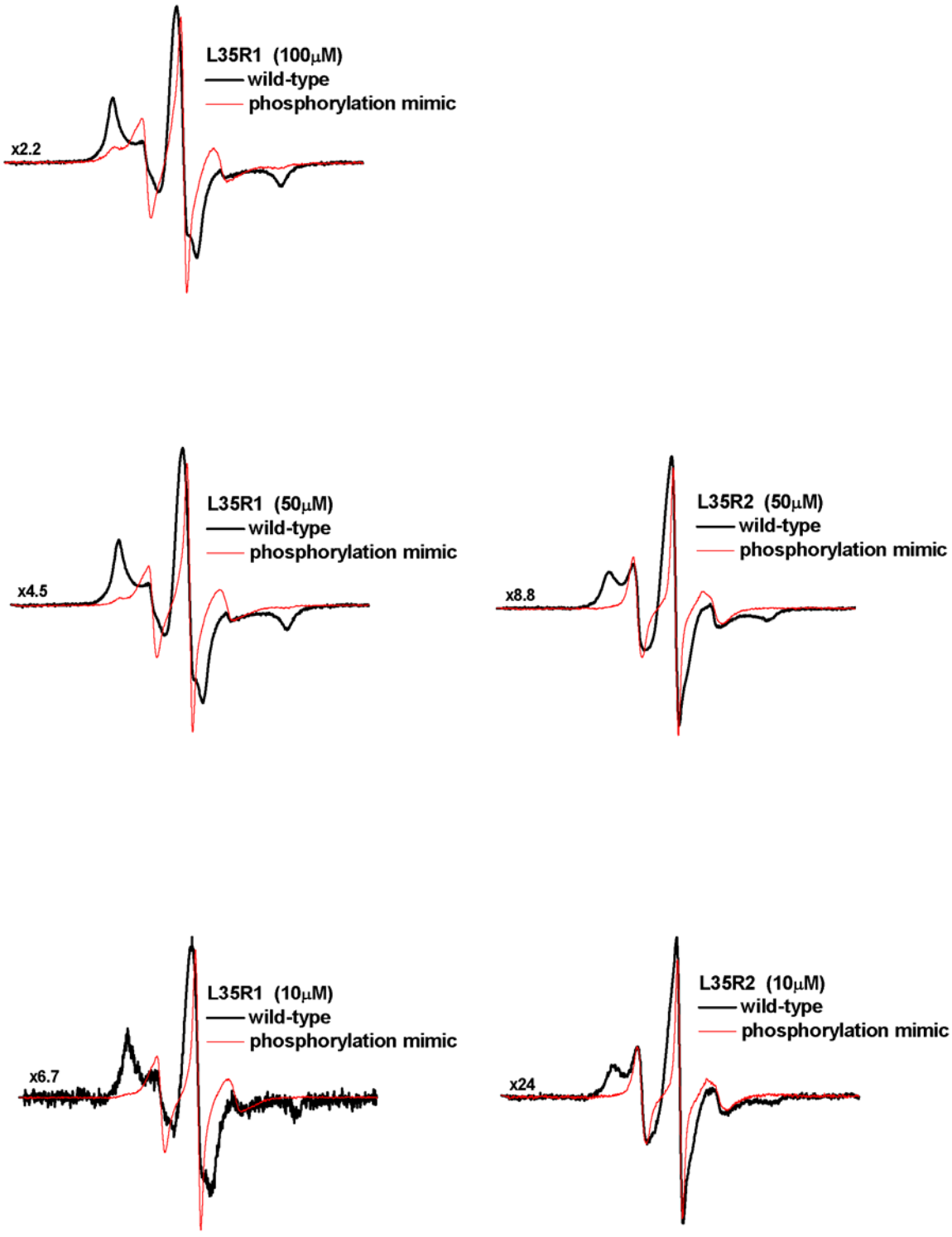


***The Hsp27-WT mutant spectra were scaled by the factor to the left of the spectrum for ease of presentation.**

**Figure A8. Hsp27-D3 & Hsp27-WT EPR Spectra**

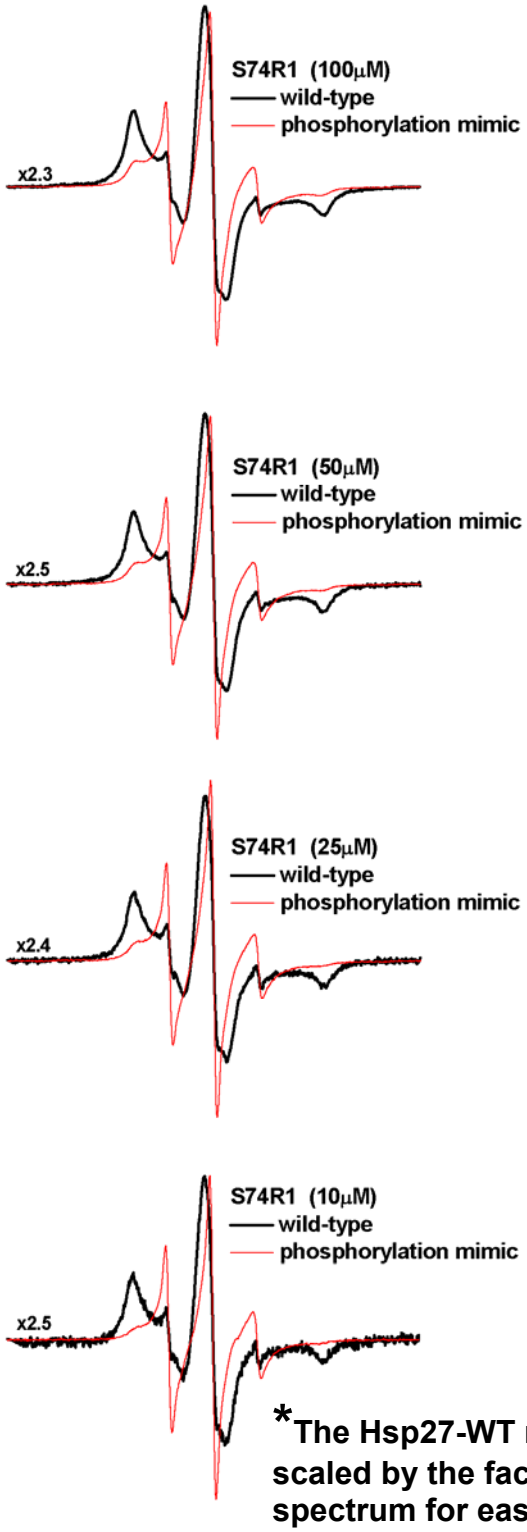


*The Hsp27-WT mutant spectra were scaled by the factor to the left of the spectrum for ease of presentation.

**Figure A9. Hsp27-D3 & Hsp27-WT EPR Spectra**

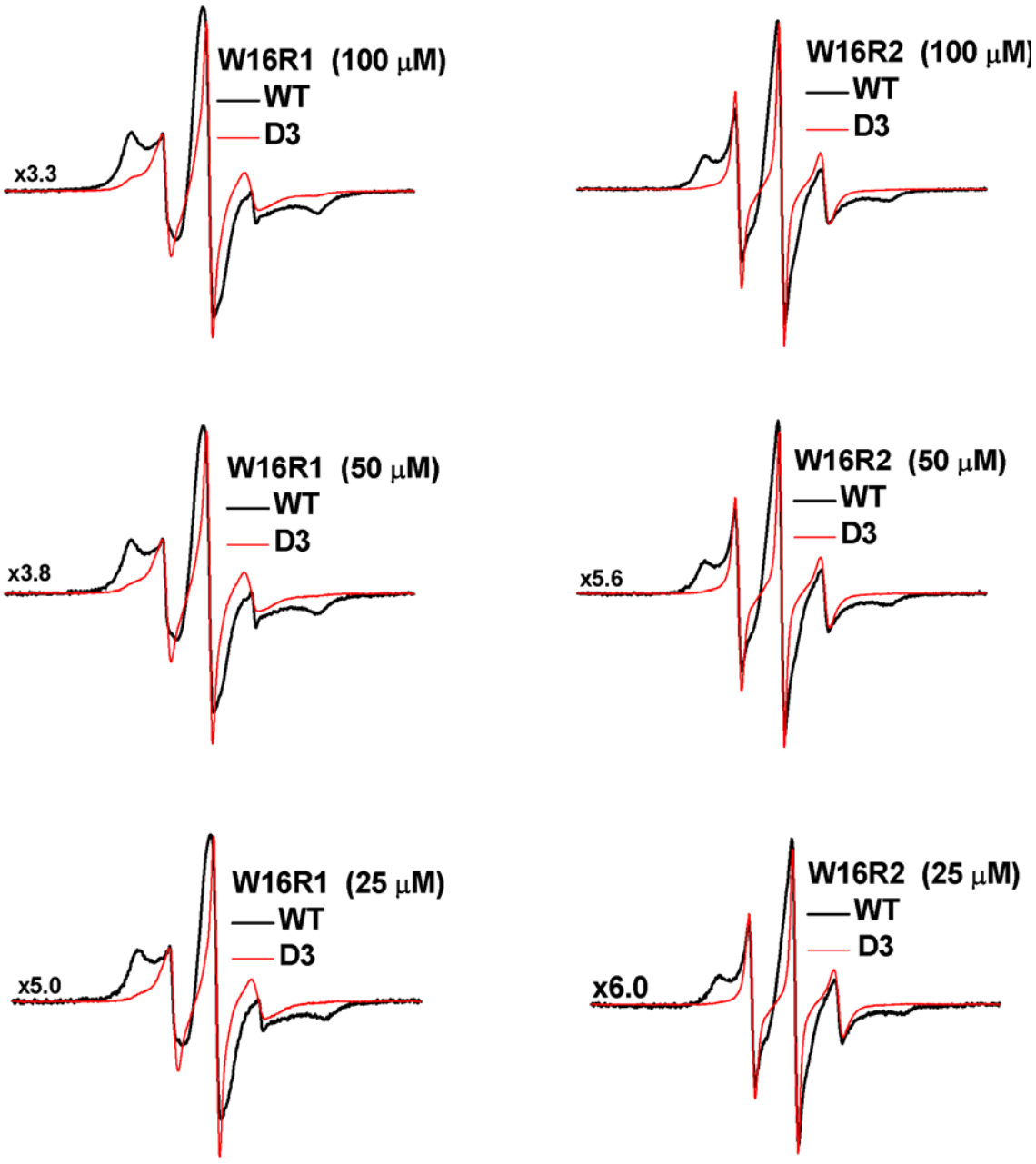


***The Hsp27-WT mutant spectra were scaled by the factor to the left of the spectrum for ease of presentation.**

**Figure A10. The Concentration Dependence of NiEDDA on Accessibility**

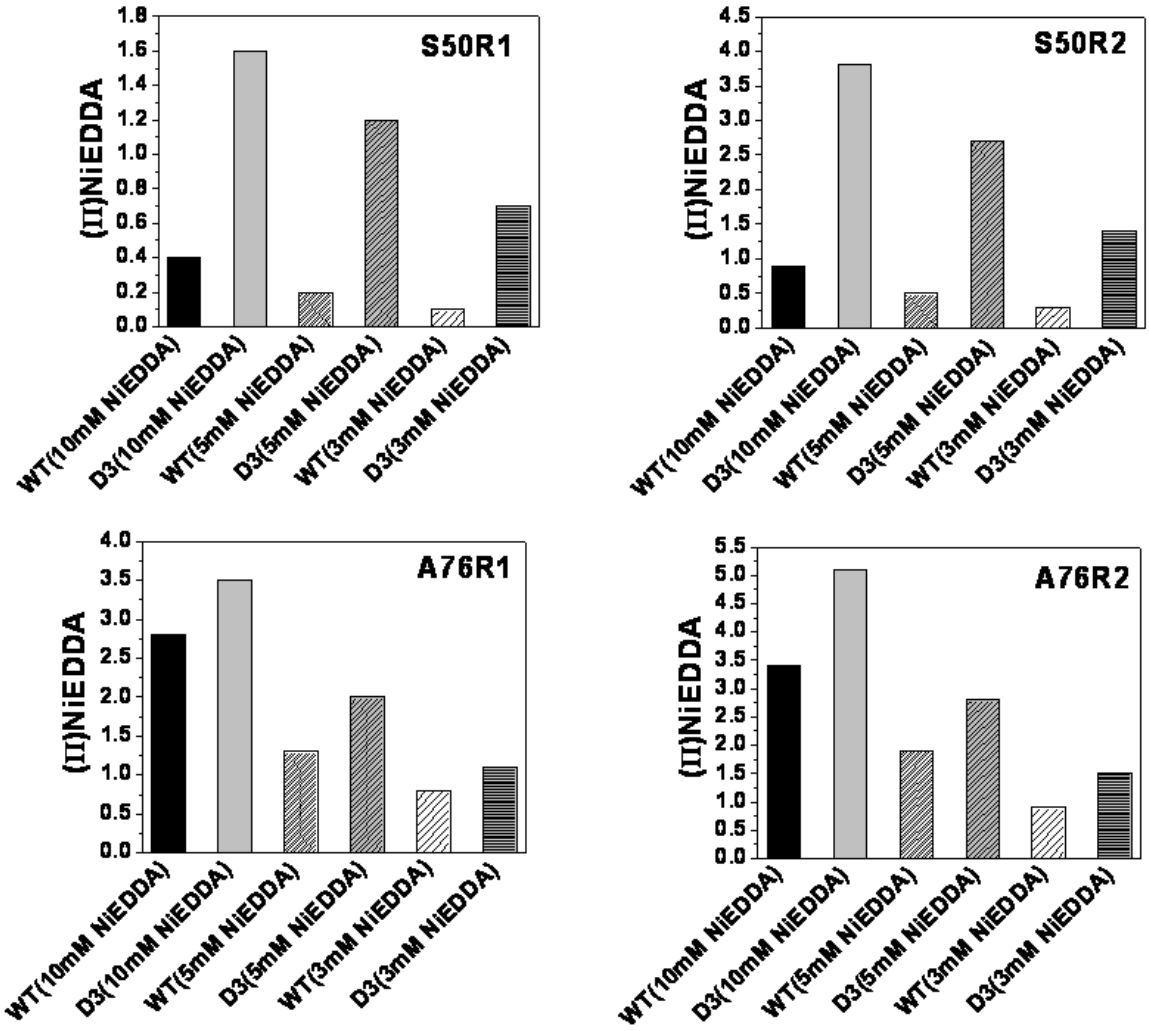

**Figure A11. Concentration Dependence of EPR Lineshape For Spin Labeled Hsp27-D3 Mutants**

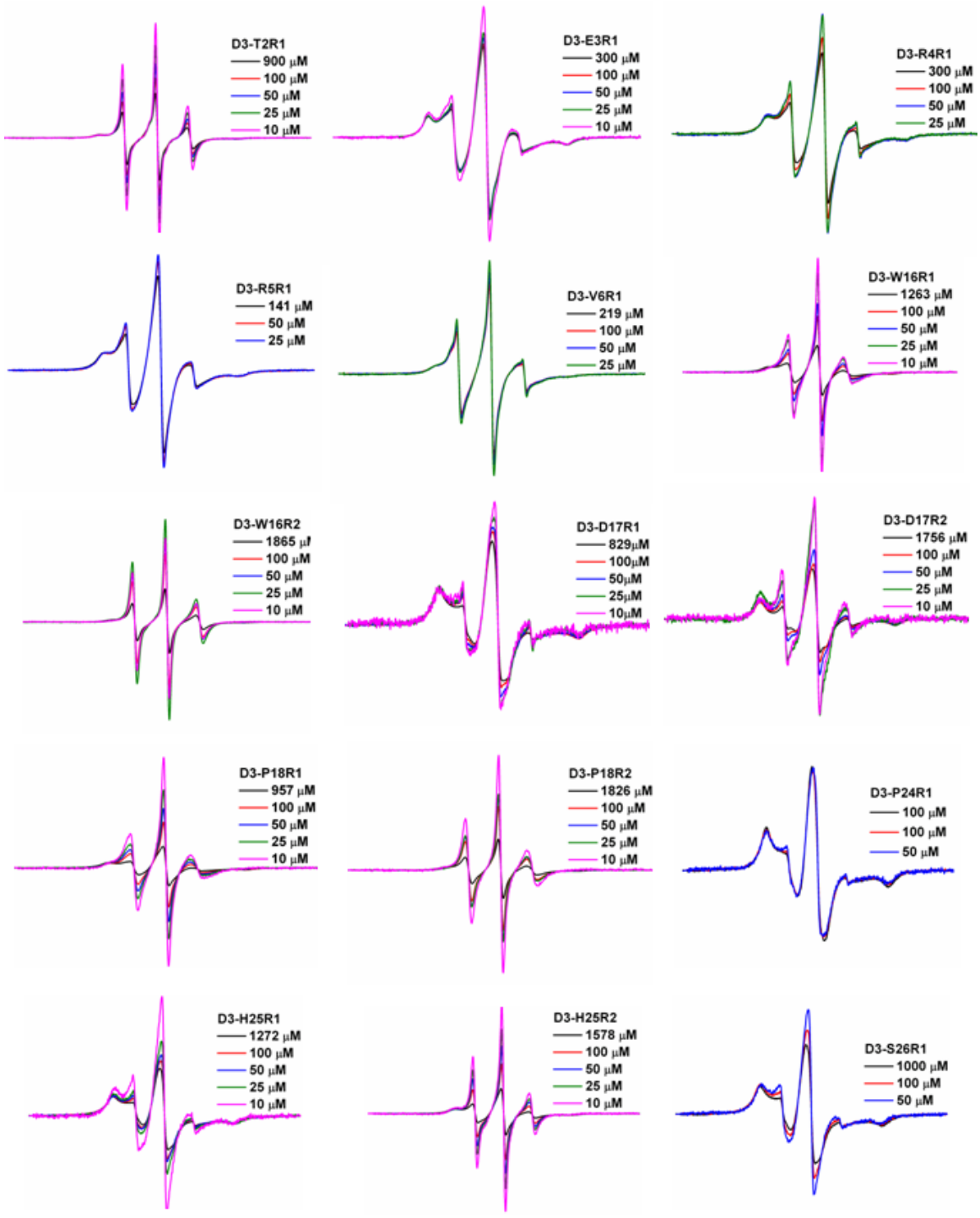

**Figure A12. Concentration Dependence of EPR Lineshape For Spin Labeled Hsp27-D3 Mutants**

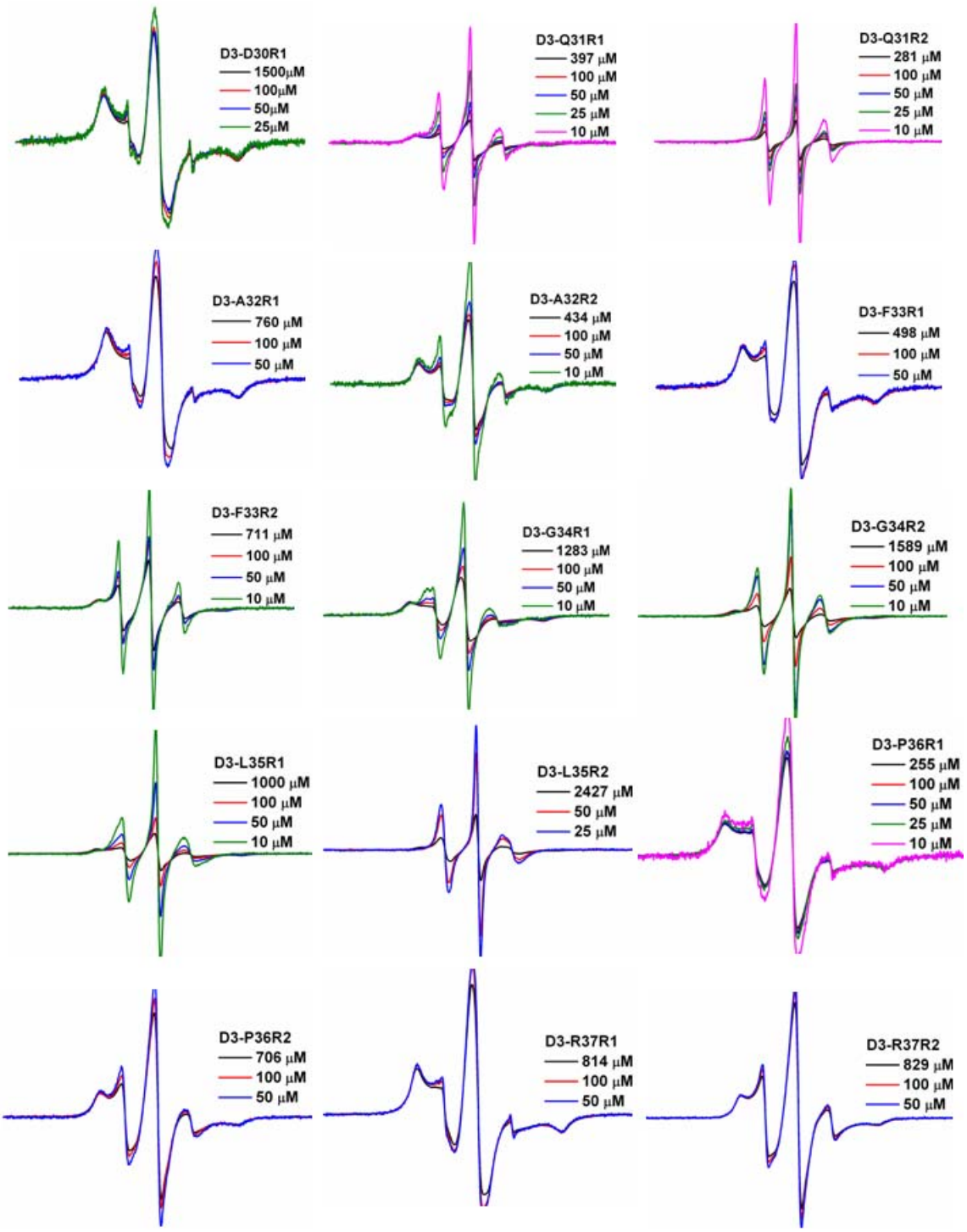

**Figure A13. Concentration Dependence of EPR Lineshape For Spin Labeled Hsp27-D3 Mutants**

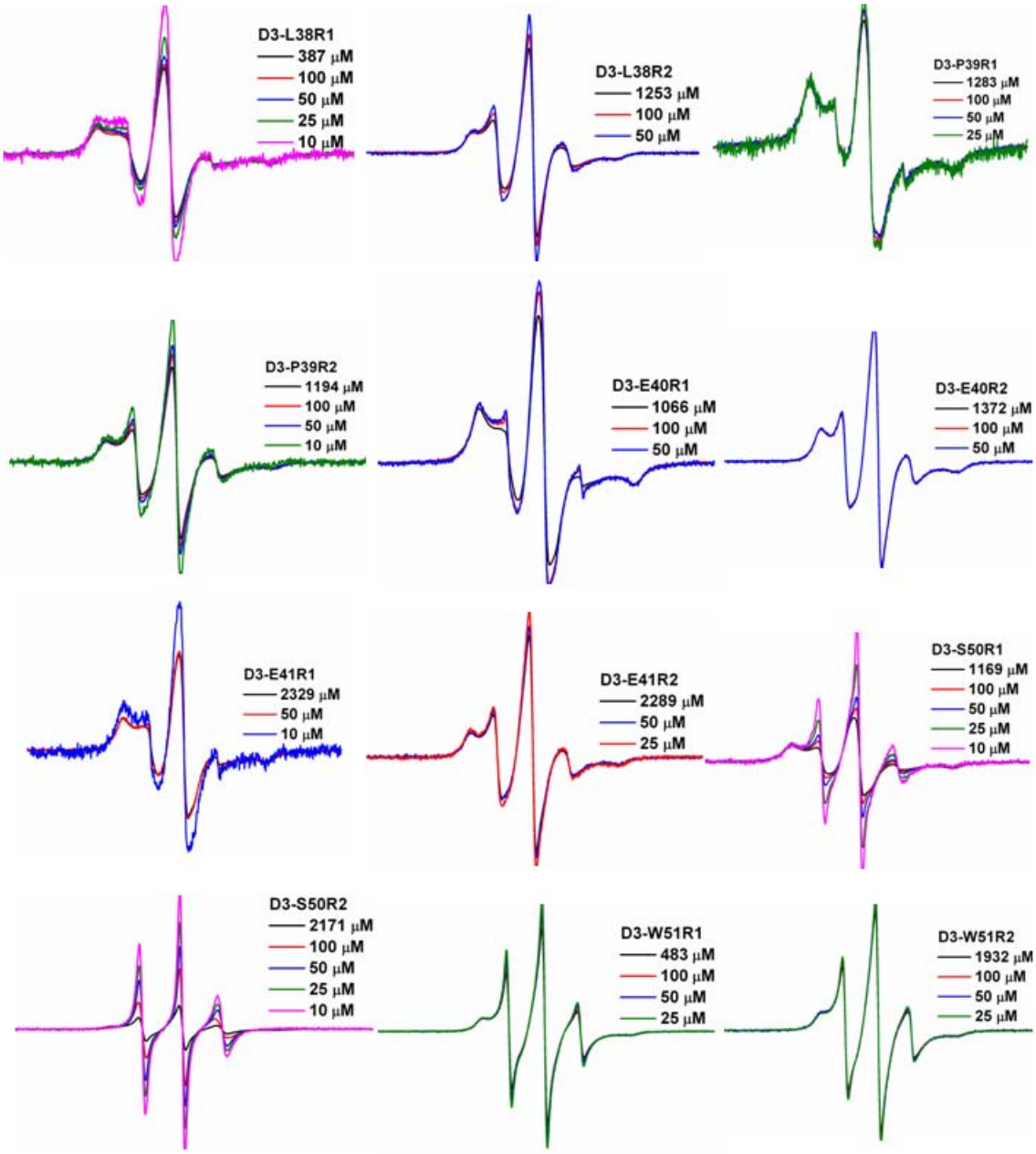

**Figure A14. Concentration Dependence of EPR Lineshape For Spin Labeled Hsp27-D3 Mutants**

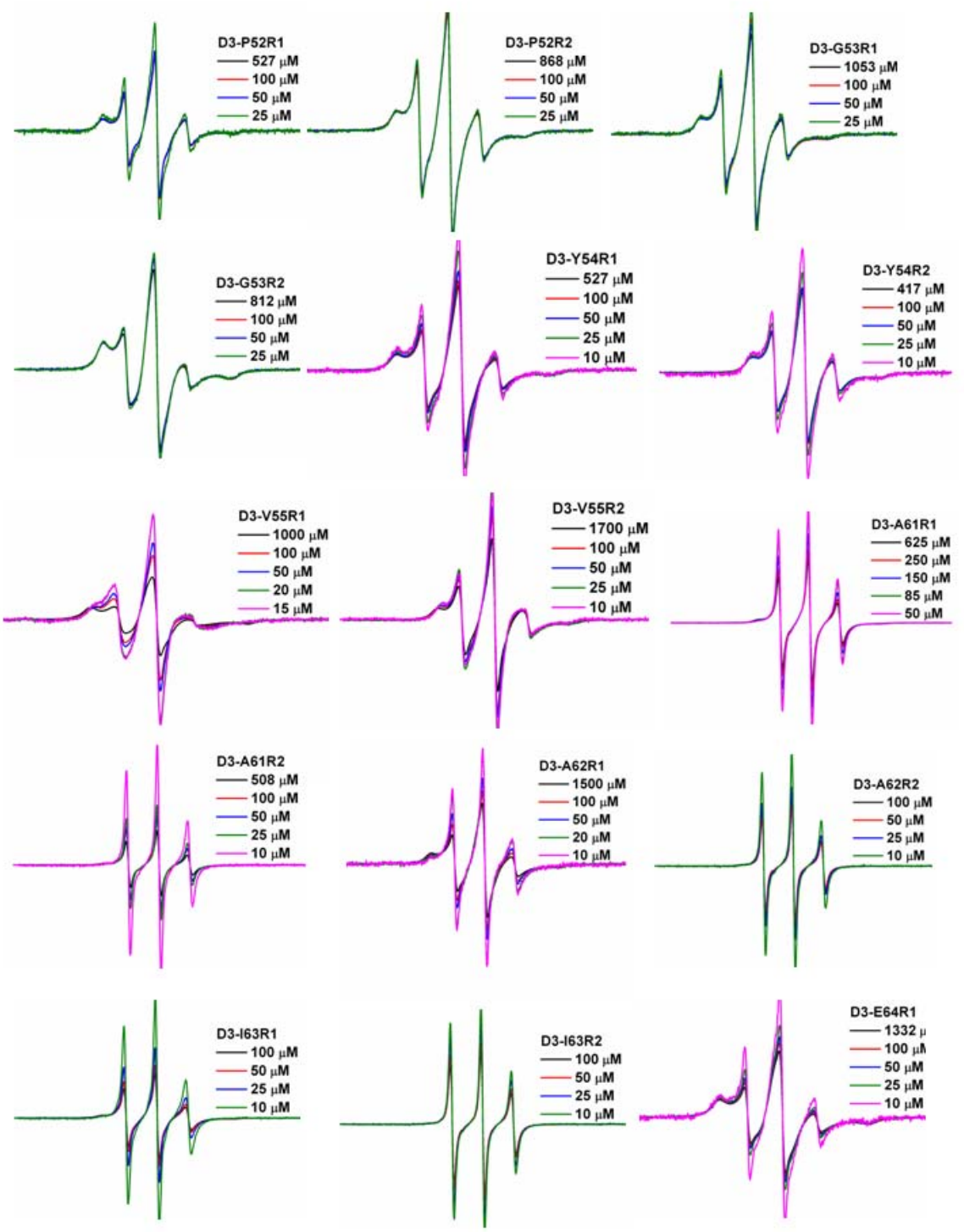

**Figure A15. Concentration Dependence of EPR Lineshape For Spin Labeled Hsp27-D3 Mutants**

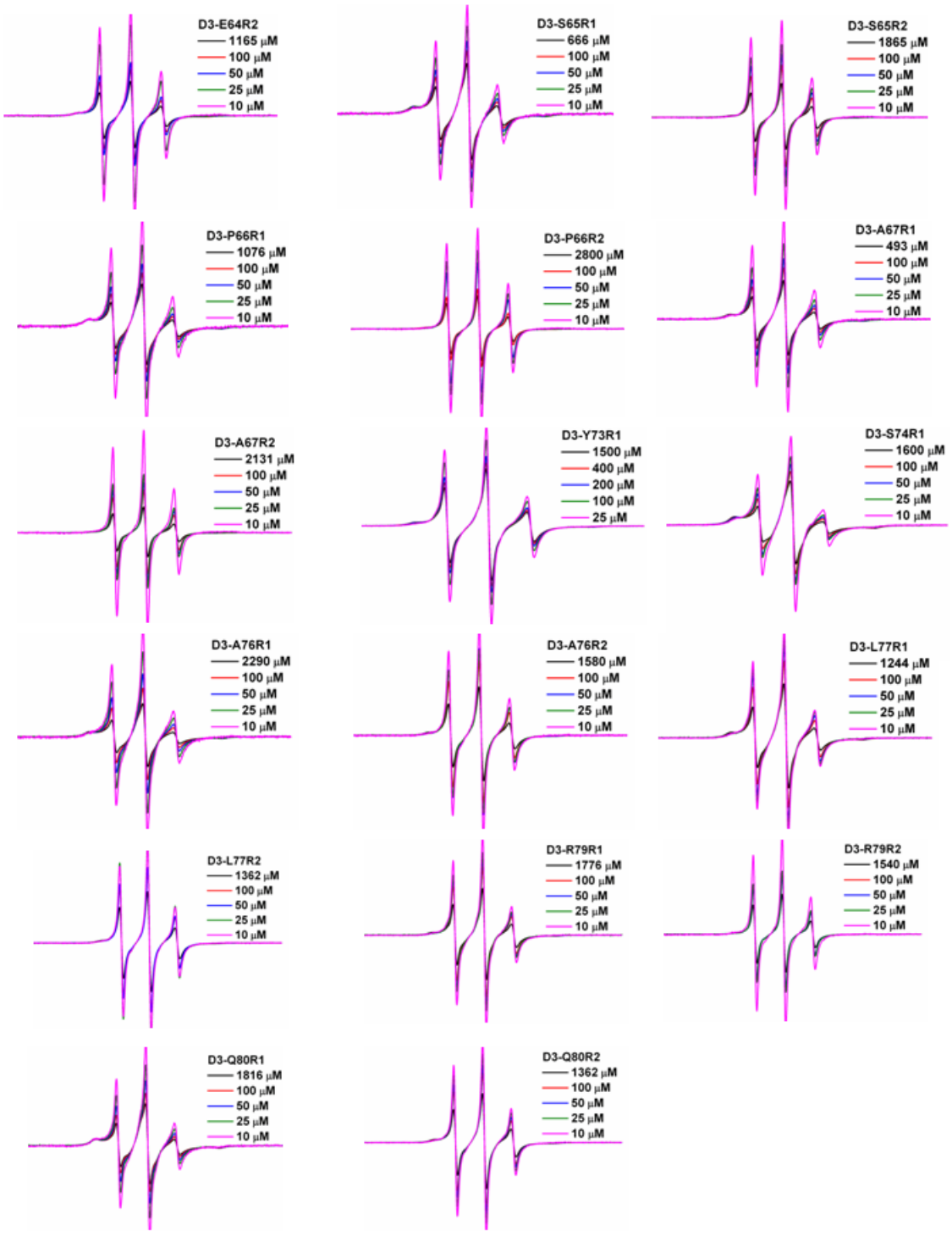

**Figure A16. Concentration Dependence of EPR Lineshape For Spin Labeled Hsp27-D3 Mutants**

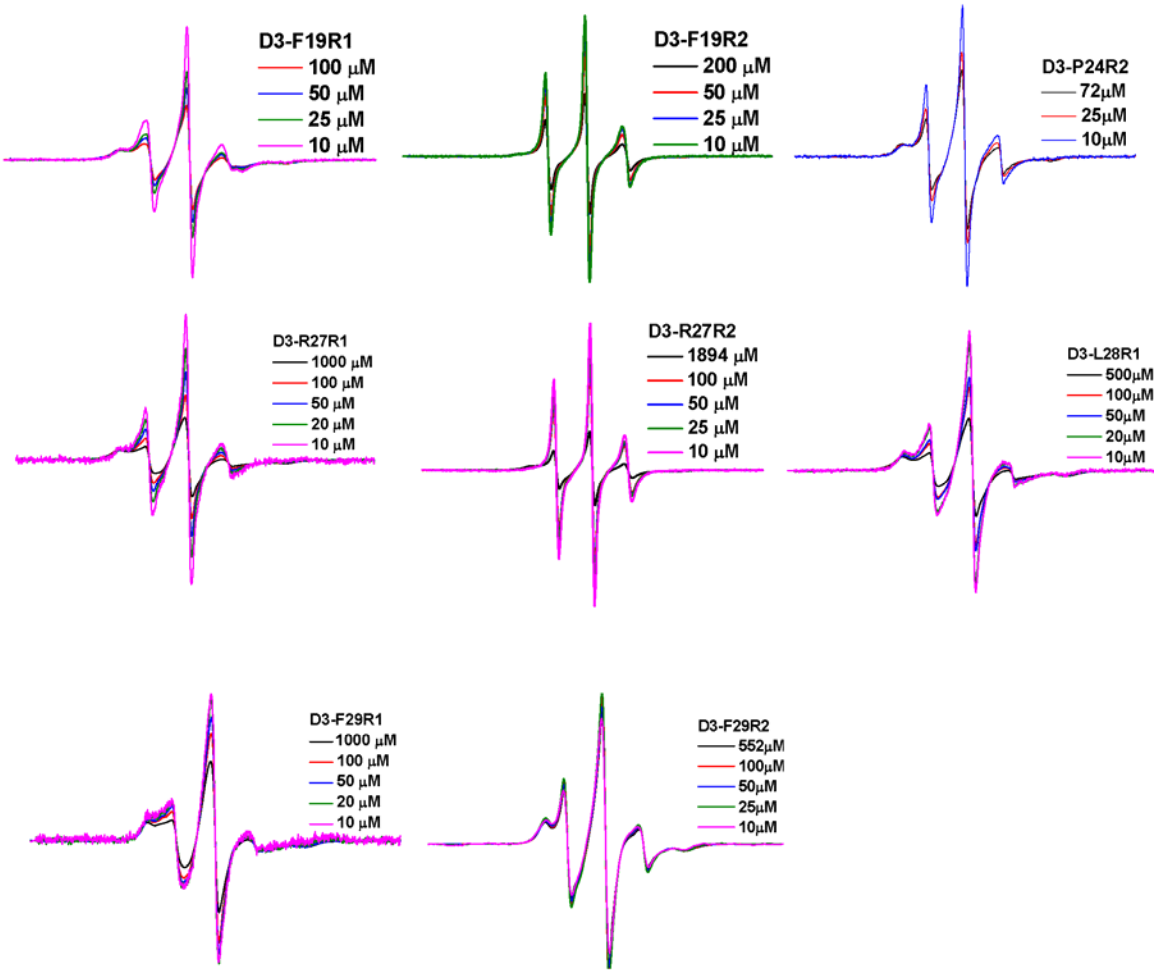

**Figure A17. pH Dependence of EPR Lineshape For Spin Labeled Hsp27-D3 Mutants**

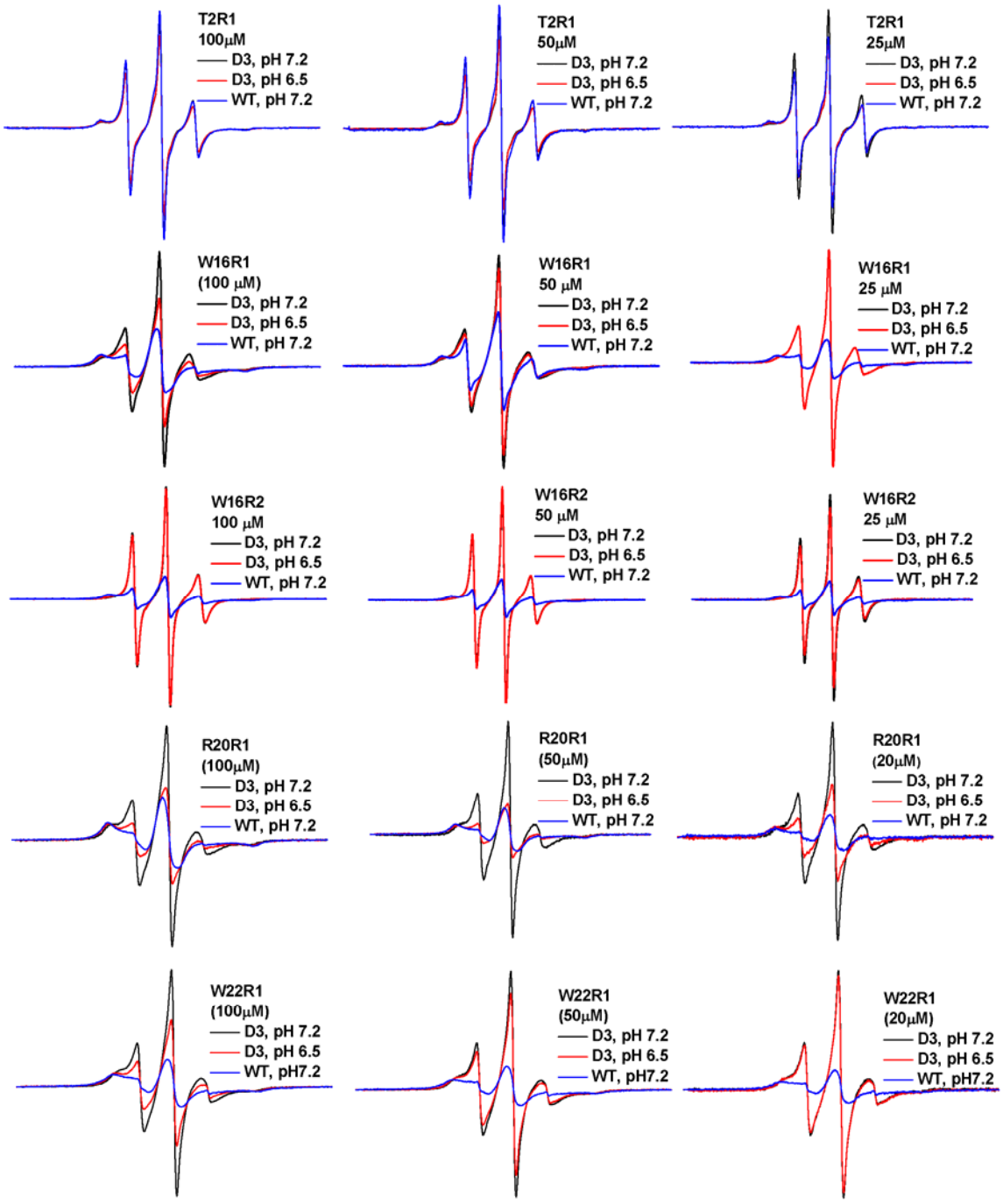

**Figure A18. pH Dependence of EPR Lineshape For Spin Labeled Hsp27-D3 Mutants**

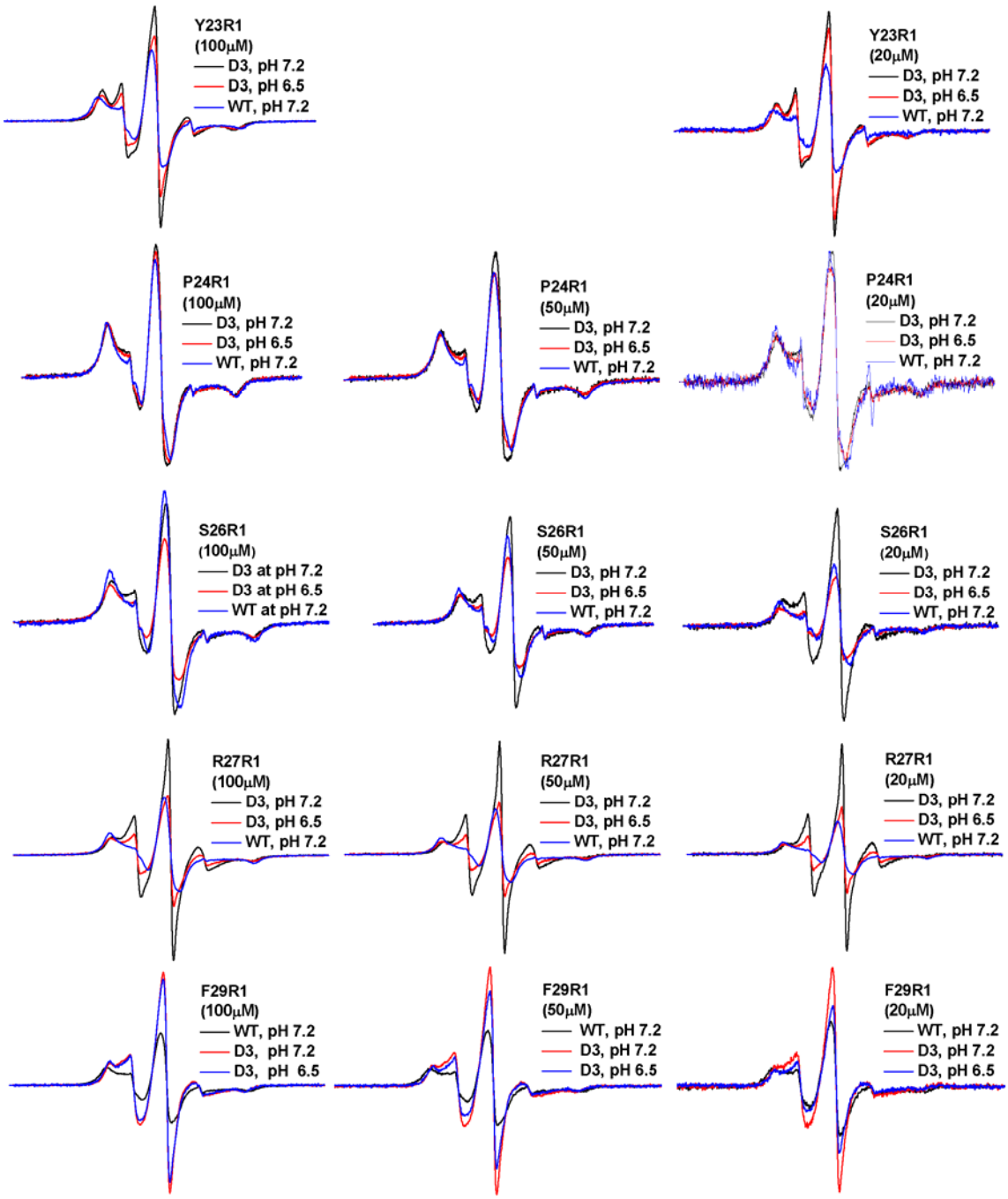

**Figure A19. pH Dependence of EPR Lineshape For Spin Labeled Hsp27-D3 Mutants**

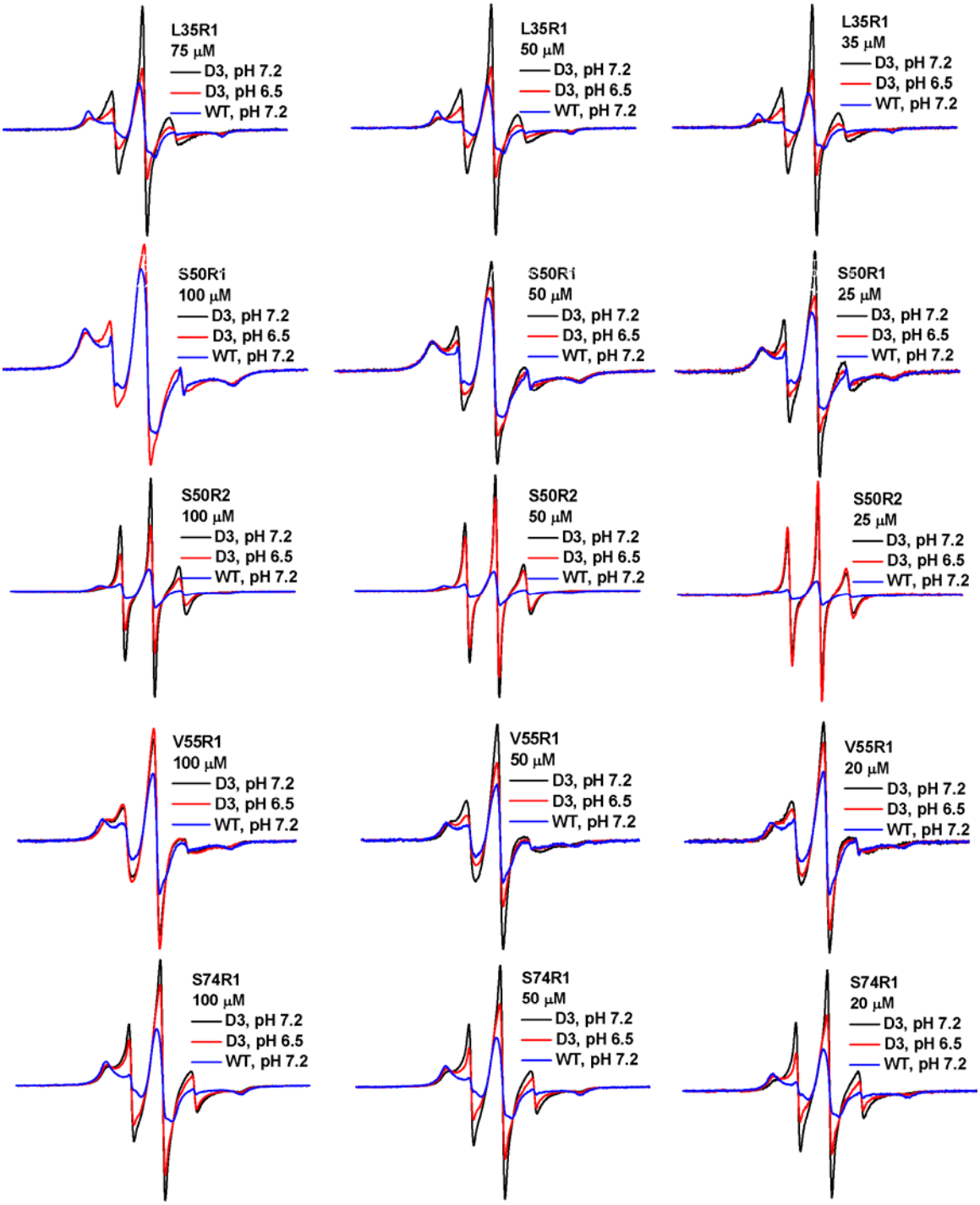

**Figure A20. pH Dependence of EPR Lineshape For Spin Labeled Hsp27-D3 Mutants**

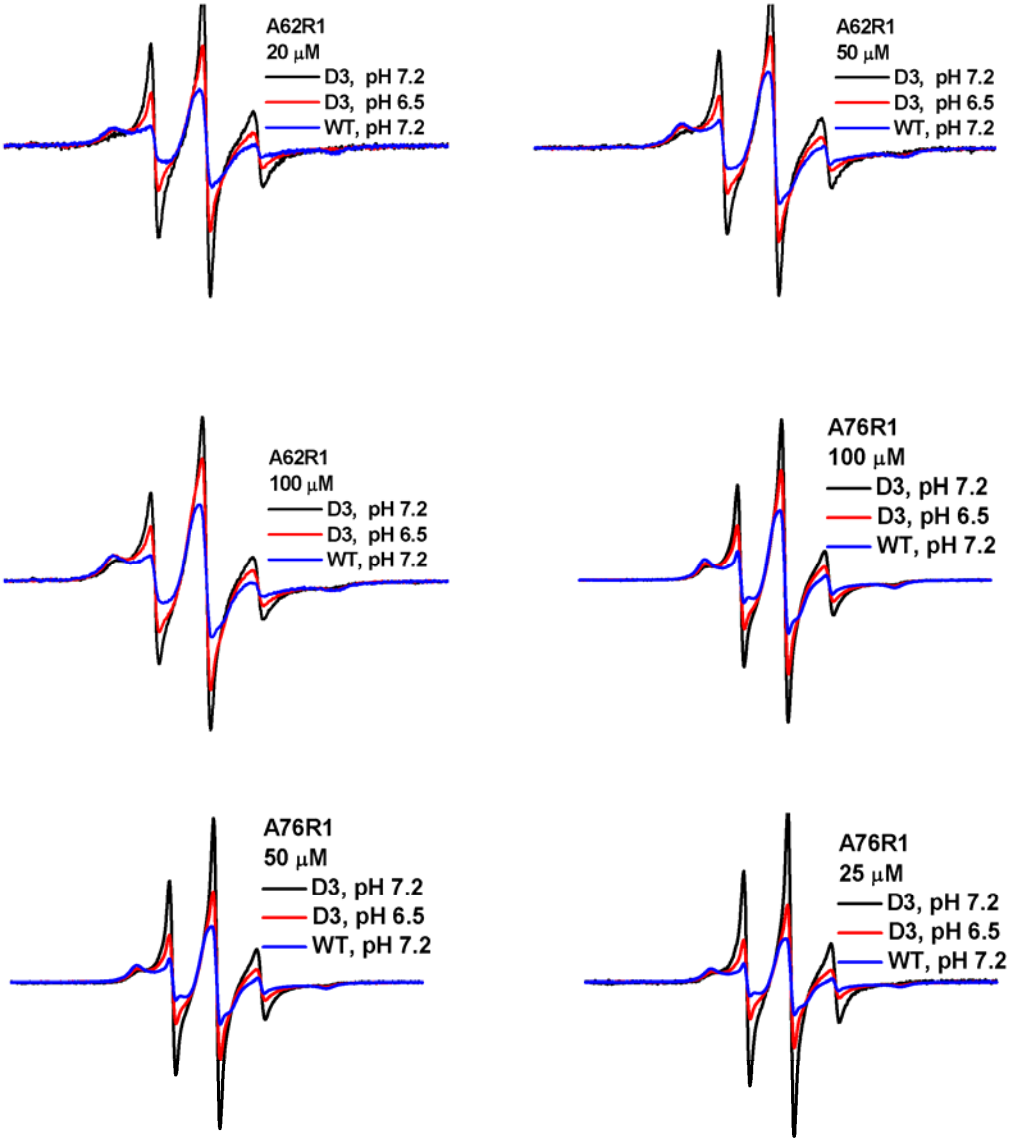

## Figure A21. Detection of Hsp27-D3/T4L Complexes By SEC

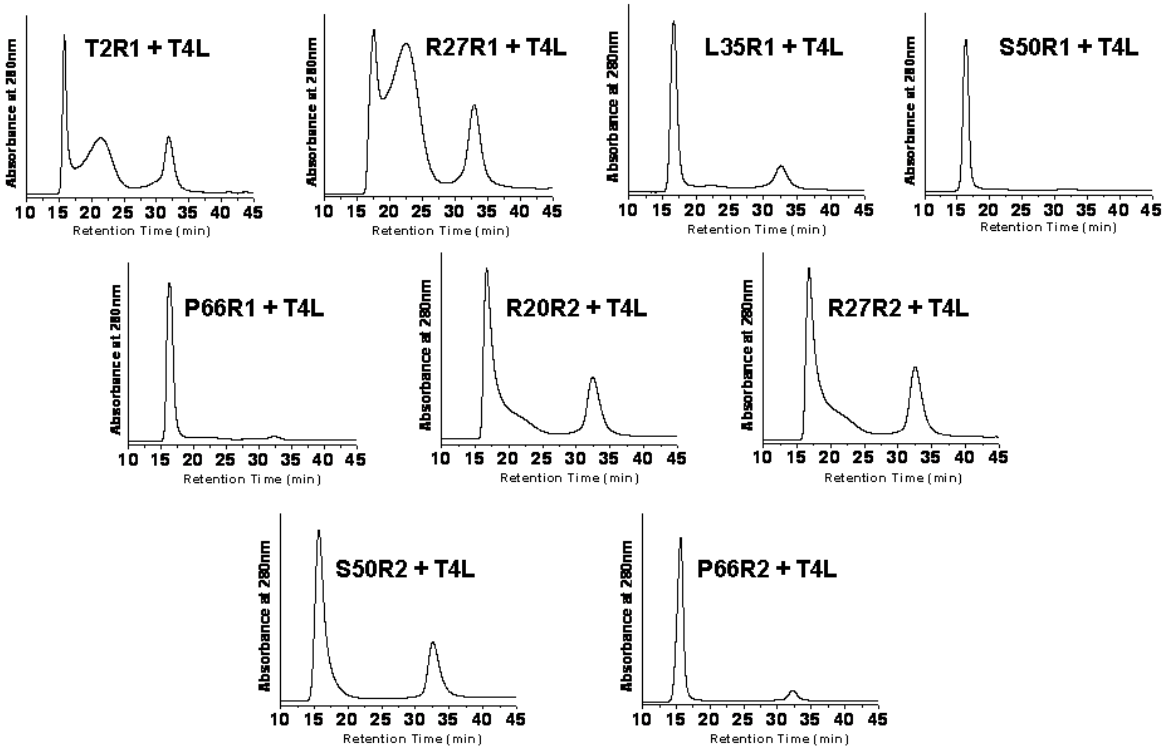


**Peaks corresponding to Hsp27-D3/T4L complexes have retention times of ~15-20 mins. The spin labeled Hsp27-D3 unbound mutants have retention times of ~32 mins.**

**Figure A22. Confirmation of Hsp27-D3/T4L Complexes By SDS-PAGE**

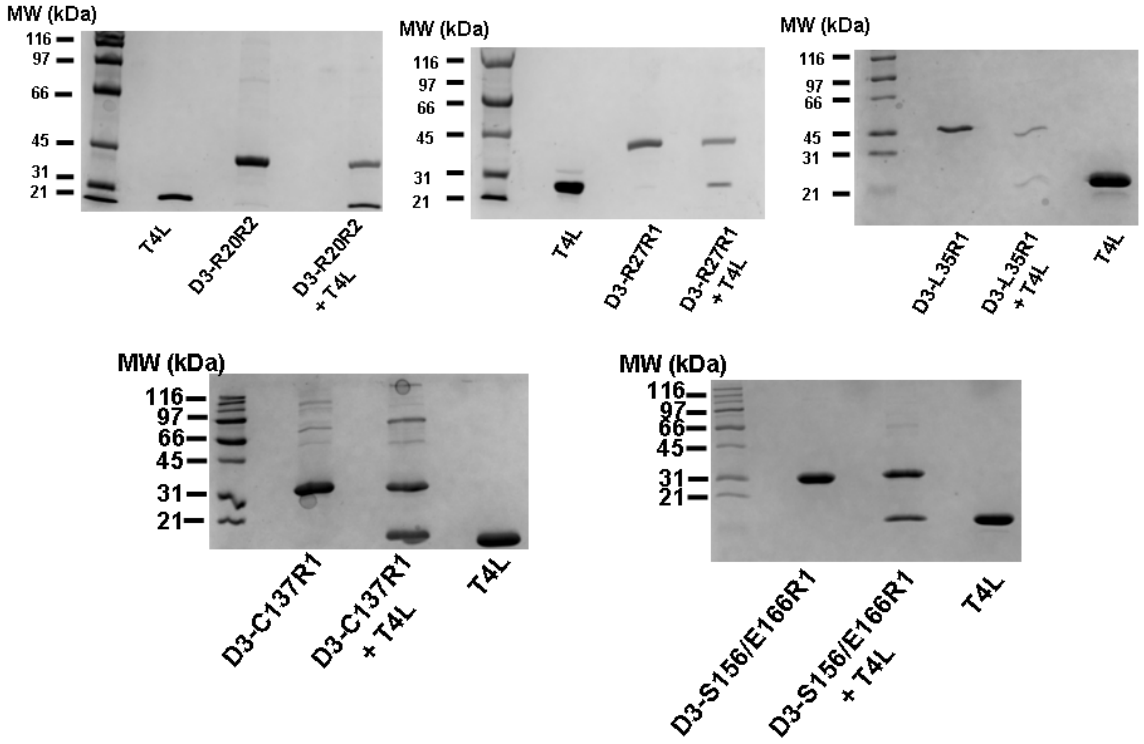

## Figure A23. SEC Data For Hsp27-D3 Mutants

### Legend

+++ Dissociated

++ Partially dissociated

+ Assembled

- No data acquired at the applicable concentration

| | Mutant | D3-T2C | D3-E3C | D3-R4C | D3-R5C | D3-R6C |
|---|---|---|---|---|---|---|
| Concentration | | | | | | |
| | | | | | | |
| 1mg/mL | | - | ++ | +++ | +++ | - |
| .7mg/mL | | - | ++ | +++ | +++ | - |
| .5mg/mL | | - | ++ | +++ | +++ | - |
| .3mg/mL | | - | ++ | +++ | +++ | - |
| .1mg/mL | | - | ++ | +++ | - | - |
| .05mg/mL | | - | ++ | +++ | - | - |
| 15µg/mL | | - | ++ | +++ | - | - |

## Figure A24. SEC Data For Hsp27-D3 Mutants

| | Mutant | D3-T2R1 | D3-E3R1 | D3-R4R1 | D3-R5R1 | D3-R6R1 |
|---|---|---|---|---|---|---|
| Concentration | | | | | | |
| | | | | | | |
| 1mg/mL | | ++ | ++ | ++ | ++ | - |
| .7mg/mL | | - | ++ | ++ | ++ | - |
| .5mg/mL | | - | ++ | ++ | ++ | - |
| .3mg/mL | | - | ++ | ++ | ++ | - |
| .1mg/mL | | - | ++ | ++ | ++ | - |
| .05mg/mL | | - | ++ | ++ | ++ | - |
| 15µg/mL | | - | ++ | ++ | ++ | - |

| | Mutant | D3-T2R2 | D3-E3R2 | D3-R4R2 | D3-R5R2 | D3-R6R2 |
|---|---|---|---|---|---|---|
| Concentration | | | | | | |
| | | | | | | |
| 1mg/mL | | - | ++ | ++ | ++ | - |
| .7mg/mL | | - | ++ | ++ | ++ | - |
| .5mg/mL | | - | ++ | ++ | ++ | - |
| .3mg/mL | | - | ++ | ++ | ++ | - |
| .1mg/mL | | - | ++ | ++ | ++ | - |
| .05mg/mL | | - | ++ | ++ | ++ | - |
| 15µg/mL | | - | ++ | ++ | ++ | - |

## Figure A25. SEC Data For Hsp27-D3 Mutants

| | Mutant | D3-W16C | D3-D17C | D3-P18C | D3-F19C | D3-R20C | D3-D21C | D3-W22C | D3-Y23C |
|---|---|---|---|---|---|---|---|---|---|
| Concentration | | | | | | | | | |
| | | | | | | | | | |
| 1mg/mL | | - | ++ | +++ | +++ | +++ | ++ | +++ | +++ |
| .7mg/mL | | - | - | - | - | - | - | - | - |
| .5mg/mL | | - | - | - | - | - | - | - | - |
| .3mg/mL | | - | - | - | - | - | - | - | - |
| .1mg/mL | | - | - | - | - | - | - | - | - |
| .05mg/mL | | - | ++ | - | - | - | ++ | - | - |
| 15μg/mL | | - | ++ | +++ | - | - | - | - | - |

| | Mutant | D3-W16R1 | D3-D17R1 | D3-P18R1 | D3-F19R1 | D3-R20R1 | D3-D21R1 | D3-W22R1 | D3-Y23R1 |
|---|---|---|---|---|---|---|---|---|---|
| Concentration | | | | | | | | | |
| | | | | | | | | | |
| 1mg/mL | | +++ | ++ | - | ++ | +++ | ++ | +++ | +++ |
| .7mg/mL | | - | - | - | - | - | - | - | - |
| .5mg/mL | | +++ | - | - | - | - | - | - | - |
| .3mg/mL | | - | - | - | - | - | - | - | - |
| .1mg/mL | | - | - | - | - | - | - | - | - |
| .05mg/mL | | +++ | ++ | - | - | - | ++ | +++ | +++ |
| 15μg/mL | | - | ++ | - | - | - | ++ | - | - |

## Figure A26. SEC Data For Hsp27-D3 Mutants

| | Mutant | D3-W16R2 | D3-D17R2 | D3-P18R2 | D3-F19R2 | D3-R20R2 | D3-D21R2 | D3-W22R2 | D3-Y23R2 |
|---|---|---|---|---|---|---|---|---|---|
| Concentration | | | | | | | | | |
| | | | | | | | | | |
| 1mg/mL | | +++ | ++ | - | +++ | +++ | ++ | +++ | ++ |
| .7mg/mL | | - | - | - | - | - | - | - | - |
| .5mg/mL | | - | - | - | - | - | - | - | - |
| .3mg/mL | | - | - | - | - | - | - | - | - |
| .1mg/mL | | - | - | - | - | - | - | - | - |
| .05mg/mL | | - | ++ | - | - | - | ++ | - | - |
| 15µg/mL | | - | ++ | - | - | - | - | - | - |

| | Mutant | D3-P24C | D3-H25C | D3-S26C | D3-R27C | D3-L28C | D3-F29C |
|---|---|---|---|---|---|---|---|
| Concentration | | | | | | | |
| | | | | | | | |
| 1mg/mL | | ++ | +++ | ++ | +++ | - | +++ |
| .7mg/mL | | - | - | - | - | - | - |
| .5mg/mL | | - | - | - | - | - | - |
| .3mg/mL | | ++ | - | ++ | - | - | - |
| .1mg/mL | | - | - | - | - | - | - |
| .05mg/mL | | ++ | - | ++ | - | - | - |
| 15µg/mL | | ++ | - | ++ | - | - | - |

## Figure A27. SEC Data For Hsp27-D3 Mutants

| | Mutant | D3-P24R1 | D3-H25R1 | D3-S26R1 | D3-R27R1 | D3-L28R1 | D3-F29R1 |
|---|---|---|---|---|---|---|---|
| Concentration | | | | | | | |
| | | | | | | | |
| 1mg/mL | | ++ | ++ | ++ | +++ | +++ | +++ |
| .7mg/mL | | - | - | - | - | - | - |
| .5mg/mL | | - | ++ | - | - | - | - |
| .3mg/mL | | - | ++ | - | - | - | - |
| .1mg/mL | | - | - | - | - | - | - |
| .05mg/mL | | ++ | - | ++ | - | +++ | - |
| 15µg/mL | | ++ | - | - | - | - | - |

| | Mutant | D3-P24R2 | D3-H25R2 | D3-S26R2 | D3-R27R2 | D3-L28R2 | D3-F29R2 |
|---|---|---|---|---|---|---|---|
| Concentration | | | | | | | |
| | | | | | | | |
| 1mg/mL | | ++ | +++ | - | +++ | - | +++ |
| .7mg/mL | | - | - | - | - | - | - |
| .5mg/mL | | - | - | - | - | - | - |
| .3mg/mL | | - | - | - | - | - | - |
| .1mg/mL | | - | - | - | - | - | - |
| .05mg/mL | | ++ | - | - | - | - | - |
| 15µg/mL | | - | - | - | - | - | - |

## Figure A28. SEC Data For Hsp27-D3 Mutants

| | Mutant | D3-D30C | D3-Q31C | D3-A32C | D3-F33C | D3-G34C | D3-L35C |
|---|---|---|---|---|---|---|---|
| Concentration | | | | | | | |
| | | | | | | | |
| 1mg/mL | | ++ | +++ | +++ | +++ | ++ | +++ |
| .7mg/mL | | - | - | - | - | - | - |
| .5mg/mL | | - | - | - | - | - | - |
| .3mg/mL | | ++ | - | - | - | - | - |
| .1mg/mL | | - | - | - | - | - | - |
| .05mg/mL | | ++ | - | +++ | - | - | - |
| 15μg/mL | | ++ | - | - | - | - | - |

| | Mutant | D3-D30R1 | D3-Q31R1 | D3-A32R1 | D3-F33R1 | D3-G34R1 | D3-L35R1 |
|---|---|---|---|---|---|---|---|
| Concentration | | | | | | | |
| | | | | | | | |
| 1mg/mL | | + | +++ | - | - | ++ | +++ |
| .7mg/mL | | - | - | - | - | - | - |
| .5mg/mL | | - | - | - | - | - | - |
| .3mg/mL | | - | - | - | - | - | - |
| .1mg/mL | | - | - | - | - | - | - |
| .05mg/mL | | ++ | - | - | - | - | - |
| 15μg/mL | | - | - | - | - | - | - |

## Figure A29. SEC Data For Hsp27-D3 Mutants

| | Mutant | D3-D30R2 | D3-Q31R2 | D3-A32R2 | D3-F33R2 | D3-G34R2 | D3-L35R2 |
|---|---|---|---|---|---|---|---|
| Concentration | | | | | | | |
| | | | | | | | |
| 1mg/mL | | ++ | +++ | ++ | ++ | ++ | +++ |
| .7mg/mL | | - | - | - | - | - | - |
| .5mg/mL | | ++ | - | - | - | - | - |
| .3mg/mL | | - | - | - | - | - | - |
| .1mg/mL | | - | - | - | - | - | - |
| .05mg/mL | | - | - | - | - | - | - |
| 15μg/mL | | - | - | - | - | - | - |

| | Mutant | D3-P36C | D3-R37C | D3-L38C | D3-P39C | D3-E40C | D3-E41C |
|---|---|---|---|---|---|---|---|
| Concentration | | | | | | | |
| | | | | | | | |
| 1mg/mL | | - | + | + | + | + | + |
| .7mg/mL | | - | + | + | + | + | - |
| .5mg/mL | | - | + | + | + | + | - |
| .3mg/mL | | - | + | + | ++ | + | - |
| .1mg/mL | | - | ++ | ++ | ++ | ++ | - |
| .05mg/mL | | - | ++ | ++ | ++ | ++ | ++ |
| 15μg/mL | | - | ++ | ++ | ++ | ++ | ++ |

## Figure A30. SEC Data For Hsp27-D3 Mutants

| | Mutant | D3-P36R1 | D3-R37R1 | D3-L38R1 | D3-P39R1 | D3-E40R1 | D3-E41R1 |
|---|---|---|---|---|---|---|---|
| Concentration | | | | | | | |
| | | | | | | | |
| 1mg/mL | | + | ++ | + | + | + | + |
| .7mg/mL | | - | - | - | - | - | - |
| .5mg/mL | | - | - | - | - | - | - |
| .3mg/mL | | - | - | - | - | - | - |
| .1mg/mL | | - | - | - | - | - | - |
| .05mg/mL | | - | - | ++ | - | - | - |
| 15µg/mL | | - | - | - | - | - | - |

| | Mutant | D3-P36R2 | D3-R37R2 | D3-L38R2 | D3-P39R2 | D3-E40R2 | D3-E41R2 |
|---|---|---|---|---|---|---|---|
| Concentration | | | | | | | |
| | | | | | | | |
| 1mg/mL | | ++ | + | ++ | ++ | + | + |
| .7mg/mL | | - | - | - | - | - | - |
| .5mg/mL | | - | - | - | - | - | - |
| .3mg/mL | | - | - | - | - | - | - |
| .1mg/mL | | - | - | - | - | - | - |
| .05mg/mL | | - | - | ++ | - | - | - |
| 15µg/mL | | - | - | - | - | - | - |

## Figure A31. SEC Data For Hsp27-D3 Mutants

| | Mutant | D3-S50C | D3-W51C | D3-P52C | D3-G53C | D3-Y54C | D3-V55C |
|---|---|---|---|---|---|---|---|
| Concentration | | | | | | | |
| | | | | | | | |
| 1mg/mL | | +++ | + | ++ | + | + | +++ |
| .7mg/mL | | - | + | ++ | + | + | - |
| .5mg/mL | | - | + | ++ | + | + | +++ |
| .3mg/mL | | - | ++ | ++ | + | + | - |
| .1mg/mL | | - | ++ | ++ | ++ | ++ | - |
| .05mg/mL | | - | ++ | ++ | ++ | ++ | - |
| 15µg/mL | | - | ++ | ++ | ++ | ++ | - |

| | Mutant | D3-S50R1 | D3-W51R1 | D3-P52R1 | D3-G53R1 | D3-Y54R1 | D3-V55R1 |
|---|---|---|---|---|---|---|---|
| Concentration | | | | | | | |
| | | | | | | | |
| 1mg/mL | | ++ | + | + | - | - | +++ |
| .7mg/mL | | - | - | - | - | - | - |
| .5mg/mL | | - | - | - | - | - | - |
| .3mg/mL | | - | - | - | - | - | - |
| .1mg/mL | | - | - | - | - | - | - |
| .05mg/mL | | - | - | - | - | - | +++ |
| 15µg/mL | | - | ++ | - | - | - | - |

## Figure A32. SEC Data For Hsp27-D3 Mutants

| | Mutant | D3-S50R2 | D3-W51R2 | D3-P52R2 | D3-G53R2 | D3-Y54R2 | D3-V55R2 |
|---|---|---|---|---|---|---|---|
| Concentration | | | | | | | |
| | | | | | | | |
| 1mg/mL | | +++ | + | + | + | ++ | +++ |
| .7mg/mL | | - | - | - | - | - | - |
| .5mg/mL | | - | - | - | - | - | +++ |
| .3mg/mL | | - | - | - | - | - | - |
| .1mg/mL | | - | - | - | - | - | - |
| .05mg/mL | | - | - | - | - | - | - |
| 15µg/mL | | - | ++ | - | - | - | - |

| | Mutant | D3-A61C | D3-A62C | D3-I63C | D3-E64C | D3-S65C | D3-P66C | D3-A67C |
|---|---|---|---|---|---|---|---|---|
| Concentration | | | | | | | | |
| | | | | | | | | |
| 1mg/mL | | +++ | +++ | +++ | ++ | - | - | - |
| .7mg/mL | | - | - | - | ++ | - | - | - |
| .5mg/mL | | - | - | - | ++ | - | - | - |
| .3mg/mL | | - | - | - | ++ | - | - | - |
| .1mg/mL | | - | - | - | ++ | - | - | - |
| .05mg/mL | | - | - | - | ++ | - | - | - |
| 15µg/mL | | - | - | - | ++ | - | - | - |

## Figure A33. SEC Data For Hsp27-D3 Mutants

| | Mutant | D3-A61R1 | D3-A62R1 | D3-I63R1 | D3-E64R1 | D3-S65R1 | D3-P66R1 | D3-A67R1 |
|---|---|---|---|---|---|---|---|---|
| Concentration | | | | | | | | |
| | | | | | | | | |
| 1mg/mL | | +++ | +++ | +++ | + | - | +++ | - |
| .7mg/mL | | - | - | - | + | - | - | - |
| .5mg/mL | | - | - | - | ++ | - | - | - |
| .3mg/mL | | - | - | - | ++ | - | - | - |
| .1mg/mL | | - | - | - | ++ | - | - | - |
| .05mg/mL | | - | - | - | ++ | - | - | - |
| 15µg/mL | | - | - | - | ++ | - | - | - |

| | Mutant | D3-A61R2 | D3-A62R2 | D3-I63R2 | D3-E64R2 | D3-S65R2 | D3-P66R2 | D3-A67R2 |
|---|---|---|---|---|---|---|---|---|
| Concentration | | | | | | | | |
| | | | | | | | | |
| 1mg/mL | | +++ | +++ | +++ | - | - | +++ | - |
| .7mg/mL | | - | - | - | - | - | - | - |
| .5mg/mL | | - | - | - | - | - | - | - |
| .3mg/mL | | - | - | - | - | - | - | - |
| .1mg/mL | | - | - | - | - | - | - | - |
| .05mg/mL | | - | - | - | - | - | - | - |
| 15µg/mL | | - | - | - | - | - | - | - |

## Figure A34. SEC Data For Hsp27-D3 Mutants

| | Mutant | D3-Y73C | D3-S74C | D3-A76C | D3-L77C | D3-R79C | D3-Q80C |
|---|---|---|---|---|---|---|---|
| Concentration | | | | | | | |
| | | | | | | | |
| 1mg/mL | | - | - | +++ | - | - | - |
| .7mg/mL | | - | - | - | - | - | - |
| .5mg/mL | | - | - | - | - | - | - |
| .3mg/mL | | - | - | - | - | - | - |
| .1mg/mL | | - | - | - | - | - | - |
| .05mg/mL | | - | - | - | - | - | - |
| 15µg/mL | | - | - | - | - | - | - |

| | Mutant | D3-Y73R1 | D3-S74R1 | D3-A76R1 | D3-L77R1 | D3-R79R1 | D3-Q80R1 |
|---|---|---|---|---|---|---|---|
| Concentration | | | | | | | |
| | | | | | | | |
| 1mg/mL | | - | +++ | +++ | - | +++ | - |
| .7mg/mL | | - | - | - | - | - | - |
| .5mg/mL | | - | - | - | - | - | - |
| .3mg/mL | | - | - | - | - | - | - |
| .1mg/mL | | - | - | - | - | - | - |
| .05mg/mL | | - | - | - | - | - | - |
| 15µg/mL | | - | - | - | - | - | - |

## Figure A35. SEC Data For Hsp27-D3 Mutants

| | Mutant | D3-Y73R2 | D3-S74R2 | D3-A76R2 | D3-L77R2 | D3-R79R2 | D3-Q80R2 |
|---|---|---|---|---|---|---|---|
| Concentration | | | | | | | |
| | | | | | | | |
| 1mg/mL | | - | - | +++ | +++ | +++ | +++ |
| .7mg/mL | | - | - | - | - | - | - |
| .5mg/mL | | - | - | - | - | - | - |
| .3mg/mL | | - | - | - | - | - | - |
| .1mg/mL | | - | - | - | - | - | - |
| .05mg/mL | | - | - | - | - | - | - |
| 15μg/mL | | - | - | - | - | - | - |

## REFERENCES


Abisambra, J. F., Blair, L. J., Hill, S. E., Jones, J. R., Kraft, C., Rogers, J., Koren, J., Jinwal, U. K., Lawson, L., Johnson, A. G., Wilcock, D., O'Leary, J. C., Jansen-West, K., Muschol, M., Golde, T. E., Weeber, E. J., Banko, J. and Dickey, C. A. (2010). "Phosphorylation Dynamics Regulate Hsp27-Mediated Rescue of Neuronal Plasticity Deficits in Tau Transgenic Mice." The Journal of Neuroscience 30(46): 15374-15382.

Aevermann, B. and Waters, E. (2008). "A comparative genomic analysis of the small heat shock proteins in Caenorhabditis elegans briggsae." Genetica 133(3): 307-319.

Altenbach, C., Flitsch, S. L., Khorana, H. G. and Hubbell, W. L. (1989). "Structural studies on transmembrane proteins. 2. Spin labeling of bacteriorhodopsin mutants at unique cysteines." Biochemistry 28(19): 7806-7812.

Altenbach, C., Froncisz, W., Hemker, R., McHaourab, H. and Hubbell, W. L. (2005). "Accessibility of Nitroxide Side Chains: Absolute Heisenberg Exchange Rates from Power Saturation EPR." Biophysical Journal 89(3): 2103-2112.

Altenbach, C., Greenhalgh, D. A., Khorana, H. G. and Hubbell, W. L. (1994). "A collision gradient method to determine the immersion depth of nitroxides in lipid bilayers: Application to spin-labeled mutants of bacteriorhodopsin." Proc. Natl. Acad. Sci. USA 91: 1667-1671.

Altenbach, C., Marti, T., Khorana, H. G. and Hubbell, W. L. (1990). "Transmembrane protein structure: spin labeling of bacteriorhodopsin mutants." Science 248(4959): 1088-1092.

Amadi, S. T., Koteiche, H. A., Mishra, S. and McHaourab, H. S. (2010). "Structure, Dynamics, and Substrate-induced Conformational Changes of the Multidrug Transporter EmrE in Liposomes." Journal of Biological Chemistry 285(34): 26710-26718.

Andersson, S. G. E., Zomorodipour, A., Andersson, J. O., Sicheritz-Ponten, T., Alsmark, U. C. M., Podowski, R. M., Naslund, A. K., Eriksson, A.-S., Winkler, H. H. and Kurland, C. G. (1998). "The genome sequence of Rickettsia prowazekii and the origin of mitochondria." Nature 396(6707): 133-140.

Arrigo, A.-P., Simon, S., Gibert, B., Kretz-Remy, C., Nivon, M., Czekalla, A., Guillet, D., Moulin, M., Diaz-Latoud, C. and Vicart, P. (2007). "Hsp27 (HspB1) and αB-crystallin (HspB5) as therapeutic targets." FEBS Letters 581(19): 3665-3674.

Arrigo, A. P. and Muller, W. E. G. (2002). Small stress proteins. Berlin, Springer Verlag.

Astashkin, A. V., Hara, H. and Kawamori, A. (1998). "The pulsed electron-electron double resonance and "2+1" electron spin echo study of the oriented oxygen-evolving and Mn-depleted preparations of photosystem II." Journal of Chemical Physics 108(9): 3805-3812.

Atherton, N. M. (1973). Electron Spin Resonance Theory and Applications. New York, John Wiley & Sons Inc.

Aubin-Tam, M.-E., Olivares, Adrian O., Sauer, R. T., Baker, T. A. and Lang, M. J. (2011). "Single-Molecule Protein Unfolding and Translocation by an ATP-Fueled Proteolytic Machine." Cell 145(2): 257-267.

Bagneris, C., Bateman, O. A., Naylor, C. E., Cronin, N., Boelens, W. C., Keep, N. H. and Slingsby, C. (2009). "Crystal Structures of α-Crystallin Domain Dimers of αB-Crystallin and Hsp20." Journal of Molecular Biology 392(5): 1242-1252.

Baldwin, R. L. (1995). "The nature of protein folding pathways: The classical versus the new view." J. Biomol. NMR 5: 103-109.

Baldwin, R. L. and Rose, G. D. (1999). "Is protein folding hierarchic? I. Local structure and peptide folding." Trends Biochem Sci. 24: 27-33.

Banham, J. E., Baker, C. M., Ceola, S., Day, I. J., Grant, G. H., Groenen, E. J. J., Rodgers, C. T., Jeschke, G. and Timmel, C. R. (2008). "Distance measurements in the borderline region of applicability of CW EPR and DEER: A model study on a homologous series of spin-labelled peptides." Journal of Magnetic Resonance 191(2): 202-218.

Baranova, E. V., Weeks, S. D., Beelen, S., Bukach, O. V., Gusev, N. B. and Strelkov, S. V. (2011). "Three-Dimensional Structure of α-Crystallin Domain Dimers of Human Small Heat Shock Proteins HSPB1 and HSPB6." Journal of Molecular Biology 411(1): 110-122.

Barnes, J. P., Liang, Z., McHaourab, H. S., Freed, J. H. and Hubbell, W. L. (1999). "A Multifrequency Electron Spin Resonance Study of T4 Lysozyme Dynamics." Biophysical Journal 76(6): 3298-3306.

Basha, E., Friedrich, K. L. and Vierling, E. (2006). "The N-terminal arm of small heat shock proteins is important for both chaperone activity and substrate specificity." J Biol. Chem. 281: 39943-39952.

Beier, C. and Steinhoff, H. J. (2006). "A structure based simulation approach for electron paramagnetic resonance spectra using molecular and stochastic dynamic simulations." Biophys. J. 91: 2647-2664.

Ben-Zvi, A. P. and Goloubinoff, P. (2002). "Proteinaceous Infectious Behavior in Non-pathogenic Proteins Is Controlled by Molecular Chaperones." Journal of Biological Chemistry 277(51): 49422-49427.

Berengian, A. R., Parfenova, M. and Mchaourab, H. S. (1999). "Site-directed Spin Labeling Study of Subunit Interactions in the α-Crystallin Domain of Small Heat-shock Proteins." J Biol. Chem. 274(10): 6305-6314.

Bersohn, M. and Baird, J. C. (1966). An introduction to electron paramagnetic resonance. New York, W.A. Benjamin.

Beth, A. H., Robinson, B. H., Cobb, C. E., Dalton, L. R., Trommer, W. E., Birktoft, J. J. and Park, J. H. (1984). "Interactions and spatial arrangement of spin-labeled NAD+ bound to glyceraldehyde-3-phosphate dehydrogenase. Comparison of EPR and X-ray modeling data." Journal of Biological Chemistry 259(15): 9717-28.

Bloch, F. (1966). "Bloch Equation for Conduction-Electron Spin Resonance." Phys. Rev. 151: 215-219.

Blumberg, W. E. (1960). "Nuclear Spin-Lattice Relaxation Caused by Paramagnetic Impurities." Phys. Rev. 119: 79-84.

Borbat, P. P., Costa-Filho, A. J., Earle, K. A., Moscicki, J. K. and Freed, J. H. (2001). "Electron Spin Resonance in Studies of Membranes and Proteins." Science 291(5502): 266-269.

Bova, M. P., McHaourab, H. S., Han, Y. and Fung, B. K. K. (2000). "Subunit Exchange of Small Heat Shock Proteins." Journal of Biological Chemistry 275(2): 1035-1042.

Brady, J. P., Garland, D., Duglas-Tabor, Y., Robison, W. G., Groome, A. and Wawrousek, E. F. (1997). "Targeted disruption of the mouse αA-crystallin gene induces cataract and cytoplasmic inclusion bodies containing the small heat shock protein αB-crystallin." Proceedings of the National Academy of Sciences 94(3): 884-889.

Braig, K., Otwinowski, Z., Hegde, R., Boisvert, D. C., Joachimiak, A., Horwich, A. L. and Sigler, P. B. (1994). "The crystal structure of the bacterial chaperonln GroEL at 2.8 A." Nature 371(6498): 578-586.

Brinda, K. V. and Vishveshwara, S. (2005). "Oligomeric protein structure networks: insights into protein-protein interactions." BMC Bioinformatics 6(1): 296.

Buchberger, A., Bukau, B. and Sommer, T. (2010). "Protein Quality Control in the Cytosol and the Endoplasmic Reticulum: Brothers in Arms." Molecular Cell 40(2): 238-252.

Budil, D. E., Lee, S., Saxena, S. and Freed, J. H. (1996). "Nonlinear-Least-Squares Analysis of Slow-Motion EPR Spectra in One and Two Dimensions Using a Modified Levenberg Marquardt Algorithm." Journal of Magnetic Resonance, Series A 120(2): 155-189.

Bukau, B. and Horwich, A. L. (1998). "The Hsp70 and Hsp60 Chaperone Machines." Cell 92: 351-366.

Bult, C. J., White, O., Olsen, G. J., Zhou, L., Fleischmann, R. D., Sutton, G. G., Blake, J. A., FitzGerald, L. M., Clayton, R. A., Gocayne, J. D., Kerlavage, A. R., Dougherty, B. A., Tomb, J.-F., Adams, M. D., Reich, C. I., Overbeek, R., Kirkness, E. F., Weinstock, K. G., Merrick, J. M., Glodek, A., Scott, J. L., Geoghagen, N. S. M., Weidman, J. F., Fuhrmann, J. L., Nguyen, D., Utterback, T. R., Kelley, J. M., Peterson, J. D., Sadow, P. W., Hanna, M. C., Cotton, M. D., Roberts, K. M., Hurst, M. A., Kaine, B. P., Borodovsky, M., Klenk, H.-P., Fraser, C. M., Smith, H. O., Woese, C. R. and Venter, J. C. (1996). "Complete Genome Sequence of the Methanogenic Archaeon, Methanococcus jannaschii." Science 273(5278): 1058-1073.

Calderwood, S. K., Murshid, A. and Prince, T. (2009). "The Shock of Aging: Molecular Chaperones and the Heat Shock Response in Longevity and Aging A Mini Review." Gerontology 55: 550-558.

Caspers, G. J., Leunissen, J. A. M. and De Jong, W. W. (1995). "The expanding small heat shock protein family, and structure predictions of the conserved $\alpha$-crystallin domain." J. Mol. Evol. 40: 238-248.

Chen, B., Zhong, D. and Monteiro, A. (2006). "Comparative genomics and evolution of the HSP90 family of genes across all kingdoms of organisms." BMC Genomics 7(1): 156.

Chen, J., Feige, M. J., Franzmann, T. M., Bepperling, A. and Buchner, J. (2010). "Regions Outside the $\alpha$-Crystallin Domain of the Small Heat Shock Protein Hsp26 Are Required for Its Dimerization." Journal of Molecular Biology 398(1): 122-131.

Cheng, M. Y., Hartl, F. U., Martin, J., Pollock, R. A., Kalousek, F., Neuper, W., Hallberg, E. M., Hallberg, R. L. and Horwich, A. L. (1989). "Mitochondrial heat-shock protein hsp60 is essential for assembly of proteins imported into yeast mitochondria." Nature 337(6208): 620-625.

Chou, C., Forouhar, F., Yeh, Y. H., Shr, H. L., Wang, C. and Hsiao, C. D. (2003). "Crystal structure of the C-terminal 10-kDa subdomain of Hsc70." J Biol. Chem. 278: 30311-30316.

Claxton, D. P., Quick, M., Shi, L., de Carvalho, F. D., Weinstein, H., Javitch, J. A. and McHaourab, H. S. (2010). "Ion/substrate-dependent conformational dynamics of a bacterial homolog of neurotransmitter:sodium symporters." Nat Struct Mol Biol 17(7): 822-829.

Claxton, D. P., Zou, P. and McHaourab, H. S. (2008). "Structure and Orientation of T4 Lysozyme Bound to the Small Heat Shock Protein α-Crystallin." Journal of Molecular Biology 375(4): 1026-1039.

Clifton, A. D., Young, P. R. and Cohen, P. (1996). "A comparison of the substrate specificity of MAPKAP kinase-2 and MAPKAP kinase-3 and their activation by cytokines and cellular stress." FEBS Letters 392(3): 209-214.

Columbus, L., Kalai, T., Jeko, J., Hideg, K. and Hubbell, W. L. (2001). "Molecular Motion of Spin Labeled Side Chains in α-Helices: Analysis by Variation of Side Chain Structure " Biochemistry 40(13): 3828-3846.

Crabbe, M. J. and Goode, D. (1994). "α-crystallin: chaperoning and aggregation." Biochem. J. 297: 653-654.

Craig, E. A., Gambill, B. D. and Nelson, R. J. (1993). "Heat Shock Proteins: Molecular Chaperones of Protein Biogenesis." Microbiol. Rev. 57(2): 402-414.

Craig, E. A. and Lindquist, S. (1988). "The heat shock proteins." Annu. Rev. Genet. 22: 631-677.

Czogalla, A., Pieciul, A., Jezierski, A. and Sikorski, A. F. (2007). "Attaching a spin to a protein: site directed spin labeling in structural biology." Acta Biochim. Pol. 54(2): 235-244.

D'Silva, P., Liu, Q., Walter, W. and Craig, E. A. (2004). "Regulated interactions of mtHsp70 with Tim44 at the translocon in the mitochondrial inner membrane." Nat Struct Mol Biol 11(11): 1084-1091.

de Jong, W. W., Caspers, G. J. and Leunissen, J. A. M. (1998). "Genealogy of the a-crystallin-small heat-shock protein superfamily." Int J Biol. Macromol 22: 151-162.

de Jong, W. W., Leunissen, J. A. M. and Voorter, C. E. M. (1993). "Evolution of the α-Crystallin/Small Heat Shock Protein Family." Mol Bio Evol 10(1): 103-126.

Dierick, I., Irobi, J., De Jonghe, P. and Timmerman, V. (2005). "Small heat shock proteins in inherited peripheral neuropathies." Annals of Medicine 37(6): 413-422.

Dill, K. A., Bromberg, S., Yue, K., Fiebig, K. M., Yee, D. P., Thomas, P. D. and Chan, H. S. (1995). "Principles of protein folding ---- A perspective from simple exact models." Protein Sci. 4: 561-602.

Dill, K. A. and Chan, H. S. (1997). "From Levinthal to pathways to funnels." Nat. Struct. Biol. 4(1): 10-19.

Dinner, A. R., Sali, A., Smith, L. J., Dobson, C. M. and Karplus, M. (2000). "Understanding protein folding via free-energy surfaces from theory and experiment." Trends in Biochemical Sciences 25(7): 331-339.

DiSalvo, S., Derdowski, A., Pezza, J. A. and Serio, T. R. (2011). "Dominant prion mutants induce curing through pathways that promote chaperone-mediated disaggregation." Nat Struct Mol Biol 18(4): 486-492.

Ditzel, L., Lowe, J., Stock, D., Stetter, K. O., Huber, H., Huber, R. and Steinbacher, S. (1998). "Crystal structure of the thermosome, the archael chaperonin and homolog of CCT." Cell 93: 125-138.

Dobson, C. M. and Karplus, M. (1999). "The fundamental of protein folding: bringing together theory and experiment." Current Opinion in Structural Biology 9: 92-101.

Dong, J., Yang, G. and Mchaourab, H. S. (2005). "Structural basis of energy transduction in the transport cycle of MsbA." Science 308(5724): 1023-1028.

Drago, R. S. (1992). Physical Methods for Chemists. New York, Saunders Harcourt Brace Jovanovich.

Dutta, R. and Inouye, M. (2000). "GHKL, an emergent ATPase/kinase superfamily." Trends Biochem Sci. 25: 24-28.

Eaton, S., Eaton, G. and Berliner, L. (2002). Distance Measurements by CW and Pulsed EPRDistance Measurements in Biological Systems by EPR, Springer US. 19**:** 1-27.

Eaton, S. S. and Eaton, G. R. (1982). "Measurement of spin-spin distances from the intensity of the EPR half-field transition." Journal of the American Chemical Society 104(18): 5002-5003.

Effantin, G., Ishikawa, T., De Donatis, G. M., Maurizi, M. R. and Steven, A. C. (2010a). "Local and Global Mobility in the ClpA AAA+ Chaperone Detected by Cryo-Electron Microscopy: Functional Connotations." Structure 18(5): 553-562.

Effantin, G., Maurizi, M. R. and Steven, A. C. (2010b). "Binding of the ClpA Unfoldase Opens the Axial Gate of ClpP Peptidase." Journal of Biological Chemistry 285(19): 14834-14840.

Ehrnsperger, M., Buchner, J. and Gaestel, M. (1997a). Molecular chaperones in the life cycle of proteins, structure, function and mode of action. New York, Marcel Dekker Inc.

Ehrnsperger, M., Graber, S., Gaestel, M. and Buchner, J. (1997b). "Binding of non-native protein to Hsp25 during heat shock creates a reservoir of folding intermediates for reactivation." EMBO J 16(2): 221-229.

Elicker, K. S. and Hutson, L. D. (2007). "Genome-wide analysis and expression profiling of the small heat shock proteins in zebrafish." Gene 403(1-2): 60-69.

Ellis, R. J. (1994). "Molecular Chaperones: Opening and closing the Anfinsen cage." Current Biology 4(7): 633-635.

Evgrafov, O. V., Mersiyanova, I., Irobi, J., Van Den Bosch, L., Dierick, I., Leung, C. L., O., S., Verpoorten, N., Van Impe, K., Fedotov, V., Dadali, E., Auer-Grumbach, M., Windpassinger, C., Wagner, K., Mitrovic, Z., Hilton-Jones, D., Talbot, K., Martin, J. J., Vasserman, N., Tverskaya, S., Polyakov, A., Leim, R. K., Gettemans, J., Robberecht, W., De Jonghe, P. and Timmerman, V. (2004). "Mutant small heat shock protein 27 causes axonal Charcot-Marie-Tooth disease and distal hereditary motor neuropathy." Nat. Genet. 36: 602-606.

Farahbakhsh, Z. T., Altenbach, C. and Hubbell, W. L. (1992). "Spin Labeled Cysteines As Sensors For Protein-Lipid Interaction and Conformation In Rhodopsin." Photochem. Photobiol. 56: 1019-1033.

Feil, I. K., Malfois, M., Hendle, J., van der Zandt, H. and Svergun, D. I. (2001). "A Novel Quaternary Structure of the Dimeric $\alpha$-Crystallin Domain with Chaperone-like Activity." Journal of Biological Chemistry 276(15): 12024-12029.

Franck, E., Madsen, O., van Rheede, T., Ricard, G., Huynen, M. A. and de Jong, W. W. (2004). "Evolutionary Diversity of Vertebrate Small Heat Shock Proteins." Journal of Molecular Evolution 59(6): 792-805.

Fraser, C. M., Gocayne, J. D., White, O., Adams, M. D., Clayton, R. A., Fleischmann, R. D., Bult, C. J., Kerlavage, A. R., Sutton, G., Kelley, J. M., Fritchman, J. L., Weidman, J. F., Small, K. V., Sandusky, M., Fuhrmann, J., Nguyen, D., Utterback, T. R., Saudek, D. M., Phillips, C. A., Merrick, J. M., Tomb, J., Dougherty, B. A., Bott, K. F., Hu, P., Lucier, T. S., Peterson, S. N., Smith, H. O., Hutchison, C. A. and Venter, J. C. (1995). "The Minimal Gene Complement of *Mycoplasma genitalium*." Science 270(5235): 397-404.

Freed, J. H. (1976). Theory of slow tumbling ESR spectra for nitroxides. In spin labeling: Theory and Application. New York, Academic Press.

Frydenberg, J., Barker, J. and Loeschcke, V. (2010). "Characterization of the shsp genes in Drosophila buzzatii and association between the frequency of Valine mutations in hsp23 and climatic variables along a longitudinal gradient in Australia." Cell Stress and Chaperones 15(3): 271-280.

Frydman, J. (2001). "Folding of newly translated proteins in vivo: The role of molecular chaperones." Annual Review of Biochemistry 70: 603-647.

Fu, X. and Chang, Z. (2006). "Identification of bis-ANS binding sites in Mycobacterium tuberculosis small heat shock protein Hsp16.3: Evidences for a two-step substrate-binding mechanism." Biochemical and Biophysical Research Communications 349(1): 167-171.

Georgopoulos, C. P., Bisig, R., Magazin, M., Eisen, H. and Court, D. (1979). "Novel bacteriophage lamda mutation affecting lambda head assembly." J. Virol. 29(2): 782-788.

Ghosh, J. G., Shenoy, A. K. and Clark, J. I. (2006). "N- and C-Terminal Motifs in Human αB Crystallin Play an Important Role in the Recognition, Selection, and Solubilization of Substrates " Biochemistry 45(46): 13847-13854.

Gidalevitz, T., Ben-Zvi, A., Ho, K. H., Brignull, H. R. and Morimoto, R. I. (2006a). "Progressive disruption of cellular protein folding in models of polyglutamine diseases." Science 311: 1471-1474.

Gidalevitz, T., Ben-Zvi, A., Ho, K. H., Brignull, H. R. and Morimoto, R. I. (2006b). "Progressive Disruption of Cellular Protein Folding in Models of Polyglutamine Diseases." Science 311(5766): 1471-1474.

Giese, K. C., Basha, E., Catague, B. Y. and Vierling, E. (2005). "Evidence for an essential function of the N-terminus of a small heat shock protein in vivo, independent of in vitro chaperone activity." PNAS 102: 18896-18901.

Goloubinoff, P. and De Los Rios, P. (2007). "The mechanism of Hsp70 chaperones: (entropic) pulling the models together." Trends Biochem Sci. 32(8): 372-380.

Graw, J. (1997). "The crystallins: genes, proteins and diseases." Biological Chemistry 378(11): 1331-48.

Griffith, O. H., Dehlinger, P. J. and Van, S. P. (1974). "Shape of the hydrophobic barrier of phospholipid bilayers (Evidence for water penetration in biological membranes)." Journal of Membrane Biology 15(1): 159-192.

Haley, D. A., Bova, M. P., Huang, Q. L., Mchaourab, H. S. and Stewart, P. L. (2000). "Small heat shock protein structures reveal a continuum from symmetric to variable assemblies." J. Mol. Biol. 298: 261-272.

Haley, D. A., Horwitz, J. and Stewart, P. L. (1998). "The Small Heat-shock Protein, αB-crystallin, has a Variable Quaternary Structure." J. Mol. Biol. 277: 27-35.

Hamilton, C. L. and McConnell, H. M. (1968). Structural Chemistry and Molecular Biology. San Franciso, W. H. Freeman.

Hartl, F. U. and Hayer-Hartl, M. (2002). "Molecular Chaperones in the Cytosol: from Nascent Chain to Folded Protein." Science 295(5561): 1852-1858.

Haslbeck, M., Franzmann, T., Weinfurtner, D. and Buchner, J. (2005). "Some like it hot: the structure and function of small heat-shock proteins." Nat Struct Mol Biol 12(10): 842-846.

Haslbeck, M., Ignatiou, A., Saibil, H., Helmich, S., Frenzi, E., Stromer, T. and Buchner, J. (2004a). "A domain in the N-terminal part of Hsp26 is essential for chaperone function and oligomerization." J. Mol. Biol. 343: 445-455.

Haslbeck, M., Ignatiou, A., Saibil, H., Helmich, S., Frenzl, E., Stromer, T. and Buchner, J. (2004b). "A Domain in the N-terminal Part of Hsp26 is Essential for Chaperone Function and Oligomerization." Journal of Molecular Biology 343(2): 445-455.

Haslberger, T., Bukau, B. and Mogk, A. (2010). "Towards a unifying mechanism for ClpB/Hsp104-mediated protein disaggregation and prion propagationThis paper is one of a selection of papers published in this special issue entitled 8th International Conference on AAA Proteins and has undergone the Journal's usual peer review process." Biochemistry and Cell Biology 88(1): 63-75.

Hemmingsen, S. M., Woolford, C., van der Vies, S. M., Tilly, K., Dennis, D. T., Georgopoulos, C. P., Hendrix, R. W. and Ellis, R. J. (1988). "Homologous plant and bacterial proteins chaperone oligomeric protein assembly." Nature 333(6171): 330-334.

Hilario, E., Martin, F. J. M., Bertolini, M. C. and Fan, L. (2011). "Crystal Structures of Xanthomonas Small Heat Shock Protein Provide a Structural Basis for an Active Molecular Chaperone Oligomer." Journal of Molecular Biology 408(1): 74-86.

Horwich, A. L., Fenton, W. A., Chapman, E. and Farr, G. W. (2007). "Two families of chaperonin: physiology and mechanism." Ann. Rev. Cell. Dev. Biol. 23: 115-145.

Horwitz, J. (1992). "Alpha-crystallin can function as a molecular chaperone." Proceedings of the National Academy of Sciences 89(21): 10449-10453.

Hsu, A.-L., Murphy, C. T. and Kenyon, C. (2003). "Regulation of Aging and Age-Related Disease by DAF-16 and Heat-Shock Factor." Science 300(5622): 1142-1145.

Hubbell, W. L., Cafiso, D. S. and Altenbach, C. (2000). "Identifying conformational changes with site-directed spin labeling." Nat Struct Mol Biol 7(9): 735-739.

Hubbell, W. L., Gross, A., Langen, R. and Lietzow, M. A. (1998). "Recent advances in site-directed spin labeling of proteins." Current Opinion in Structural Biology 8(5): 649-656.

Hubbell, W. L., Mchaourab, H. S., Altenbach, C. and Lietzow, M. A. (1996). "Watching proteins move using site-directed spin labeling." Structure 4(7): 779-783.

Hunt, J. F., Weaver, A. J., Landry, S. J., Gierasch, L. and Deisenhofer, J. (1996). "The crystal structure of the GroES co-chaperonin at 2.8 A resolution." Nature 379(6560): 37-45.

Hustedt, E. J. and Beth, A. H. (1999). "NITROXIDE SPIN-SPIN INTERACTIONS: Applications to Protein Structure and Dynamics." Annual Review of Biophysics and Biomolecular Structure 28(1): 129-153.

Hustedt, E. J., Smirnov, A. I., Laub, C. F., Cobb, C. E. and Beth, A. H. (1997). "Molecular distances from dipolar coupled spin-labels: the global analysis of multifrequency continuous wave electron paramagnetic resonance data." Biophysical Journal 72(4): 1861-1877.

Hustedt, E. J., Stein, R. A., Sethaphong, L., Brandon, S., Zhou, Z. and DeSensi, S. C. (2006). "Dipolar Coupling between Nitroxide Spin Labels: The Development and Application of a Tether-in-a-Cone Model." Biophysical Journal 90(1): 340-356.

Ingolia, T. D. and Craig, E. A. (1982). "Drosophila gene related to the major heat shock-induced gene is transcribed at normal temperatures and not induced by heat shock." Proc. Natl. Acad. Sci. USA 79: 525-529.

Ito, H., Kamei, K., Iwamoto, I., Inaguma, Y., Nohara, D. and Kato, K. (2001). "Phosphorylation-induced Change of the Oligomerization State of αB-crystallin." Journal of Biological Chemistry 276(7): 5346-5352.

Jakob, U., Gaestel, M., Engel, K. and Buchner, J. (1993). "Small heat shock proteins are molecular chaperones." Journal of Biological Chemistry 268(3): 1517-20.

Jascur, T., Brickner, H., Salles-Passador, I., Barbier, V., El Khissiin, A., Smith, B., Fotedar, R. and Fotedar, A. (2005). "Regulation of p21WAF1/CIP1 Stability by WISp39, a Hsp90 Binding TPR Protein." Molecular Cell 17(2): 237-249.

Jaya, N., Garcia, V. and Vierling, E. (2009a). "Substrate binding site flexibility of the small heat shock protein molecular chaperones." PNAS 106: 15604-15609.

Jaya, N., Garcia, V. and Vierling, E. (2009b). "Substrate binding site flexibility of the small heat shock protein molecular chaperones." Proceedings of the National Academy of Sciences 106(37): 15604-15609.

Jehle, S., van Rossum, B., Stout, J. R., Noguchi, S. M., Falber, K., Rehbein, K., Oschkinat, H., Klevit, R. E. and Rajagopal, P. (2009). "αB-Crystallin: A Hybrid Solid-State/Solution-State NMR Investigation Reveals Structural Aspects of the Heterogeneous Oligomer." Journal of Molecular Biology 385(5): 1481-1497.

Jeschke, G. (2002). "Distance Measurements in the Nanometer Range by Pulse EPR." ChemPhysChem 3(11): 927-932.

Jeschke, G. and Polyhach, Y. (2007). "Distance measurements on spin-labelled biomacromolecules by pulsed electron paramagnetic resonance." Physical Chemistry Chemical Physics 9(16): 1895-1910.

Jeschke, G., Wegener, C., Nietschke, M., Jung, H. and Steinhoff, H.-J. r. (2004). "Interresidual Distance Determination by Four-Pulse Double Electron-Electron Resonance in an Integral Membrane Protein: The Na+/Proline Transporter PutP of Escherichia coli." Biophysical Journal 86(4): 2551-2557.

Kampinga, H. H. and Craig, E. A. (2010). "The HSP70 chaperone machinery: J proteins as drivers of functional specificity." Nat. Rev. Mol. Cell Biol. 11: 579-592.

Kappe, G., Franck, E., Verschuure, P., Boelens, W. C., Leunissen, J. A. M. and de Jong, W. W. (2003). "The human genome encodes 10 $\alpha$-crystallin-related small heat shock proteins: HspB1-10." Cell Stress Chaperones 8(1): 53-61.

Karagoz, G. E., Duarte, A. M. S., Ippel, H., Uetrecht, C., Sinnige, T., van Rosmalen, M., Hausmann, J., Heck, A. J. R., Boelens, R. and Rudiger, S. G. D. (2011). "N-terminal domain of human Hsp90 triggers binding to the cochaperone p23." Proceedings of the National Academy of Sciences 108(2): 580-585.

Kazutoyo, T. and Oike, Y. (2010). "Multiple Molecules of Hsc70 and a dimer of DjA1 independently bind to an unfolded protein." J Biol. Chem. 285(22): 16789-16797.

Kim, K. K., Kim, R. and Kim, S.-H. (1998). "Crystal structure of a small heat-shock protein." Nature 394(6693): 595-599.

Kirstein, J., Moliere, N., Dougan, D. A. and Turgay, K. (2009). "Adapting the machine: adaptor proteins for Hsp100/Clp and AAA+ proteases." Nat. Rev. Microbiol. 7: 589-599.

Klug, C. S. and Feix, J. B. (2008). Methods and Applications of Site-Directed Spin Labeling EPR Spectroscopy. Biophysical Toos For Biologist: Vol. 1 In Vitro Techniques. J. J. Correia and H. W. Detrich. New York, Elsevier. 84.

Klumpp, M., Baumeister, W. and Essen, L.-O. (1997). "Structure of the Substrate Binding Domain of the Thermosome, an Archaeal Group II Chaperonin." Cell 91(2): 263-270.

Kokke, B. P. A., Leroux, M. R., Candido, E. P. M., Boelens, W. C. and de Jong, W. W. (1998). "Caenorhabditis elegans small heat-shock proteins Hsp12.2 and Hsp12.3 form tetramers and have no chaperone-like activity." FEBS Letters 433(3): 228-232.

Kokorin, a. I., Zamaraev, K. I., Grigorian, G. L., Ivanov, V. P. and Rozantsev, E. G. (1972). "Measurement of distance between paramagnetic centres in solid solutions of nitrosyl radicals, biradicals, and spin-labeled proteins." Biofizika 17: 34-41.

Koteiche, H. A., Berengian, A. R. and Mchaourab, H. S. (1998). "Identification of Protein Folding Patterns Using Site-Directed Spin Labeling. Structural Characterization of a β-Sheet and Putative Substrate Binding Regions in the Conserved Domain of αA-Crystallin " Biochemistry 37(37): 12681-12688.

Koteiche, H. A. and Mchaourab, H. S. (1999). "Folding pattern of the [alpha]-crystallin domain in [alpha]A-crystallin determined by site-directed spin labeling." Journal of Molecular Biology 294(2): 561-577.

Koteiche, H. A. and Mchaourab, H. S. (2002). "The determinants of the oligomeric structure in Hsp16.5 are encoded in the α-crystallin domain." FEBS Letters 519(1): 16-22.

Koteiche, H. A. and Mchaourab, H. S. (2003). "Mechanism of Chaperone Function in Small Heat-shock Proteins." Journal of Biological Chemistry 278(12): 10361-10367.

Koteiche, H. A. and Mchaourab, H. S. (2006). "Mechanism of a Hereditary Cataract Phenotype." Journal of Biological Chemistry 281(20): 14273-14279.

Kuwajima, K. (1989). "The molten globule state as a clue for understanding the folding and cooperativity of globular-protein structure." Proteins 6: 87-103.

Laganowsky, A., Benesch, J. L. P., Landau, M., Ding, L., Sawaya, M. R., Cascio, D., Huang, Q., Robinson, C. V., Horwitz, J. and Eisenberg, D. (2010). "Crystal structures of truncated alphaA and alphaB crystallins reveal structural mechanisms of polydispersity important for eye lens function." Protein Science 19(5): 1031-1043.

Lambert, H., Charette, S. J., Bernier, A. F., Guimond, A. and Landry, J. (1999). "HSP27 Multimerization Mediated by Phosphorylation-sensitive Intermolecular Interactions at the Amino Terminus." Journal of Biological Chemistry 274(14): 9378-9385.

Langen, R., Oh, K. J., Cascio, D. and Hubbell, W. L. (2000). "Crystal Structures of Spin Labeled T4 Lysozyme Mutants: Implications for the Interpretation of EPR Spectra in Terms of Structure " Biochemistry 39(29): 8396-8405.

Langer, T., Rosmus, S. and Fasold, H. (2003). "Intracellular localization of the 90 kDa heat shock protein (Hsp90$\alpha$) determined by expression of a EGFP-HSP90$\alpha$-fusion protein in unstressed and heat stressed 3T3 cells." Cell Biol. Int. 27(1): 47-52.

Larmor, J. (1900). Aether and Matter: A development of the dynamical relations of the aether to material systems. Cambridge, Cambridge University Press.

Laskowska, E., Matuszewska, E. and Kuczynska-Wisnik, D. (2010). "Small heat shock proteins and protein-misfolding diseases." Curr. Pharm. Biotechnol. 11(2): 146-157.

Launay, N., Goudeau, B., Kato, K., Vicart, P. and Lilienbaum, A. (2006). "Cell signaling pathways to $\alpha$B-crystallin following stresses of the cytoskeleton." Experimental Cell Research 312(18): 3570-3584.

Lazaridis, T. and Karplus, M. (1997). ""New View" of Protein Folding Reconciled with the Old Through Multiple Unfolding Simulations." Science 278(5345): 1928-1931.

Lee, G. J., Roseman, A. M., Saibil, H. R. and Vierling, E. (1997). "A small heat shock protein stably binds heat-denatured model substrates and can maintain a substrate in a folding-competent state." EMBO J 16(3): 659-671.

Lee, G. J. and Vierling, E. (2000). "A Small Heat Shock Protein Cooperates with Heat Shock Protein 70 Systems to Reactivate a Heat-Denatured Protein." Plant Physiology 122(1): 189-198.

Leifson, O. S. and Jeffries, C. D. (1961). "Dynamic Polarization of Nuclei by Electron-Nuclear Dipolar Coupling in Crystals." Phys. Rev. 122: 1781-1795.

Leroux, M. R., Melki, R., Gordon, B., Batelier, G. r. and Candido, E. P. M. (1997). "Structure-Function Studies on Small Heat Shock Protein Oligomeric Assembly and Interaction with Unfolded Polypeptides." Journal of Biological Chemistry 272(39): 24646-24656.

Levinthal, C. J. (1968). "Are there pathways for protein folding." J. Chim. Phys. 65: 44-45.

Li, J., Richter, K. and Buchner, J. (2011). "Mixed Hsp90-cochaperone complexes are important for the progression of the reaction cycle." Nat. Struct. Mol. Biol. 18(1): 61-67.

Liberek, K., Lewandowska, A. and Zietkiewicz, S. (2008). "Chaperones in control of protein disaggregation." EMBO J 27(2): 328-335.

Lindquist, S. (1986). "The Heat Shock Response." Ann. Rev. Biochem. 55: 1151-1191.

Liu, M., Ke, T., Wang, Z., Yang, Q., Chang, W., Jiang, F., Tang, Z., Li, H., Ren, X., Wang, X., Wang, T., Li, Q., Yang, J., Liu, J. and Wang, Q. K. (2006). "Identification of a CRYAB Mutation Associated with Autosomal Dominant Posterior Polar Cataract in a Chinese Family." Investigative Ophthalmology & Visual Science 47(8): 3461-3466.

Liu, Y.-S., Sompornpisut, P. and Perozo, E. (2001). "Structure of the KcsA channel intracellular gate in the open state." Nat Struct Mol Biol 8(10): 883-887.

Lorimer, G. H. (1993). Advances in protein chemistry: Accessory folding proteins. New York, Academic Press.

Maglica, Z., Striebel, F. and Weber-Ban, E. (2008). "An Intrinsic Degradation Tag on the ClpA C-Terminus Regulates the Balance of ClpAP Complexes with Different Substrate Specificity." Journal of Molecular Biology 384(2): 503-511.

Maillard, R., Chistol, G., Sen, M., Righini, M., Tan, J., Kaiser, C. M., Hodges, C., Martin, A. and Bustamante, C. (2011). "ClpX(P) Generates Mechanical Force to Unfold and Translocate Its Protein Substrates." Cell 145(3): 459-469.

Marshall, J. S., DeRocher, A. E., Keegstra, K. and Vierling, E. (1990). "Identification of heat shock protein hsp70 homologues in chloroplasts." Proc. Natl. Acad. Sci. USA 87(1).

Martin, A., Baker, T. A. and Sauer, R. T. (2005). "Rebuilt AAA+ motors reveal operating principles for ATP-fuelled machines." Nature 437: 1115-1119.

Mayer, M. P. and Bukau, B. (2005). "Hsp70 chaperones: Cellular functions and molecular mechanism." Cell. Mol. Life Sci. 62: 670-684.

Mchaourab, H. S., Berengian, A. R. and Koteiche, H. A. (1997a). "Site-Directed Spin-Labeling Study of the Structure and Subunit Interactions along a Conserved Sequence in the a-Crystallin Domain of Heat Shock Protein 27. Evidence of a Conserved Subunit Interface." Biochemistry 36(48): 14627-14634.

Mchaourab, H. S., Dodson, E. K. and Koteiche, H. A. (2002). "Mechanism of Chaperone Function in Small Heat Shock Proteins." J Biol. Chem. 277(43): 40557-40566.

Mchaourab, H. S., Godar, J. A. and Stewart, P. L. (2009). "Structure and mechanism of protein stability sensors." Biochemistry 48(18): 3828-3837.

Mchaourab, H. S., Lietzow, M. A., Hideg, K. and Hubbell, W. L. (1996). "Motion of Spin-Labeled Side Chains in T4 Lysozyme. Correlation with Protein Structure and Dynamics " Biochemistry 35(24): 7692-7704.

Mchaourab, H. S., Oh, K. J., Fang, C. J. and Hubbell, W. L. (1997b). "Conformation of T4 Lysozyme in Solution. Hinge-Bending Motion and the Substrate-Induced Conformational Transition Studied by Site-Directed Spin Labeling " Biochemistry 36(2): 307-316.

Mehlen, P., Hickey, E., Weber, L. A. and Arrigo, A.-P. (1997). "Large Unphosphorylated Aggregates as the Active Form of hsp27 Which Controls Intracellular Reactive Oxygen Species and Glutathione Levels and Generates a Protection against TNFα in NIH-3T3-ras Cells." Biochemical and Biophysical Research Communications 241(1): 187-192.

Mehta, R., Steinkraus, K. A., Sutphin, G. L., Ramos, F. J., Shamieh, L. S., Huh, A., Davis, C., Chandler-Brown, D. and Kaeberlein, M. (2009). "Proteasomal Regulation of the Hypoxic Response Modulates Aging in C. elegans." Science 324(5931): 1196-1198.

Meirovitch, E., Nayeem, A. and Freed, J. H. (1984). "Analysis of protein-lipid interactions based on model simulations of electron spin resonance spectra." The Journal of Physical Chemistry 88(16): 3454-3465.

Merck, K. B., De Haard-Hoekman, W. A., Oude Essink, B. B., Bloemendal, H. and De Jong, W. W. (1992). "Expression and aggregation of recombinant αA-crystallin and its two domains." Biochimica et Biophysica Acta (BBA) - Gene Structure and Expression 1130(3): 267-276.

Merck, K. B., Horwitz, J., Kersten, M., Overkamp, P., Gaestel, M., Bloemendal, H. and de Jong, W. W. (1993). "Comparison of the homologous carboxy-terminal domain and tail of α-crystallin and small heat shock protein." Molecular Biology Reports 18(3): 209-215.

Millhauser, G. L., Fiori, W. R., Miick, S. M. and Kenneth, S. (1995). Electron spin labels. Methods in Enzymology, Academic Press. 246**:** 589-610.

Milov, A. D., Maryasov, A. G., Tsvetkov, Y. D. and Raap, J. (1999). "Pulsed ELDOR in spin-labeled polypeptides." Chemical Physics Letters 303(1-2): 135-143.

Mims, W. B., Nassau, K. and McGee, J. D. (1961). "Spectral Diffusion in Electron Resonance Lines." Phys. Rev. 123: 2059-2069.

Muchowski, P. J. and Wacker, J. L. (2005). "Modulation of Neurodegeneration by Molecular Chaperones." Nature Reviews Neuroscience 6: 11-22.

Munro, S. and Pelham, H. R. B. (1986). "An hsp70-like protein in the ER: Identitiy with the 78 kd glucose-regulated protein and immunoglobulin heavy chain binding protein." Cell 46(2): 291-300.

Narberhaus, F. (2002). "α-crystallin-type heat shock proteins: socializing minichaperones in the context of a multichaperone network." Microbiol. Mol. Biol. Rev. 66(1): 64-93.

Nelson, K. E., Clayton, R. A., Gill, S. R., Gwinn, M. L., Dodson, R. J., Haft, D. H., Hickey, E. K., Peterson, J. D., Nelson, W. C., Ketchum, K. A., McDonald, L., Utterback, T. R., Malek, J. A., Linher, K. D., Garrett, M. M., Stewart, A. M., Cotton, M. D., Pratt, M. S., Phillips, C. A., Richardson, D., Heidelberg, J., Sutton, G. G., Fleischmann, R. D., Eisen, J. A., White, O., Salzberg, S. L., Smith, H. O., Venter, J. C. and Fraser, C. M. (1999). "Evidence for lateral gene transfer between Archaea and Bacteria from genome sequence of Thermotoga maritima." Nature 399(6734): 323-329.

Nikolic, A., Baud, S., Rauscher, S. and Pomès, R. (2011). "Molecular mechanism of β-sheet self-organization at water-hydrophobic interfaces." Proteins: Structure, Function, and Bioinformatics 79(1): 1-22.

Osheroff, D. D., Gully, W. J., Richardson, R. C. and Lee, D. M. (1972). "New Magnetic Phenomena in Liquid $He^3$ below 3mK." Phys. Rev. Lett. 29: 920-923.

Pake, G. E. (1962). Paramagnetic Resonance. New York, W. A. Benjamin Inc.

Pannier, M., Veit, S., Godt, A., Jeschke, G. and Spiess, H. W. (2000). "Dead-Time Free Measurement of Dipole Dipole Interactions between Electron Spins." Journal of Magnetic Resonance 142(2): 331-340.

Pappenberger, G., Wilsher, J. A., Mark Roe, S., Counsell, D. J., Willison, K. R. and Pearl, L. H. (2002). "Crystal Structure of the CCTγ Apical Domain: Implications for Substrate Binding to the Eukaryotic Cytosolic Chaperonin." Journal of Molecular Biology 318(5): 1367-1379.

Parsell, D. A. and Lindquist, S. (1993). "The function of heat-shock proteins in stress tolerance: degredation and reactivation of damaged proteins." Annu. Rev. Genet. 27: 437-496.

Pasta, S. Y., Raman, B., Ramakrishna, T. and Rao, C. M. (2003). "Role of the Conserved SRLFDQFFG Region of α-Crystallin, a Small Heat Shock Protein." Journal of Biological Chemistry 278(51): 51159-51166.

Patel, Y. J. K., Payne Smith, M. D., de Belleroche, J. and Latchman, D. S. (2005). "Hsp27 and Hsp70 administered in combination have a potent protective effect against FALS-associated SOD1-mutant-induced cell death in mammalian neuronal cells." Molecular Brain Research 134(2): 256-274.

Perutz, M. F. and Raidt, H. (1975). "Stereochemical basis of heat stability in bacterial ferredoxins and in haemoglobin A2." Nature 255(5505): 256-259.

Phipps, B. M., Typke, D., Hegerl, R., Volker, S., Hoffmann, A., Stetter, K. O. and Baumeister, W. (1993). "Structure of a molecular chaperone from a thermophilic archaebacterium." Nature 361(6411): 475-477.

Picard, D. (2002). "Heat-shock protein 90, a chaperone for folding and regulation " Cell Mol. Life Sci. 59: 1640-1648.

Pivovarova, A. V., Mikhailova, V. V., Chernik, I. S., Chebotareva, N. A., Levitsky, D. I. and Gusev, N. B. (2005). "Effects of small heat shock proteins on the thermal denaturation and aggregation of F-actin." Biochemical and Biophysical Research Communications 331(4): 1548-1553.

Portis, A. M. (1953). "Electronic Structure of F Centers: Saturation of the Electron Spin Resonance." Phys. Rev. 91: 1071-1079.

Pridgeon, J. W., Olzmann, J. A., Chin, L.-S. and Li, L. (2007). "PINK1 Protects against Oxidative Stress by Phosphorylating Mitochondrial Chaperone TRAP1." PLoS Biol 5(7): 1494-1503.

Ptitsyn, O. B. (1996). "How molten is the molten globule." Nature Struct Biol. 3: 488-490.

Pyka, J., Ilnicki, J., Altenbach, C., Hubbell, W. L. and Froncisz, W. (2005). "Accessibility and dynamics of nitroxide side chains in T4 lysozyme measured by saturation recovery EPR." Biophys. J. 89: 2059-2068.

Rabenstein, M. D. and Shin, Y. K. (1995). "Determination of the distance between two spin labels attached to a macromolecule." Proceedings of the National Academy of Sciences 92(18): 8239-8243.

Rajendar, B. and Lucius, A. L. (2010). "Molecular Mechanism of Polypeptide Translocation Catalyzed by the Eschericia coli ClpA Protein Translocase." J. Mol. Biol. 399: 665-679.

Raman, B. and Rao, C. M. (1997). "Chaperone-like Activity and Temperature-induced Structural Changes of α-Crystallin." Journal of Biological Chemistry 272(38): 23559-23564.

Read, T. D., Brunham, R. C., Shen, C., Gill, S. R., Heidelberg, J. F., White, O., Hickey, E. K., Peterson, J., Utterback, T., Berry, K., Bass, S., Linher, K., Weidman, J., Khouri, H., Craven, B., Bowman, C., Dodson, R., Gwinn, M., Nelson, W., DeBoy, R., Kolonay, J., McClarty, G., Salzberg, S. L., Eisen, J. and Fraser, C. M. (2000). "Genome sequences of Chlamydia trachomatis MoPn and Chlamydia pneumoniae AR39." Nucleic Acids Research 28(6): 1397-1406.

Richter, K., Haslbeck, M. and Buchner, J. (2010). "The heat shock response: Life on the verge of death." Mol. Cell 40(2): 253-266.

Rogalla, T., Ehrnsperger, M., Preville, X., Kotlyarov, A., Lutsch, G., Ducasse, C. c., Paul, C., Wieske, M., Arrigo, A.-P., Buchner, J. and Gaestel, M. (1999). "Regulation of Hsp27 Oligomerization, Chaperone Function, and Protective Activity against Oxidative Stress/Tumor Necrosis Factor Î± by Phosphorylation." Journal of Biological Chemistry 274(27): 18947-18956.

Roy, S. K. and Nakamota, H. (1998). "Cloning, characterization, and transcriptional analysis of a gene encoding an α-crystallin-related, small heat shock protein from the thermophillic cyanobacterium *Synechococcus vulcanus*." J. Bacteriol. 180: 3997-4001.

Rudiger, S., Buchberger, A. and Bukau, B. (1997). "Interaction of Hsp70 chaperones with substrates." Nat Struct Mol Biol 4(5): 342-349.

Rye, H. S., Roseman, A. M., Chen, S., Furtak, K., Fenton, W. A., Saibil, H. R. and Horwich, A. L. (1999). "GroEL-GroES Cycling: ATP and Nonnative Polypeptide Direct Alternation of Folding-Active Rings." Cell 97(3): 325-338.

Saibil, H. R. (2008). "Chaperone machines in action." Curr. Opin. Struct. Biol. 18: 35-42.

Saibil, H. R., Zheng, D., Roseman, A. M., Hunter, A. S., Watson, G. M. F., Chen, S., auf der Mauer, A., O'Hara, B. P., Wood, S. P., Mann, N. H., Barnett, L. K. and Ellis, R. J. (1993). "ATP induces large quaternary rearrangements in a cage-like chaperonin structure." Current Biology 3(5): 265-273.

Sathish, H. A., Stein, R. A., Yang, G. and McHaourab, H. S. (2003). "Mechanism of Chaperone Function in Small Heat-shock Proteins." Journal of Biological Chemistry 278(45): 44214-44221.

Sauer, R. T., Bolon, D. N., Burton, B. M., Burton, R. E., Flynn, J. M., Grant, R. A., Hersch, G. L., Joshi, S. A., Kenniston, J. A., Levchenko, I., Neher, S. B., Oakes, E. S. C., Siddiqui, S. M., Wah, D. A. and Baker, T. A. (2004). "Sculpting the proteome with AAA+ proteases and disassembly machines." Cell 119(1): 9-18.

Saxena, S. and Freed, J. H. (1997). "Theory of double quantum two dimensional electron spin resonance with application to distance measurements." J. Chem. Phys. 107: 1317-1340.

Schroder, H., Langer, T., Hartl, F. U. and Bukau, B. (1993). "DnaK, DnaJ, and GrpE form a cellular chaperone machinery capable of repairing heat induced protein damage." The EMBO Journal 12(11): 4137-4144.

Sharma, K. K., Kaur, H. and Kester, K. (1997). "Functional Elements in Molecular Chaperone $\alpha$-Crystallin: Identification of Binding Sites in $\alpha$B-Crystallin." Biochemical and Biophysical Research Communications 239(1): 217-222.

Sharma, M., Burre, J. and Sudhof, T. C. (2011). "CSP$\alpha$ promotes SNARE-complex assembly by chaperoning SNAP-25 during synaptic activity." Nat Cell Biol 13(1): 30-39.

Shashidharamurthy, R., Koteiche, H. A., Dong, J. and McHaourab, H. S. (2005). "Mechanism of Chaperone Function in Small Heat Shock Proteins." Journal of Biological Chemistry 280(7): 5281-5289.

Sherman, M. Y. and Goldberg, A. L. (2001). "Cellular Defenses against Unfolded Proteins: A Cell Biologist Thinks about Neurodegenerative Diseases." Neuron 29(1): 15-32.

Shi, J., Koteiche, H. A., Mchaourab, H. S. and Stewart, P. (2006). "Cryoelectron microscopy and EPR analysis of Engineered Symmetric and Polydisperse Hsp16.5 Assemblies Reveals Determinants of Polydispersity and Substrate Binding." J. Biol. Chem. 281(52): 40420-40428.

Shiau, A. K., Harris, S. F., Southworth, D. R. and Agard, D. A. (2006). "Structural Analysis of E.coli hsp90 Reveals Dramatic Nucleotide-Dependent Conformational Rearrangements." Cell 127: 329-340.

Shigenobu, S., Watanabe, H., Hattori, M., Sakaki, Y. and Ishikawa, H. (2000). "Genome sequence of the endocellular bacterial symbiont of aphids Buchnera sp. APS." Nature 407(6800): 81-86.

Slack, F. J., Serror, P., Joyce, E. and Sonenshein, A. L. (1995). "A gene required for nutritional repression of the Bacillus subtilis dipeptide permease operon." Molecular Microbiology 15(4): 689-702.

Smith, W. V., Sorokin, P. P., Gelles, I. L. and Lasher, G. J. (1959). "Electron-Spin Resonance of Nitrogen Donors in Diamond." Physical Review 115(6): 1546.

Smulders, R. H. P. H., Carver, J. A., Lindner, R. A., van Boekel, M. A. M., Bloemendal, H. and de Jong, W. W. (1996). "Immobilization of the C-terminal Extension of Bovine αA-Crystallin Reduces Chaperone-like Activity." Journal of Biological Chemistry 271(46): 29060-29066.

Smulders, R. H. P. H. and de Jong, W. W. (1997). "The hydrophobic probe 4,4-bis(1-anilino-8-naphthalene sulfonic acid) is specifically photoincorporated into the N-terminal domain of αB-crystallin." FEBS Letters 409(1): 101-104.

Solomon, I. (1955). "Relaxation Processes in a System of Two Spins." Phys. Rev. 99: 559-565.

Stamler, R., Kappe, G., Boelens, W. and Slingsby, C. (2005). "Wrapping the α-Crystallin Domain Fold in a Chaperone Assembly." Journal of Molecular Biology 353(1): 68-79.

Standley, K. J. and Vaughan, R. A. (1969). Electron spin relaxation phenomena in solids. New York, Plenum Press.

Steinhoff, H.-J. r. (2004). "Inter- and intra-molecular distances determined by EPR spectroscopy and site-directed spin labeling reveal protein-protein and protein-oligonucleotide interaction." Biological Chemistry 385(10): 913-920.

Steinhoff, H. J., Radzwill, N., Thevis, W., Lenz, V., Brandenburg, D., Antson, A., Dodson, G. and Wollmer, A. (1997). "Determination of interspin distances between spin labels attached to insulin: comparison of electron paramagnetic resonance data with the X-ray structure." Biophysical Journal 73(6): 3287-3298.

Stetler, R. A., Signore, A. P., Gao, Y., Cao, G. and Chen, J. (2009). "HSP27: Mechanisms of Cellular Protection Against Neuronal Injury." Curr. Mol. Med. 9(7): 863-872.

Stokoe, D., Engel, K., Campbell, D. G., Cohen, P. and Gaestel, M. (1992). "Identification of MAPKAP kinase 2 as a major enzyme responsible for the phosphorylation of the small mammalian heat shock proteins." FEBS Letters 313(3): 307-313.

Stromer, T., Fischer, E., Richter, K., Haslbeck, M. and Buchner, J. (2004). "Analysis of the Regulation of the Molecular Chaperone Hsp26 by Temperature-induced Dissociation." Journal of Biological Chemistry 279(12): 11222-11228.

Studier, F. W. (2005). "Protein production by auto-induction in high density shaking cultures." Protein Expr. Purif. 41(1): 207-234.

Subramaniam, S. (1998). "The biology workbench A seamless database and analysis environment for the biologist." Proteins: Structure, Function, and Bioinformatics 32: 1-2.

Suzuki, T. C., Krawitz, D. C. and Vierling, E. (1998). "The Chloroplast Small Heat-Shock Protein Oligomer Is Not Phosphorylated and Does Not Dissociate during Heat Stress in Vivo." Plant Physiology 116(3): 1151-1161.

Taipale, M., Jarosz, D. F. and Lindquist, S. (2010). "HSP90 at the hub of protein homeostasis: emerging mechanistic insights." Nat. Rev. Mol. Cell Biol. 11: 515-528.

Taylor, R. P. and Benjamin, I. J. (2005). "Small heat shock proteins: a new classification scheme in mammals." J. Mol. Cell Cardiol. 38: 433-444.

Theriault, J. R., Lambert, H., Chavez-Zobel, A. T., Charest, G., Lavigne, P. and Landry, J. (2004). "Essential Role of the NH2-terminal WD/EPF Motif in the Phosphorylation-activated Protective Function of Mammalian Hsp27." Journal of Biological Chemistry 279(22): 23463-23471.

Thompson, J. D., Higgins, D. G. and Gibson, T. J. (1994). "CLAUSTAL W: improving the sensitivity of progressive multiple sequence alignment through sequence weighting, position-specific gap penalties and weight matrix choice. ." Nucleic Acids Res 22: 4673-4680.

Todd, A. P., Cong, J., Levinthal, F., Levinthal, C. and Hubell, W. L. (1989). "Site-directed mutagenesis of colicin E1 provides specific attachment sites for spin labels whose spectra are sensitive to local conformation." Proteins: Structure, Function, and Bioinformatics 6(3): 294-305.

Tomko Jr, R. J., Funakoshi, M., Schneider, K., Wang, J. and Hochstrasser, M. (2010). "Heterohexameric Ring Arrangement of the Eukaryotic Proteasomal ATPases: Implications for Proteasome Structure and Assembly." Molecular Cell 38(3): 393-403.

Ungewickell, E., Ungewickell, H., Holstein, S. E. H., Lindner, R., Prasad, K., Barouch, W., Martini, B., Greene, L. E. and Eisenberg, E. (1995). "Role of auxilin in uncoating clathrin-coated vesicles." Nature 378(6557): 632-635.

van de Klundert, F. A. J. M., Smulders, R. H. P. H., Gijsen, M. L. J., Lindner, R. A., Jaenicke, R., Carver, J. A. and de Jong, W. W. (1998). "The mammalian small heat-shock protein Hsp20 forms dimers and is a poor chaperone." European Journal of Biochemistry 258(3): 1014-1021.

van Montfort, R. L. M., Basha, E., Friedrich, K. L., Slingsby, C. and Vierling, E. (2001). "Crystal structure and assembly of a eukaryotic small heat shock protein." Nat Struct Mol Biol 8(12): 1025-1030.

Van Vleck, J. H. (1948). "The dipolar broadening of magnetic resonance lines in crystals." Phys. Rev. 74: 1168-1183.

Vasquez, V., Sotomayor, M., Cordero-Morales, J., Schulten, K. and Perozo, E. (2008). "A Structural Mechanism for MscS Gating in Lipid Bilayers." Science 321(5893): 1210-1214.

Vetriani, C., Maeder, D. L., Tolliday, N., Yip, K. S. P., Stillman, T. J., Britton, K. L., Rice, D. W., Klump, H. H. and Robb, F. T. (1998). "Protein thermostability above 100Â°C: A key role for ionic interactions." Proceedings of the National Academy of Sciences 95(21): 12300-12305.

Vicart, P., Caron, A., Guicheney, P., Li, Z., Prevost, M. C., Faure, A., Chateau, D., Chapon, F., Tome, F., Dupret, J. M., Paulin, D. and Fardeau, M. (1998). "A missense mutation in the aB-crystallin chaperone gene causes a desmin-related myopathy." Nat. Genet. 20: 92-95.

Voos, W., Martin, H., Krimmer, T. and Pfanner, N. (1999). "Mechanisms of protein translocation into mitochondria." Biochim Biophys Acta 1422: 232-254.

Voss, J., Salwinski, L., Kaback, H. R. and Hubbell, W. L. (1995). "A method for distance determination in proteins using a designed metal ion binding site and site-directed spin labeling: evaluation with T4 lysozyme." Proceedings of the National Academy of Sciences 92(26): 12295-12299.

Walker, J. E., Wonacott, A. J. and Harris, J. I. (1980). "Heat Stability of a Tetrameric Enzyme, D-Glyceraldehyde-3-PhosphateDehydrogenase." European Journal of Biochemistry 108(2): 581-586.

Wang, F., Mei, Z., Qi, Y., Yan, C., Hu, Q., Wang, J. and Shi, Y. (2011). "Structure and mechanism of the hexameric MecA-ClpC molecular machine." Nature 471(7338): 331-335.

Waters, E. R. (1995). "The Molecular Evolution of the Small Heat-Shock Proteins in Plants." Genetics 141(2): 785-795.

Waters, E. R., Lee, G. J. and Vierling, E. (1996). "Evolution, structure and function of the small heat shock proteins in plants." Journal of Experimental Botany 47(3): 325-338.

Weese, J. (1992). "A reliable and fast method for the solution of Fredholm integral equations of the first kind based on Tikhonov regularization." Comp. Phys. Commun. 69: 99-111.

White, H. E., Orlova, E. V., Chen, S., Wang, L., Ignatiou, A., Gowen, B., Stromer, T., Franzmann, T. M., Haslbeck, M., Buchner, J. and Saibil, H. R. (2006). "Multiple Distinct Assemblies Reveal Conformational Flexibility in the Small Heat Shock Protein Hsp26." Structure 14(7): 1197-1204.

Wolynes, P. G., Onuchic, J. N. and Thirumalai, D. (1995). "Navigating the folding routes." Science 267: 1619-1620.

Wyttenbach, A., Sauvageot, O., Carmichael, J., Diaz-Latoud, C., Arrigo, A.-P. and Rubinsztein, D. C. (2002). "Heat shock protein 27 prevents cellular polyglutamine toxicity and suppresses the increase of reactive oxygen species caused by huntingtin." Human Molecular Genetics 11(9): 1137-1151.

Xi, J., Bai, J., Gross, J., Townsend, R. R., Menko, A. S. and Andley, U. P. (2008). "Mechanism of small heat shock protein function in vivo, a knock in mouse model demonstrates that the R49C mutation in αA-crystallin enhances protein insolubility and cell death." J Biol. Chem. 283: 5801-5814.

Xiao, W., Shin, Y.-K., Berliner, L., Eaton, G. and Eaton, S. (2002). EPR Spectroscopic Ruler: the Deconvolution Method and its Applications Distance Measurements in Biological Systems by EPR, Springer US. 19**:** 249-276.

Xu, Z., Horwich, A. L. and Sigler, P. B. (1997). "The crystal structure of the asymmetric GroEL-GroES-(ADP)7 chaperonin complex." Nature 388(6644): 741-750.

Yaffe, M. B., Farr, G. W., Miklos, D., Horwich, A. L., Sternlicht, M. L. and Sternlicht, H. (1992). "TCP1 complex is a molecular chaperone in tubulin biogenesis." Nature 358(6383): 245-248.

Young, J. C., Agashe, V. R., Siegers, K. and Hartl, F. U. (2004). "Pathways of chaperone-mediated protein folding in the cytosol." Nat Rev Mol Cell Biol 5(10): 781-791.

Young, J. C., Obermann, W. M. J. and Hartl, F. U. (1998). "Specific Binding of Tetratricopeptide repeat proteins to the C-terminal 12-kDa Domain of hsp90." J Biol. Chem. 273(29): 18007-18010.

Yuan, J. and Rozengurt, E. (2008). "PKD, PKD2, and p38 MAPK mediate Hsp27 serine-82 phosphorylation induced by neurotensin in pancreatic cancer PANC-1 cells." Journal of Cellular Biochemistry 103(2): 648-662.

Zhu, X., Zhao, X., Burkholder, W. F., Gragerov, A., Ogata, C. M., Gottesman, M. E. and Hendrickson, W. A. (1996). "Structural analysis of substrate binding of molecular chaperone DnaK." Science 272: 1606-1614.

Zimmer, C., Van Gabin, A. and Henics, T. (2001). "Analysis of sequence-specific binding of RNA to Hsp70 and its various homologs indicates the involvement of N-and C-terminal interactions." RNA 7: 1628-1637.

Zou, P., Bortolus, M. and McHaourab, H. S. (2009). "Conformational Cycle of the ABC Transporter MsbA in Liposomes: Detailed Analysis Using Double Electron Electron Resonance Spectroscopy." Journal of Molecular Biology 393(3): 586-597.

Zourlidou, A., Payne Smith, M. D. and Latchman, D. S. (2004). "HSP27 but not HSP70 has a potent protective effect against α-synuclein-induced cell death in mammalian neuronal cells." Journal of Neurochemistry 88(6): 1439-1448.